TRIBHUVAN UNIVERSITY

INSTITUTE OF ENGINEERING

PULCHOWK CAMPUS

THESIS NO: 079/MSPSE/004

Fault Localization and Classification in Distribution Feeder Utilizing Voltage Sag Data

By

Awnish Kumar Thakur

A THESIS

SUBMITTED TO THE DEPARTMENT OF ELECTRICAL ENGINEERING IN

PARTIAL FULFILMENT OF THE REQUIREMENTS FOR THE

DEGREE OF MASTERS OF SCIENCE IN

POWER SYSTEM ENGINEERING

DEPARTMENT OF ELECTRICAL ENGINEERING

Lalitpur, Nepal

APRIL, 2025

COPYRIGHT©

त्रिभुवन विश्वविद्यालय
TRIBHUVAN UNIVERSITY
इन्जिनियरिङ्ग अध्ययन संस्थान
INSTITUTE OF ENGINEERING
पुल्चोक क्याम्पस
PULCHOWK CAMPUS
DEPARTMENT OF ELECTRICAL ENGINEERING
Pulchowk, Lalitpur

Accredited by University Grants Commission (UGC) Nepal 2020

Institute of Engineering Electrical Engineering Department Pulchowk Campus

CERTIFICATE OF APPROVAL

The undersigned certify that they have read, and recommended to the Institute of Engineering for acceptance, a thesis entitled **"Fault Localization and Classification in Distribution Feeder Utilizing Voltage Sag Data"** submitted by Awnish Kumar Thakur in partial fulfilment of the requirements for the degree of Master of Science in Power System Engineering.

.....

Asst. Prof. Anil Kumar Panjiyar
Deputy Head of Department
Department of Electrical Engineering
Pulchowk Campus, Lalitpur
(Supervisor)

.....

Er. Kedar Raj Silwal
Director
Nepal Electricity Authority
(External Examiner)

.....

Asst. Prof. Dr. Bishal Silwal
Program Coordinator
MSc. in Power System Engineering
Department of Electrical Engineering
Pulchowk Campus, Lalitpur

.....

Assoc. Prof. Dr. Basanta Kumar Gautam
Head of Department
Department of Electrical Engineering
Pulchowk Campus, Lalitpur
(Supervisor)

April 2025

ABSTRACT

Nepal's power distribution feeders often struggle with reliability due to aging infrastructure and extreme weather, which frequently lead to insulator punctures and short-circuit faults. Currently, fault detection and clearance rely on manual inspections, making it difficult to visually identify damaged insulators and causing delays in power restoration. This contributes to extended outages, negatively impacting economic activity and service quality.

This study introduces a fault localization and classification method based on voltage sag analysis and circuit modeling, reducing the need for widespread sensor deployment and offering a cost-efficient solution. The approach requires two synchronized time measurement units—one at the substation and one at a terminal node—for fault classification, while other terminal nodes only need non-synchronized units.

The method uses voltage data, with synchronized units also providing phase angle information. Its linear equation framework simplifies computations, and the impact of fault resistance, DG presence, and load variation on accuracy is minimal. The algorithm is implemented in Python and OpenDSS and tested on both IEEE 33-bus and real Nepalese feeders. GIS integration enhances visualization by mapping fault locations.

Simulation results confirm high fault localization precision and effective classification of fault types, indicating the approach’s potential to strengthen Nepal’s distribution system reliability and support future automation and resilience strategies.

Table of Contents

LIST OF TABLES

LIST OF FIGURES

ABBREVIATIONS

NEA	Nepal Electricity Authority
LG	Single Line to Ground Fault
LLG	Double Line to Ground Fault
LL	Double Line Fault
LLL	Tripple Line Fault
LLLG	Tripple Line to Ground Fault
DT	Decision Tree
BIBC	Bus Injection to Branch Current
BCBV	Branch Current to Bus Voltage
ANN	Artificial Neural Network
IED	Intelligent Electronic Device
BFS	Breadth First Search
DG	Distributed Generation
PV	Photovoltaic
PMU	Phasor Measurement Unit
GIS	Geographical Information System
MHP	Micro Hydro Power
AI	Artificial Intelligence
IEEE	Institute of Electrical and Electronics Engineers

CHAPTER ONE: INTRODUCTION

1.1 Background

Electric utilities face numerous reliability issues in distribution systems, which directly impact consumers through power outages and utilities through revenue losses. The power systems in many developing countries were originally designed to serve basic lighting and limited industrial loads. However, with improving economic conditions and increasing load demand, these systems are now under significant strain. One of the primary causes of poor reliability is aging infrastructure, including outdated transformers and inadequate distribution line capacity [1].

Weather conditions play a crucial role in power outages at consumer premises. Extreme events with high impact but low probability, such as hurricanes, wildfires, and ice storms, can severely damage critical infrastructure like distribution lines. A notable example is Hurricane Sandy, which struck the U.S. East Coast in 2012, leaving approximately 7.5 million customers without power across 15 states and Washington, DC. This event underscores the vulnerability of power grids to natural disasters. According to the Congressional Research Service [2], annual revenue losses in the U.S. due to outages ranged from $25 million to $70 million.

The adoption of distributed generation (DG) technologies, such as solar and wind, is increasingly prevalent in distribution systems, greatly enhancing power quality in distribution feeders. However, operating these advanced technologies necessitates grid modernization and the implementation of sophisticated systems to maintain stability. Ensuring reliability requires substantial investments in grid upgrades, advanced monitoring systems, and resilient infrastructure to guarantee a dependable power supply.

Extensive research and various algorithms have been developed for fault localization in transmission lines. However, identifying precise fault locations in distribution systems remains a crucial challenge for electric utilities. Accurate fault localization is vital for minimizing downtime, reducing repair costs, and ensuring efficient service restoration [3]. Traditional methods often rely on manual inspection, which can be time-consuming, especially in large or remote areas. In contrast, modern systems leverage

advanced technologies such as smart meter grids, sensors, phasor measurement units (PMUs), and fault indicators to detect anomalies in voltage, current, or impedance.

The electric distribution network in Nevada experienced approximately 50,000 customer outage hours that affected 40,000 customers due to sustained fault in the year of 2016 AD [4].

Based on logbook data collected from the Barahathawa Distribution and Consumers Services of the Solati distribution feeder, approximately 6,320 consumers experienced a total of 936 hours of outages annually due to faults in the 11 kV distribution feeder. Considering the average energy interruption and outage duration, the annual revenue loss for Nepal Electricity Authority (NEA) is estimated as NRs 6,460,240 in the fiscal year 2023.24 AD.

In rural areas, the distribution feeders (Modified Chapagaun Distribution Feeder) extend up to 70.85 km, including branches, making fault identification and restoration time-consuming due to the manual fault-clearing process (Source: GIS diagram of Chapagaun Distribution Feeder-NEA). When a fault occurs, NEA's response teams are dispatched with spare equipment to identify and repair the issue. The fault-finding process often involves patrolling the feeder, visually inspecting for faults, and, in some cases, utilizing manual load break switches to sectionalize the feeder and locate the fault.

This approach heavily depends on the operator's expertise, prolonging outage durations, especially during adverse weather conditions. Rainy seasons, windstorms, and floods increase these challenges, with fallen trees frequently contacting lines and insulator failures due to punctures. Such failures are particularly difficult to detect, resulting in prolonged outages and delayed system restoration.

In this context, an efficient fault localization and classification system is critical to improving the reliability of Nepal's distribution network. Advanced solutions can significantly reduce outage times and enhance NEA's ability to provide a reliable power supply to consumers.

1.2 Problem Statement

Nepal's power distribution system faces significant challenges in maintaining reliability due to aging infrastructure, inadequate capacity, and adverse weather conditions such as heavy rains, windstorms, and floods. These factors frequently cause faults in distribution lines, leading to power outages and service disruptions. However, the lack of advanced fault localization mechanisms further exacerbates the issue. Traditional fault location finding methods rely on manual inspections and visual assessments, which are time-consuming, error-prone, and lead to prolonged restoration times.

Existing fault localization methods, such as traveling wave-based and impedance-based techniques, are well-suited for transmission networks but face limitations in distribution systems. The presence of multiple laterals, wave reflections, and the heterogeneous nature of distribution feeders significantly reduce their accuracy. Additionally, the increasing penetration of distributed generation (DG) sources, such as photovoltaic (PV) systems and micro-hydropower plants (MHPs), alters voltage profiles and complicates fault location finding. The variability in fault resistance due to environmental factors—such as tree contact, insulator failures, or steel pole contact—further challenges accurate fault localization.

Machine learning and artificial intelligence (AI)-based fault localization methods offer promising alternatives but require extensive datasets for training. However, variations in DG penetration and dynamic load conditions significantly impact their accuracy, making them less reliable in real-world applications. Given these limitations, there is a critical need for a more robust fault localization and classification methodology that can effectively utilize voltage sag data and circuit analysis to improve fault detection accuracy and response times in Nepal’s distribution network.

1.3 Objectives

The major objective of this thesis is to determine the fault location within distribution system and integrate this information with Geographic Information Systems (GIS) for enhanced fault location visualization.

In order to achieve the main objective, a number of sub-objectives have been defined, which are listed below:

- To develop and evaluate fault classification methodology for distribution feeder.
- To validate the methodology in IEEE 33 bus distribution system and practical Nepalese distribution feeder.
- To check the impact of load variation, DG and line impedance error on the accuracy of the fault localization.

1.4 Scope and Limitation of the Study

- The developed methodology has been tested in under simulated environment, and the meshed distribution network is not considered in the simulation.
- The distribution feeder analyzed operates at a primary voltage level of 11 kV, and the study does not cover the secondary distribution system at 400 V.
- In the real system, data transmission error and noise in data transmission are also presented which in not considered in this research.
- The loading condition of for the system is considered as rating of transformer in this simulation work at 70% loading, 100% loading and 120% loading. Thus, variation of load profile is not taken in the study.
- The location and capacity of distributed generation considered in this study are randomly selected to validate the algorithm under future uncertainty conditions.

1.5 Report Organization

Chapter One: This chapter contains the introduction, problem statement, objectives, scope of the study and limitation of the study.

Chapter Two: This chapter gives the overview of different fault localization techniques with their limitations. This chapter also provides insight into the various earlier research works done in the field.

Chapter Three: This chapter outlines the methodology used to achieve the study's objectives. It covers the mathematical background adopted for fault localization, a novel fault classification methodology along with its classification logic, and the integration of results into a GIS map. Additionally, it provides details on the software tools utilized and the test systems employed, including the IEEE 33-bus system and a practical Nepalese distribution system.

Chapter Four: This chapter presents the results obtained for the IEEE 33-bus test system and a practical Nepalese distribution feeder. The results include numerical data for fault localization, fault visualization on a GIS map, and sensitivity analysis considering the impact of load variation. Additionally, it explores the effects of modeling errors in line impedance, the impact of distributed generation (DG) penetration, and resistance variations. Finally, fault classification results for each system are provided.

Chapter Five: Conclusion from the research work and future recommendation of this works are summarized in this chapter.

CHAPTER TWO: LITERATURE REVIEW

Fault localization in the power system means either finding the exact fault location, finding faulted areas, or finding the fault closest to the bus in order to minimize service disruption and repair time. There are several methods involved in fault localization depending upon the purpose and type of system.

Figure 1 illustrates the research work on fault localization in distribution systems published in IEEE Transactions papers from 2005 to 2024. It is evident that since 2020, extensive work has been conducted and published in IEEE Transactions. This surge in research highlights both progress and opportunities to address fault localization errors in distribution systems.

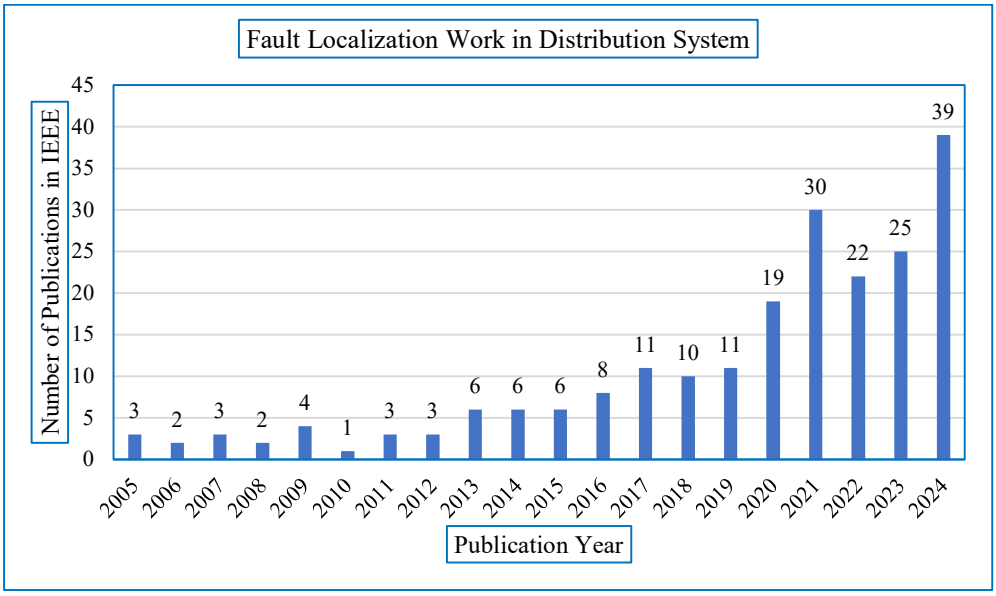

Figure 1: Number of publications in IEEE for fault localization in the distribution system from 2005 AD to 2024 AD

The paper titled “Fault detection, classification and location in power distribution smart grid using smart meters data” is presented in [5]. This paper reviews various fault detection, identification, and localization methods while proposing a novel approach integrating fuzzy logic and neural networks. The proposed method utilizes sensor and smart meter data, tested on the IEEE 37-bus system using the OpenDSS-MATLAB platform, achieving 99.9% accuracy. OpenDSS handles system modeling and load flow analysis, while MATLAB processes smart meter data for fault analysis.

Key methodologies explored include:

- **Fuzzy Logic & Discrete Wavelet Transform:** Detects faults and their effects, validated on the IEEE 13-bus system and an Indian network.
- **Neural Networks:** Applied for fault classification and detection, adapting dynamically with a correlation coefficient of 0.93788.
- **Voltage Fluctuation-Based Detection:** Neural networks identify and classify faults with a 0.2% detection error.
- **Kalman Filter & Euclidean Detector:** Enhance fault detection in smart grids by handling nonlinear variations and analyzing variable relationships.
- **Linear Regression for Fault Localization:** Considers network variability but is ineffective for looped microgrids.
- **Protective Relay-Based Detection:** Uses nonlinear operations for hidden fault detection, achieving 98% accuracy on the IEEE 39-bus system.
- **State Estimation Algorithms:** Optimize power loss reduction using smart meter data in real distribution networks.
- **Intelligent Fault Management:** Enhances grid self-healing through autonomous data exchange, analyzing overvoltage events.

The paper titled "Fault location methods for distribution networks using smart meters" is presented in [6]. This paper presents an algorithm that employs a changeable weighting matrix-based bad data identification technique for fault location detection. The algorithm is independent of fault types, and its accuracy is validated through extensive simulations on a real 13.8 kV, 134-node distribution network under various fault scenarios. It operates under the assumption that voltage and current measurements are available at specific nodes within the distribution network and at the substation. Additionally, measured load demand and forecasted data are incorporated as pseudo-measurements. Given the limited availability of real-time measurements in distribution systems, pseudo-measurements are essential to maintain network observability.

The paper titled "Voltage sag data utilization for distribution fault location" is presented in [7]. This paper presents a fault location algorithm that utilizes voltage sag data from

selected nodes for fault detection and localization. The algorithm is validated on the IEEE 123-node distribution system using Alternative Transient Program Software (ATPS) and comprises four key components: Voltage Sag Characterization, Fault Resistance Estimation, Load Variation Analysis, and Implementation of the Proposed Schemes.

Simulations are conducted for various fault scenarios, with the generated data compared to real-time smart meter data from the distribution center. Unlike conventional impedance-based methods, the proposed approach significantly reduces the number of smart meters required for accurate fault detection and localization.

For instance, in a single-line-to-ground fault scenario, an impedance-based method identifies four possible fault locations when only three smart meters are used, requiring 39 meters for precise localization. In contrast, the proposed method is more cost-effective, minimizing the need for extensive smart meter deployment.

By leveraging voltage sag characterization, the algorithm also reduces data transmission requirements to the distribution center. It considers both voltage magnitude and phase angle variations during faults while accounting for load fluctuations. Finally, a flag value is assigned to each node, with a higher flag indicating the faulted location.

The paper entitled “Enhancing Accuracy While Reducing Computation Complexity for Voltage Sag Based Distribution Fault Location” is presented in [8]. This paper leverages decision tree (DT) techniques to enhance fault detection efficiency while reducing computational complexity by 90%. Two professional software tools are used: Alternate Transient Program (ATP) for modeling the IEEE 134-node distribution feeder and CART for developing the decision tree to identify faulted segments. The feeder is divided into multiple segments based on protective device placement, with each zone treated as a segment.

Load flow analysis is performed using BIBC (Bus Injection to Branch Current) and BCBV (Branch Current to Bus Voltage) algorithms, utilizing voltage and current phasors from the feeder root and voltage sag data from sparse sensors. Voltage measurements are obtained using power quality meters or similar sensors. The DT estimates the faulted node by calculating error values, selecting the node with the

smallest error. The optimal weighting factor (α) depends on measurement accuracy and system modeling, with adjustments made based on error levels.

Six sensors are deployed in the tested feeder, and an artificial neural network (ANN) is trained using 49,210 fault scenarios. Random errors with a 0.5% deviation are introduced to reflect real-world conditions. Fault parameters, including resistance, location, and pre-fault load patterns, are considered. Completing one scenario for six voltage outputs takes three seconds. While placing sensors at every feeder node improves accuracy, financial constraints necessitate optimal sensor placement to maximize faulted segment identification.

The paper entitled “Sensitivity Analysis of Voltage Sag based Fault Location with Distributed Generation” is presented in [9]. This paper examines the impact of distributed generation (DG) on the accuracy of fault location algorithms based on voltage sag characterization. A sensitivity analysis is performed on a real-world distribution feeder using ATP software for steady-state modeling and SimLab for analysis.

The first step in fault detection is identifying the faulted node by calculating a flag value based on voltage sag mismatches, comparing simulated and measured voltage magnitudes during faults. The study assumes 15 smart meters placed at the start and end of the feeder branches for measuring voltage. The node with the highest flag value is selected as the faulted node. Binary search algorithms are then used to pinpoint the fault location by halving the search range and calculating flag values for each iteration.

Results show that DG can cause similar voltage magnitudes at different buses during faults, which reduces the accuracy of fault location algorithms. The effect of DG on fault detection depends on its location and penetration levels.

The paper titled “A New Fault Location Algorithm Using Direct Circuit Analysis for Distribution Systems” is presented in [10]. This paper introduces a fault location algorithm for unbalanced distribution systems using direct three-phase circuit analysis. Unlike traditional methods designed for balanced transmission networks, which rely on symmetrical components and sequence networks, this approach addresses the unbalanced conditions typical in distribution systems due to factors like single-phase laterals, loads, and non-transposed lines.

The proposed algorithm eliminates the need for symmetrical components, enabling accurate fault location in both balanced and unbalanced systems. By deriving a fault location equation using the matrix inverse lemma, the algorithm simplifies the fault detection process while maintaining high accuracy. Extensive EMTP simulations validate the approach, with results showing a maximum error of just 0.08% in unbalanced systems, compared to 25% in conventional methods.

This research offers a more accurate and practical fault location solution for distribution systems, particularly in scenarios where traditional methods are ineffective due to system asymmetry.

The paper titled “Fault Location in Distribution Systems Based on Smart Feeder Meters” is presented in [11]. This paper presents a fault-location method that leverages smart feeder meters with voltage sag monitoring to estimate fault locations. By correlating voltage deviations at different buses with estimated fault currents and using the bus impedance matrix, the method accurately identifies the faulted section. Unlike traditional substation-based techniques, this approach offers improved accuracy through distributed voltage measurements from feeder meters.

The study validates the method through extensive simulations on a real distribution system, showing that fault resistance, meter placement, and load variations have minimal impact on accuracy. This makes the method practical and scalable for modern distribution networks. The integration of automated outage mapping further enhances fault location precision, reducing the need for multiple estimations and lowering computational effort.

This research highlights the potential of smart meter technology in improving fault localization while reducing infrastructure costs, offering a foundation for modernized fault management in smart grids.

The paper titled "Fault Location in Distribution Networks by Compressive Sensing" is presented in [12]. This paper presents a new method for locating faults in distribution networks using compressive sensing and voltage sag measurements from smart meters. The method estimates the fault location by calculating a sparse current vector and performing $\ell 1$-norm minimization. It is robust to noise, effective in various fault conditions, and does not require expensive infrastructure like Phasor Measurement

Units (PMUs). Compared to existing methods, it performs better in noisy environments, with low fault resistances, and in cases where synchronized load data is unavailable. The method was tested on a 13.8-kV, 134-bus network, showing accurate fault location estimates.

2.1 Type of Fault

A fault in the power system refers to abnormal condition in system that causes flow of current in unintended path as well as larger magnitude. The type of short circuit fault can be classified as below [5]:

1. **Symmetrical Short Circuit Fault:** A symmetrical short circuit fault occurs when a short circuit affects all three phases equally. In this condition, the magnitude of current flowing through each phase remains the same, while the phase angles remain unchanged. Although this type of fault is rare, it has severe consequences on the power system. Symmetrical short circuit faults can be further classified into Three-Phase Fault (LLL) and Three-Phase to Ground Fault (LLLG).
2. **Unsymmetrical Short Circuit Fault:** During the short circuit condition either one or two phase involve, this type of fault is termed as unsymmetrical fault. During this type of fault magnitude of fault current through each phase are different as well as change in phase angle. Further, this type of fault can be classified as single phase to ground (LG) fault, double line to ground (LLG) fault, and double line (LL) fault.
    a) **Single Line to Ground (LG) Fault:** In case of LG fault, there is involvement of only single line to ground. When bolted LG fault occurs, the healthy phases voltage may vary from phase voltage to line voltage that depends upon the earthing condition.
    b) **Double Line (LL) Fault:** In case of LL fault, there is involvement of two line. When bolted LL fault occurs in system, the healthy phase voltage remains as same.
    c) **Double Line to Ground (LLG) Fault:** In case of LLG fault, there is involvement of two phase to ground. When bolted LLG fault occurs in system, the healthy phase voltage varies from phase voltage to 1.5 times of phase voltage depending upon condition.

Figure 2 illustrates classification of short circuit faults, in which symmetrical fault LLL, LLG, unsymmetrical fault LG, LL, and LLLG are shown in a, b, c, d, and e respectively.

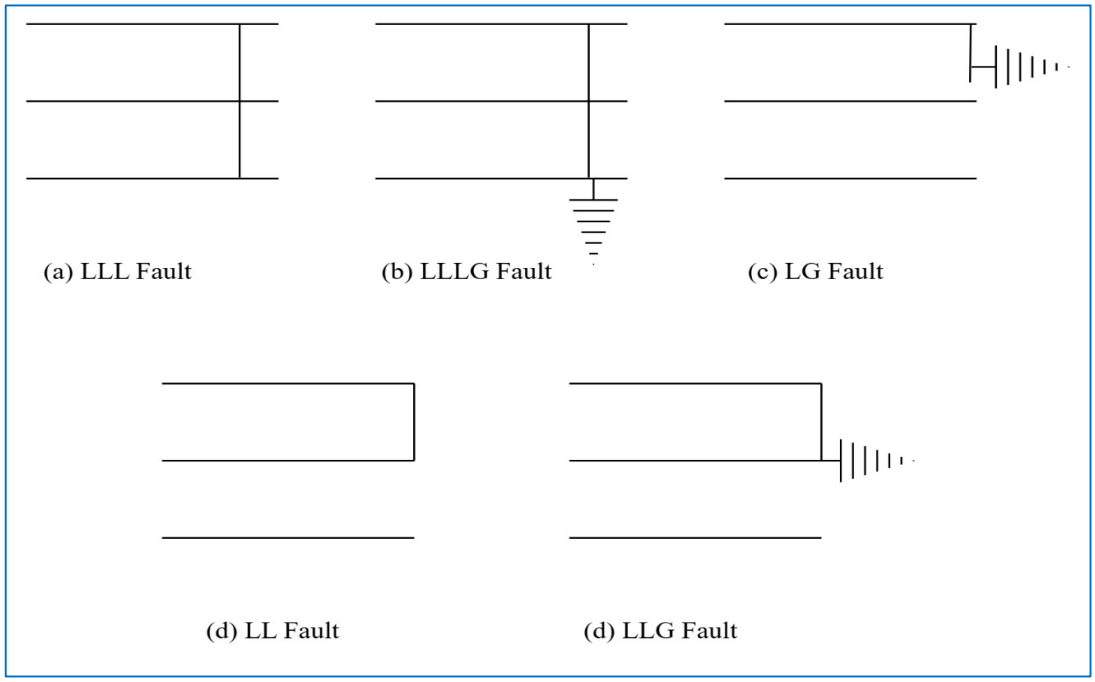

Figure 2: Classification of short circuit fault

2.2 Occurrence Probability of Fault

Various of short circuit fault types, the relative frequency of occurrence [13] of fault in distribution system in order to decreasing severity is presented in Table 1.

Table 1: Relative frequency of occurrence of fault

Type of Faults	Relative Frequency of Occurrence
Three phase (3L) faults	5%
Double line to ground (LLG) faults	10%
Double line (LL) faults	15%
Single line (LG) faults	70%

2.3 Fault Localization Approaches

There are a various of methods are applied in transmission line for fault localization, and are working with high accuracy. But in case of distribution line, there is presence of laterals, load tap, heterogenous nature, and varying loading condition, it is difficult

to locate fault in real distribution system [9]. The popular method for fault localization is listed below with brief summary about its strength as well as limitations.

a) **Travelling wave-based method:** When a fault occurs in the distribution line, the fault point generates traveling waves that propagate in both directions—toward the substation end and the opposite end. The waves travel at a speed nearly equal to the speed of light. The location of the fault is determined by detecting the time difference between two consecutive traveling waves. This approach necessitates high-frequency sampling, which depends on the tower configuration. Moreover, it requires expensive high-sampling-rate equipment capable of capturing waveforms moving at speeds close to that of light. The traveling wave-based method accurately localizes faults in transmission lines; however, its application in distribution systems is highly complex due to the presence of multiple laterals and the resulting reflected waves [14].
b) **Impedance based method:** Fault localization using impedance-based methods involves calculating the virtual fault impedance from measurements taken at specific points within the distribution network, typically at the substation. When a fault occurs, there is a sudden drop in voltage and a significant rise in current. By taking the ratio of voltage to current, the virtual fault impedance is estimated. This impedance is then compared with the known impedance profile of the distribution system. Since the impedance of a line is proportional to its length, the location of the fault can be determined accordingly. However, these methods often present challenges by providing multiple possible fault locations. One of the tested cases in the paper demonstrates that for a single line-to-ground fault, the impedance-based algorithm identifies four potential fault locations when only three smart energy meters are deployed in the system [7].
c) **Super imposed components method:** It calculates the faulted system's state by superimposing the normal (pre-fault) system state with the deviation caused by the fault, known as the superimposed components. By isolating these deviations, the method simplifies fault location and analysis by focusing only on the incremental changes. This approach is effective for analyzing transient and steady-state fault behavior, especially in radial distribution systems. However, its limitations include sensitivity to measurement inaccuracies, dependency on accurate pre-fault conditions, and reduced effectiveness in

complex, meshed systems where multiple pathways can dilute the superimposed signals. Additionally, integrating it with real-time monitoring systems can be computationally intensive [7].

d) **Intelligent system-based method:** It employs artificial intelligence (AI) techniques, such as neural networks, fuzzy logic, expert systems, and machine learning, to analyze and locate faults in power distribution systems. These methods utilize historical and real-time data to identify patterns and anomalies associated with faults. They can handle the complexities of nonlinear, dynamic systems and adapt to changing system conditions, making them suitable for modern smart grids. However, their limitations include the need for large datasets for training, potential overfitting, and challenges in interpreting the model's decision-making process. Additionally, their accuracy heavily depends on the quality and quantity of input data and the robustness of the system's design [7].

e) **Voltage sag-based method:** The voltage sag-based method identifies and locates faults in distribution systems by analyzing the voltage sags caused by faults. When a fault occurs, it creates a characteristic drop in voltage magnitude at different buses, with the severity and pattern of the sag depending on the fault's location, type, and impedance. By comparing the measured voltage sags with a pre-calculated fault signature database or using analytical models, the fault's location can be pinpointed [7].

The voltage sag during different type of fault occurrence with fault duration is reported in Table 2 [15].

Table 2: Voltage sag during different type of fault

S.N.	Type of Fault	Voltage Sag Magnitude (pu)	Typical Duration (ms)
1.	Single Line to Ground (LG) Fault	0.5 – 0.9	60 – 600
2.	Double Line (LL) Fault	0.7 – 0.9	60 – 600
3.	Double Line to Ground (LLG) Fault	0.3 – 0.7	60 – 600
4.	Three Phase (LLL) Fault	0.0 – 0.3	60 – 600
5.	Three Phase to Ground Fault (LLLG)	0.0	60 – 600

2.4 Research Gap

While reviewing research paper [9], [6], [8] and [15] following research gaps are identified that are presented below:

Most existing research on fault localization has concentrated on transmission systems, where techniques such as impedance-based methods or intelligent system-based approaches, like those using artificial intelligence, have shown accurate results. However, when applied to distribution systems, these methods tend to be less effective due to the unique complexities present in such networks. Distribution systems often include laterals (branching lines), exhibit diverse configurations, and experience highly variable loading conditions, making fault localization more challenging.

Moreover, very few methodologies effectively account for the impact of distributed generation (DG), such as solar or wind power, on the accuracy of fault detection. The presence of DG can alter voltage profiles and fault characteristics, complicating the localization process. Another critical challenge is the variability of fault resistance, which can change significantly depending on environmental factors like weather conditions. For example, wet or rainy weather often reduces fault resistance, while dry conditions can increase it, further affecting detection accuracy.

A significant limitation of many existing techniques is their failure to identify the specific phase of the fault. Fault phase identification is crucial for precise fault management and restoration, as it enables more targeted repairs and faster resolution of issues.

These limitations emphasize the need for a more cost-effective and reliable approach to fault localization. Such an approach must be specifically designed to address the distinct challenges of Nepalese distribution systems, including their complex topology, the integration of distributed generation, and variable fault conditions.

CHAPTER THREE: METHODOLOGY

To meet the proposed objectives of the thesis, the following methodology has been adopted.

3.1 Literature Review

The literature review focused on analyzing research papers concerning current fault localization and classification methods in distribution networks. This examination revealed a research gap, which prompted the development of a proposed methodology for fault localization and classification within the system. The majority of the reviewed papers were sourced from IEEE Transactions.

3.2 Fault Localization and Classification Methodology

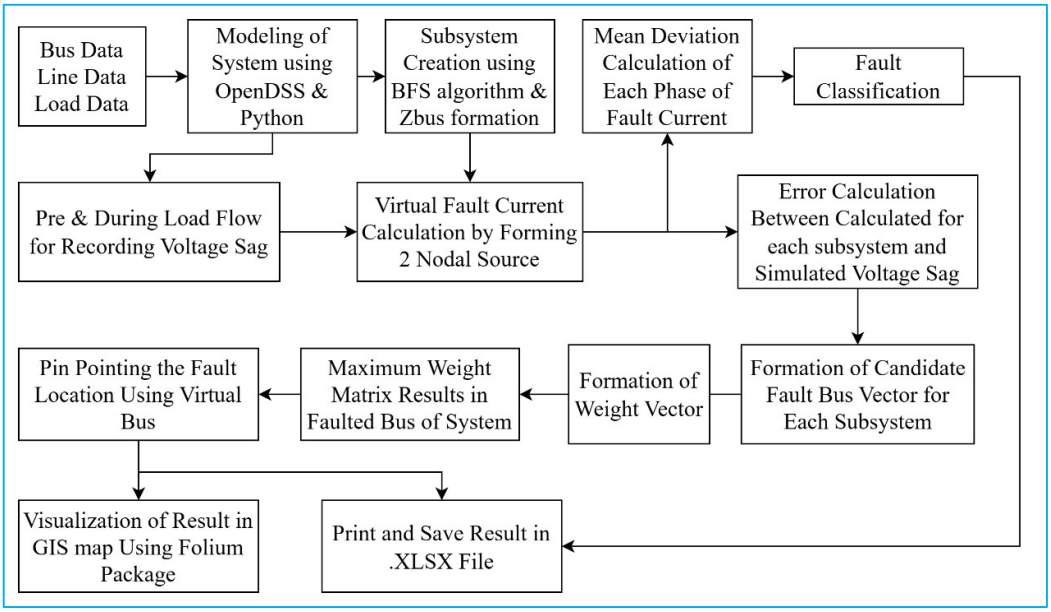

Figure 3: Fault localization and classification methodology

For the implementation of the fault localization and classification algorithm, some assumptions are taken into account. The assumptions are listed below:

Assumptions:

- The distribution system should be equipped with a fault indicator to accurately detect the fault condition in the system.

- Two nodes (the substation node and one end of a lateral) should be equipped with synchronized time measurement units capable of capturing voltage magnitude and phase angle data both before and during a fault, which is then transmitted to the data center.
- Intelligent Electronic Devices (IEDs) should be installed at the ends of laterals, enabling them to transmit voltage magnitude data both before and during fault conditions.
- All IEDs installed along the distribution line must function flawlessly, ensuring that no measurement errors occur during operation.
- During the fault condition, the power consumptions of the load should remain constant for this short transient period.

Figure 3 illustrates the integrated methodology for fault localization and classification in the distribution feeder. The distribution system is modeled by integrating OpenDSS with Python. To model the distribution feeder, line parameters such as conductor length and type, line configuration, node details along with their geographical information system (GIS) coordinates, and load types with their magnitudes and connections at buses are organized in an Excel file. This Excel file serves as the input interface for distribution network modeling, meaning that if data for any distribution feeder is entered into this file, the system automatically generates the corresponding model.

The subsystem of the distribution feeder involves dividing the network into multiple laterals, extending from the substation node to the terminal ends of the laterals, with the primary consideration being the series impedance between these points. The number of subsystems formed corresponds to the number of terminal buses. These terminal buses are identified using the Breadth First Search (BFS) algorithm. Once the subsystems are established, the admittance matrix for each subsystem is extracted from OpenDSS. By inverting this admittance matrix, the impedance matrix for each subsystem is derived.

3.2.1 Subsystem Creation

Figure 4 illustrates a sample 7-node distribution feeder used to demonstrate the formation of subsystems. This feeder is equipped with two types of Intelligent Electronic Devices (IEDs): one type includes synchronized time measurement units, such as micro-phasor measurement units (μPMUs), phasor measurement units (PMUs),

or other similar sensors, and the other type consists of smart meters capable of transmitting data to the server during transient conditions. The synchronized time measurement units are represented as IED1.1 and IED1.2.

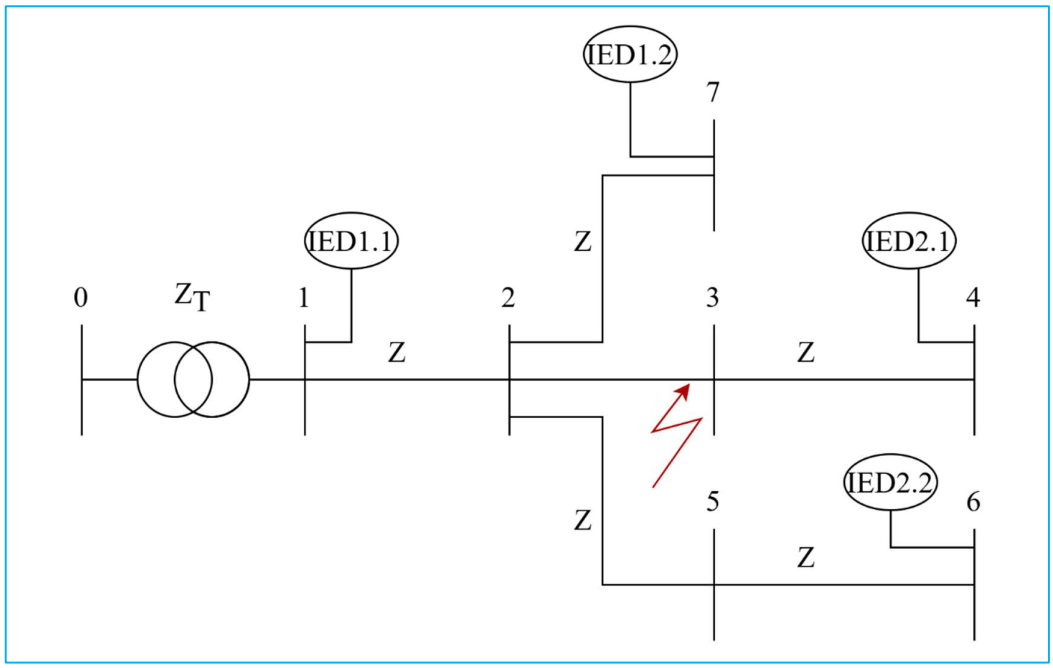

Figure 4: Sample 7 node distribution feeder

The non-synchronized time measurement units are represented by 2.1 and 2.2 [16]. The number of synchronized time measurement units is independent of the topology of the distribution feeder i.e. only two measurement units is required.

The feeder includes three terminal buses, leading to the formation of three subsystems. Each subsystem comprises the series impedance between the substation node and the end of each lateral. Figure 5 demonstrates the subsystem formation for the 7-node distribution feeder. In this setup, Subsystem 3 is equipped with synchronized time measurement units, which provide two nodal current sources at terminal nodes 7 and 1. By summing these two nodal currents, the total fault current is obtained. Similarly, the other subsystems, which lack synchronized time measurement units, are responsible for calculating the error between the computed voltage sag and the actual voltage sag at the terminal buses. For simplicity in demonstration, all sections of the distribution feeder are assumed to be of equal length. Since the distribution line segments share the same length and conductor type, they provide an identical impedance matrix.

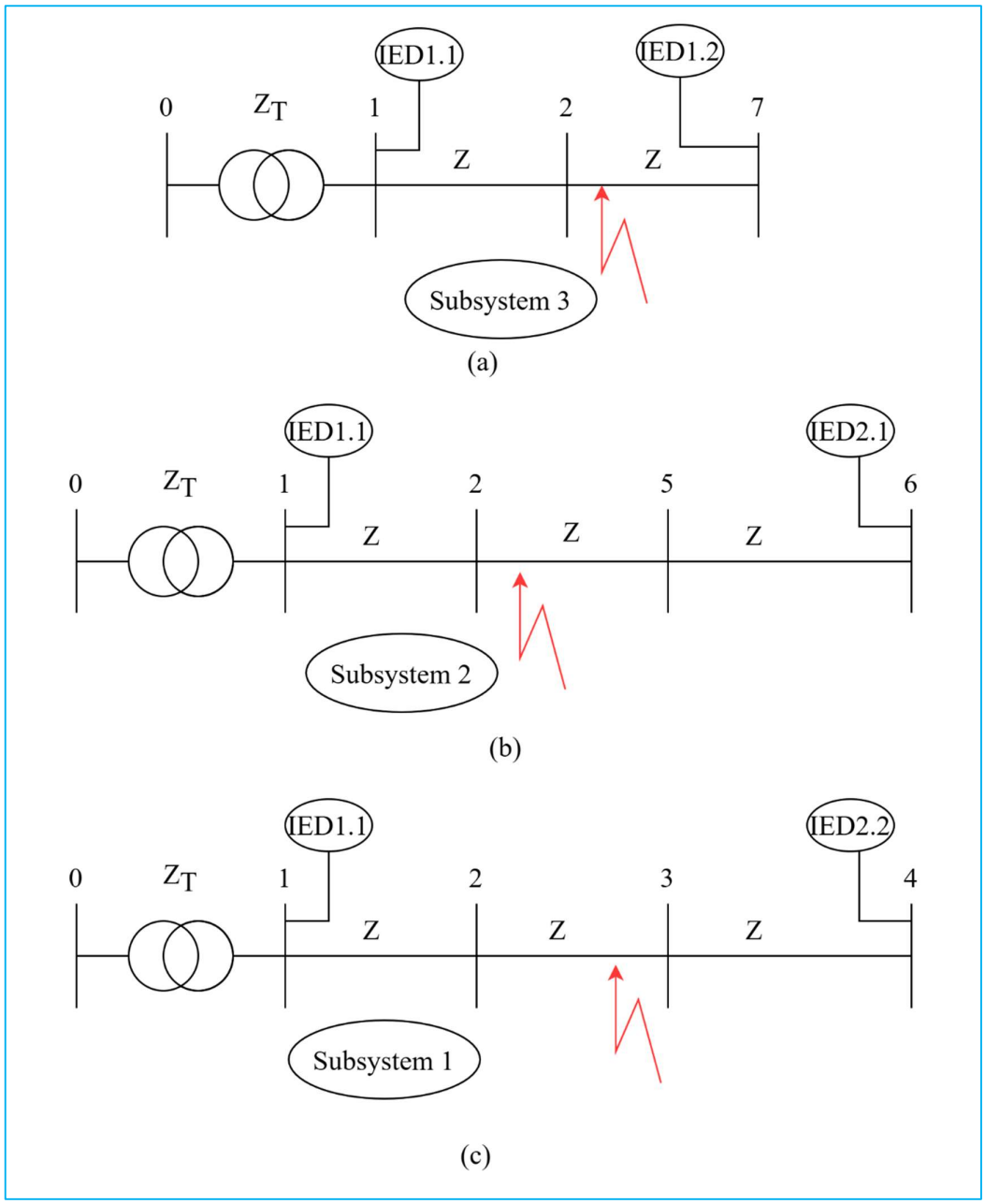

Figure 5: Subsystem formation for 7 node distribution feeders

3.2.2 Impedance Matrix Creation

Figure 6 illustrates a section of a three-phase distribution feeder. In which (a) represents healthy system, (b) represents fault at various point, and (c) represents fault current are modeled as two current sources.

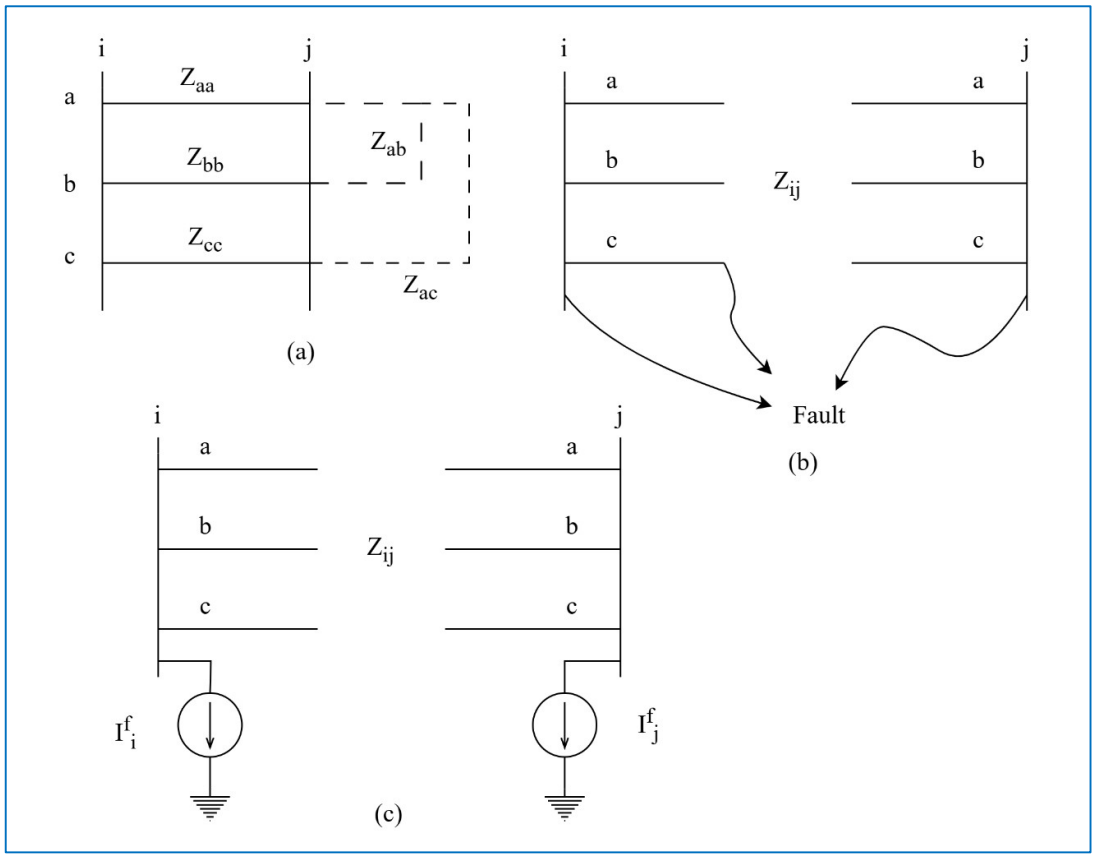

Figure 6: Section of three phase distribution system

The bus voltages at bus i, j, and impedance matrix is presented in (1), (2), and (3), respectively [4].

$$V_i = \begin{bmatrix} V_i^a \\ V_i^b \\ V_i^c \end{bmatrix}_{3\times1} \quad 1$$

$$V_j = \begin{bmatrix} V_j^a \\ V_j^b \\ V_j^c \end{bmatrix}_{3\times1} \quad 2$$

$$Z_{ij} = \begin{bmatrix} Z_{ij}^{aa} & Z_{ij}^{ab} & Z_{ij}^{ac} \\ Z_{ij}^{ba} & Z_{ij}^{bb} & Z_{ij}^{bc} \\ Z_{ij}^{ca} & Z_{ij}^{cb} & Z_{ij}^{cc} \end{bmatrix}_{3\times3} \quad 3$$

For a three-phase distribution line, the impedance matrix between two buses is a 3×3 matrix, incorporating both the series impedance of the line and the mutual coupling

impedance between phases. The diagonal element represents series impedance, while off-diagonal impedance represents mutual impedance coupling.

In fault localization, it is essential to consider the 3×3 matrix for each line section. While a simplified per-phase representation may be used for easier representation of the mathematical background, the actual implementation must account for all three phases.

The three-phase pre-fault and during-fault current can be calculated using (4), and (5), respectively.

$$I_{ij}^{pre} = Z_{ij}^{-1} \times \left(V_i^{pre} - V_j^{pre}\right) \quad 4$$

$$I_{ij}^{during} = Z_{ij}^{-1} \times \left(V_i^{during} - V_j^{during}\right) \quad 5$$

The fault current is considerably greater than both the pre-fault and during-fault load currents. Therefore, the fault current can be calculated by subtracting the pre-fault current from the during-fault current. Consequently, the final equation for the fault current is expressed in (6).

$$I_{ij}^{F} = Z_{ij}^{-1} \times \left(\Delta V_i - \Delta V_j\right) \quad 6$$

The voltage sag for a n^{th} bus is calculated using (7).

$$\Delta V_n^{abc} = \begin{bmatrix} V_n^{a,pf} - V_n^{a,f} \\ V_n^{b,pf} - V_n^{b,f} \\ V_n^{c,pf} - V_n^{c,f} \end{bmatrix}_{3\times 1} \quad 7$$

Voltage sag in a distribution feeder is influenced by the fault resistance during a fault event. Since the Intelligent Electronic Devices (IEDs) installed in the feeder are tasked with measuring real-time voltage data, the resulting voltage sag is determined as a function of the fault resistance. The behavior of the line current during phase unbalance differs from that during a fault, leading to distinct voltage drop characteristics in each scenario. Additionally, a fault indicator is installed on the distribution line to distinguish between fault conditions and phase unbalance conditions.

The three-phase impedance between the substation node and the lateral end node, where IEDs are installed, is calculated using relation (3) and a step-by-step Zbus building

algorithm. The fault currents injected at nodes 1 and 7 are determined using equation (8).

$$\begin{bmatrix} i_1^{abc} \\ i_7^{abc} \end{bmatrix}_{6\times1} = \begin{bmatrix} Z_T & Z_T \\ Z_T & Z_T + 2Z \end{bmatrix}_{6\times6}^{-1} \begin{bmatrix} \Delta V_1^{abc} \\ \Delta V_7^{abc} \end{bmatrix}_{6\times1} \quad 8$$

The fault current is calculated by summing up two individual currents of buses, which is calculated by using (9).

$$i_f^{abc} = i_1^{abc} + i_7^{abc} \quad 9$$

The inclusion of distributed generation (DG) in the distribution feeder has a notable impact on voltage sag compared to a system without DGs. However, in this methodology, the effect of DGs is already incorporated during the fault current calculation. Consequently, the process of creating subsystems remains consistent, irrespective of whether DGs are present in the system or not.

3.2.3 Finding Closest Fault Bus

The fault current calculated using equation (9) is injected into every bus of each subsystem, and the corresponding voltage sag is computed in the virtual environment. For the demonstration subsystem illustrated in the Figure 5, subsystem 3 is selected to calculate the voltage sag by injecting the fault current. In equation (10), the fault current is injected at node 1, and the resulting voltage sag is calculated at nodes 1, 2, and 7, where IEDs are installed. Similarly, the fault current is injected at nodes 2 and 7, and the corresponding voltage sags are calculated using equations (11) and (12), respectively. This process is repeated for every subsystem that has been formed.

$$\begin{bmatrix} \Delta V_{1,1}^{abc,3} \\ \Delta V_{2,1}^{abc,3} \\ \Delta V_{7,1}^{abc,3} \end{bmatrix}_{9\times1} = \begin{bmatrix} Z_T & Z_T & Z_T \\ Z_T & Z_T + Z & Z_T + Z \\ Z_T & Z_T + Z & Z_T + 2Z \end{bmatrix}_{9\times9} \begin{bmatrix} i_f^{abc} \\ 0 \\ 0 \end{bmatrix}_{9\times1} \quad 10$$

$$\begin{bmatrix} \Delta V_{1,2}^{abc,3} \\ \Delta V_{2,2}^{abc,3} \\ \Delta V_{7,2}^{abc,3} \end{bmatrix}_{9\times1} = \begin{bmatrix} Z_T & Z_T & Z_T \\ Z_T & Z_T + Z & Z_T + Z \\ Z_T & Z_T + Z & Z_T + 2Z \end{bmatrix}_{9\times9} \begin{bmatrix} 0 \\ i_f^{abc} \\ 0 \end{bmatrix}_{9\times1} \quad 11$$

$$\begin{bmatrix} \Delta V_{1,7}^{abc,3} \\ \Delta V_{2,7}^{abc,3} \\ \Delta V_{7,7}^{abc,3} \end{bmatrix}_{9\times1} = \begin{bmatrix} Z_T & Z_T & Z_T \\ Z_T & Z_T + Z & Z_T + Z \\ Z_T & Z_T + Z & Z_T + 2Z \end{bmatrix}_{9\times9} \begin{bmatrix} 0 \\ 0 \\ i_f^{abc} \end{bmatrix}_{9\times1} \quad 12$$

The error matrix is determined by subtracting the measured voltage at the terminal node of each subsystem, as the IED is installed at the end of the subsystem from the calculated voltage sag. This IED records real-time voltage data both before and during a fault. In Subsystem 3, the sensor is equipped at node 7, which is considered the reference node for measuring voltage sag. Errors are calculated for each scenario of current injection by comparing the actual voltage sag at node 7 with the voltage drop caused by current injections at nodes 1, 2, and 7. The voltage sag at node 7 for subsystem 3 is computed using equation (13). The same process is repeated for subsystems 1 and 2, with their error matrices represented by equations (14) and (15), respectively.

$$Error_7^{abc,3} = \begin{bmatrix} Error_{7,1}^{abc,3} \\ Error_{7,2}^{abc,3} \\ Error_{7,7}^{abc,3} \end{bmatrix} = \begin{bmatrix} |\Delta V_7^{abc}| \\ |\Delta V_7^{abc}| \\ |\Delta V_7^{abc}| \end{bmatrix} - \begin{bmatrix} |\Delta V_{7,1}^{abc,3}| \\ |\Delta V_{7,2}^{abc,3}| \\ |\Delta V_{7,7}^{abc,3}| \end{bmatrix} \quad 13$$

$$Error_4^{abc,3} = \begin{bmatrix} Error_{4,1}^{abc,3} \\ Error_{4,2}^{abc,3} \\ Error_{4,3}^{abc,3} \\ Error_{4,4}^{abc,3} \end{bmatrix} = \begin{bmatrix} |\Delta V_4^{abc}| \\ |\Delta V_4^{abc}| \\ |\Delta V_4^{abc}| \\ |\Delta V_4^{abc}| \end{bmatrix} - \begin{bmatrix} |\Delta V_{4,1}^{abc,3}| \\ |\Delta V_{4,2}^{abc,3}| \\ |\Delta V_{4,3}^{abc,3}| \\ |\Delta V_{4,4}^{abc,3}| \end{bmatrix} \quad 14$$

$$Error_6^{abc,3} = \begin{bmatrix} Error_{6,1}^{abc,3} \\ Error_{6,2}^{abc,3} \\ Error_{6,5}^{abc,3} \\ Error_{6,6}^{abc,3} \end{bmatrix} = \begin{bmatrix} |\Delta V_6^{abc}| \\ |\Delta V_6^{abc}| \\ |\Delta V_6^{abc}| \\ |\Delta V_6^{abc}| \end{bmatrix} - \begin{bmatrix} |\Delta V_{6,1}^{abc,3}| \\ |\Delta V_{6,2}^{abc,3}| \\ |\Delta V_{6,5}^{abc,3}| \\ |\Delta V_{6,6}^{abc,3}| \end{bmatrix} \quad 15$$

For each subsystem, distinct errors are obtained when the fault current is injected into each node individually. The node with the smallest error in each subsystem is selected as the candidate bus. A new vector, "X" is formed, containing the candidate buses for all subsystems. In the demonstration scenario, the fault is located between lines 2 and 3, closer to node 3. In Subsystem 1, node 3 is identified as the candidate bus since the fault is near node 3. However, in Subsystems 2 and 3, node 3 is not present, so the closest bus, node 2, is selected as the candidate bus for both Subsystems. Among the candidate nodes identified, it is necessary to determine which one is closest to the actual

To achieve this, two vectors are defined: "Y," which indicates how many times a selected candidate bus appears in each subsystem, and "J," which indicates how many

times each bus is selected as a candidate bus. A weight vector is calculated using equation (16).

$$W = \frac{[J]}{[Y]} \qquad 16$$

For the sample system, the vector X, Y, and J is calculated as:

X = [3 2 2]

Y = [1 3 3]

J = [1 2 2]

W = [1 2/3 2/3]

The value of the weight matrix should lie between 0 and 1. A higher value is selected as candidate buses. Here, bus 3 is selected as the candidate bus.

3.2.4 Finding Exact Fault Location

Once the node closest to the fault is identified, the process of pinpointing the exact fault location begins. First, the lines connected to the candidate fault buses are determined, along with the subsystems they belong to. These lines are virtually divided into 10 equal sections. For each subsystem containing the relevant line, a new impedance matrix is constructed. The process from equations (10) to (16) is then repeated, and the virtual node with the smallest error is identified as the final fault location in the system.

3.2.5 Noval Fault Classification Approach

The fault classification approach is developed using the fault current calculation equation (9), which relies on the mean deviation of each phase and establishes the threshold for identifying the fault type. The absolute mean value of the fault current for each phase is determined by equation (17).

$$I_f^m = \frac{abs\left(I_f^a\right) + abs\left(I_f^b\right) + abs\left(I_f^c\right)}{3} \qquad 17$$

The mean deviation value for each phase is computed using equations (18) through (20).

$$D_{IA} = abs\left(\frac{I_f^a - I_f^m}{I_f^m}\right) \quad 18$$

$$D_{IB} = abs\left(\frac{I_f^b - I_f^m}{I_f^m}\right) \quad 19$$

$$D_{IC} = abs\left(\frac{I_f^c - I_f^m}{I_f^m}\right) \quad 20$$

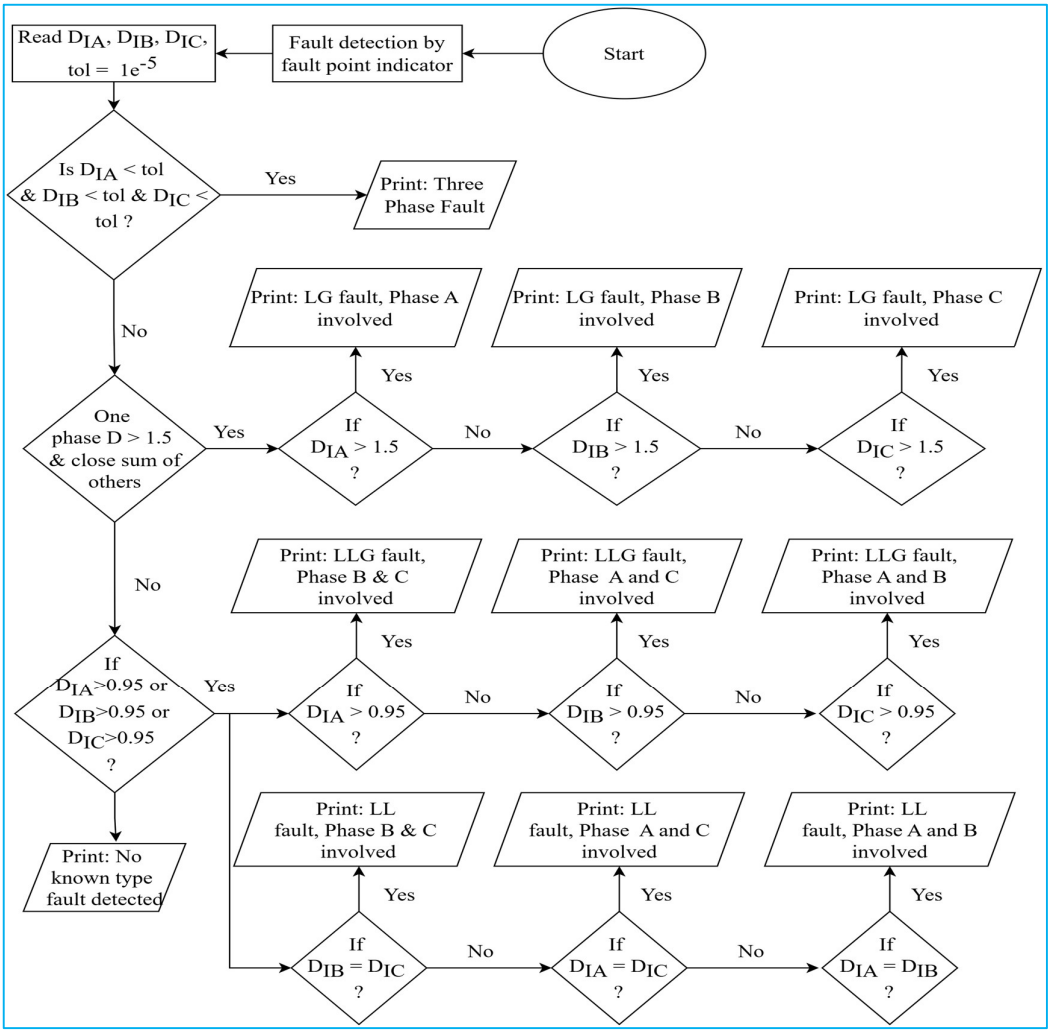

Figure 7: Flowchart showing decision logic for fault classification approach

Figure 7 illustrates that the fault classification algorithm is designed to identify and categorize different types of faults in a three-phase power system based on the mean deviation values of each phase fault current. The algorithm begins by reading these deviation values and setting a threshold value tolerance. It first checks if all three deviation values are below this threshold. If they are, the algorithm identifies the fault

as a Three-Phase Fault. If not, it proceeds to evaluate the conditions for a Single Line to Ground Fault. This is done by checking if the deviation of one phase exceeds 1.5 while the sum of the deviations of the other two phases is approximately 1.5. If this condition is met, the algorithm identifies the specific phase involved and classifies the fault accordingly. If the single line to ground fault condition is not satisfied, the algorithm checks for Double Line Faults by verifying if any two phases have deviations greater than 0.95. Depending on which phases meet this criterion, the algorithm classifies the fault as involving those specific phases. Similar way, this algorithm also distinguishes between the double line or double line to ground fault. If none of the predefined conditions are met, the algorithm concludes that there is no fault or that the fault type does not match the specified criteria. This systematic approach ensures accurate fault identification and classification, aiding in the effective management and resolution of faults in the power system.

3. 3 Simulation

The simulation section provides a comprehensive overview of the detailed modeling and automation approach used for implementing the fault localization and classification algorithm. It includes the process of data acquisition in Excel format, which is utilized for system modeling. The section elaborates on the creation of subsystems and the logic modeling approach, detailing how each component of the system is designed and integrated. Furthermore, it explains the step-by-step implementation logic of the algorithm, highlighting how the fault classification criteria are applied to the acquired data. This section ensures a clear understanding of the methodology and the systematic approach adopted for accurate fault classification and classification within the power system.

3.3.1 Modeling of Distribution System

A distribution system modeling program has been developed in Python, which takes input data from Excel and performs the final system modeling in OpenDSS. The program acts as a bridge between the input data and the OpenDSS model. To create the system, the following data sets are required: line data, bus data, load data, and bus coordinates.

For modeling the distribution lines, the necessary information includes the connections between buses, the type of line (single-phase or three-phase), line length, resistance, reactance, the units of the line, and the emergency current (ampere) capacity. The data format required for modeling the distribution line is reported in Table 3.

Table 3: Line modeling data format

Line_Name	B1	B2	Length	Units	R(Ω)	X(Ω)	Current Capacity (A)	Phase

The load modeling plays a crucial role in the convergence of the load flow convergence. Six types of loads can be modeled into the distribution system. The description of the load type along with their application is described below:

i. Constant PQ Load Model: This model is known as the constant power load. This model is widely used in the load flow analysis. There is one problem associated with this load model, which is that the convergence may deviate if the voltage level is far away from the rated voltage. While modeling this load in OpenDSS, the model is set to 1.
ii. Constant Impedance Load Model: The active and reactive power consumption of the load is varied with the square of the voltage. This model guarantees the convergence of the load flow in any loading condition. The model is essentially linear. If the terminal voltage is greater than the rated value, the power consumption is increased. While modeling this load in OpenDSS, the model is set to 2.
iii. Constant P and Quadratic Q Load Model: The reactive power varies quadratically with voltage, while the active power remains constant. The load seems like a motor load. For modeling this load, the model is set to 3.
iv. Exponential Load Model: The voltage dependencies of P and Q are defined by exponential parameters. This model is typically used for conservation voltage studies (CVR). It is also used for general distribution feeder load mix models when the exact behavior of the load is not known. For modeling this load in OpenDSS, the model is set to the 4.
v. Constant Current Magnitude Load Model: The active power and reactive power varies linearly with the voltage magnitude while the load current remains

constant. This is common in the distribution system analysis program. For modeling this load in OpenDSS, the model is set to 5.

vi. ZIP Load Model: The active power and reactive power are described as a mixture of the constant power and constant current load that can be exempt from load shape multipliers. All the loads are reverted to the constant impedance load (Z type) in an attempt to guarantee convergence even if the voltage is very low. This load modeling is very important for performing annual simulations. For modeling this load in OpenDSS, the model is set to 6.

In this simulation work, the constant PQ load flow model is employed under the assumption that the load remains constant even during transient periods. This assumption simplifies the analysis by maintaining consistent real (P) and reactive (Q) power demands, regardless of fluctuations in voltage or frequency. By using the constant PQ model, the simulation achieves better convergence during load flow calculations, ensuring stable and reliable results.

The line load and bus information data modeling formats are reported in Table 4 and Table 5 respectively.

Table 4: Load modeling data format

Load_Name	Phases	B1	Voltage (kV)	Model	Active Power (kW)	Reactive Power (kVar)
Seller	3	6	11	1	40	30
Pranami_Mandir	3	8	11	1	80	60

Table 5: Bus information data

Bus_Name	Longitude	Latitude
1	85.469879	27.008212
2	85.470307	27.008198

The distribution system modeling program is attached in A.1 in Annex 2.

3.3.2 Creation of Subsystem

OpenDSS and Python are interfaced using the win32com mode, offering complete flexibility in controlling OpenDSS. A “while” loop iterates through all the modeled lines to identify the connected buses of the selected line. All its operational

characteristics, including length, resistance, and reactance, are stored in variables. The root node and terminal nodes are determined based on the concept that terminal buses are those connected to only one line. The code for extracting the terminal node is provided below.

```
leaf_nodes = sorted({int(bus) for bus, connections in bus_connections.items() if len(connections) == 1})
```

All the nodes are stored in the variable "leaf_nodes". Since the buses obtained from OpenDSS are in string format, they are converted into integers to enable sorting in ascending order. To remove the root node from the terminal nodes, node 1 is considered the substation node and is excluded from the list of terminal nodes.

```
leaf_nodes = [bus for bus in leaf_nodes if bus != int(root_node)]
leaf_nodes = [str(bus) for bus in leaf_nodes]
```

The breadth-first search (BFS) algorithm is employed to determine the shortest path between the substation node and the terminal node [17]. BFS is a method used to explore or search through tree or graph structures. It begins at the root node and examines all adjacent nodes at the current depth level before proceeding to nodes at the subsequent level. The algorithm initiates at the source node and utilizes a queue to manage the nodes to be visited, ensuring exploration occurs level by level. Initially, the starting node is added to the queue and marked as visited. The algorithm then enters a loop where it removes a node from the queue, visits all unvisited neighboring nodes, marks them as visited, and places them into the queue. This process continues until the queue is empty or a predefined condition, such as reaching the target nodes, is met. The entire process for subsystem creation is depicted in the flowchart (Figure 8). The corresponding Python code can be found in Annex 2, Section A.2.

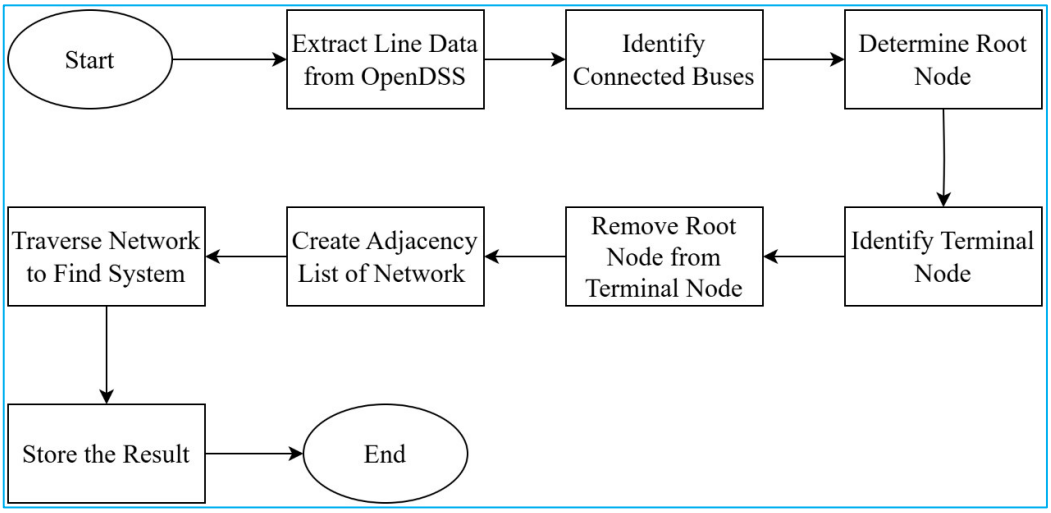

Figure 8: Flowchart showing methodology of subsystem creation using OpenDSS and Python

3.3.3 Formation of subsystem Zbus

The admittance matrix for each subsystem is extracted from OpenDSS and stored in the variable matrix. By inverting this admittance matrix, the corresponding impedance matrix is obtained. This impedance matrix is then used in the Python code for calculating voltage sags within the system.

3.3.4 Fault Localization and Classification Implementation

The fault localization and classification algorithms are implemented in Python, incorporating all the equations outlined in the previous sections. The simulation process involves calculating the voltage sag by comparing pre-fault and during-fault voltages, determining the impedance matrix for the subsystems, and calculating the fault current. The fault classification logic is applied, followed by the identification of the fault location at the bus and line levels. Finally, the results are visualized on a GIS diagram for better representation. The overall code for this process is reported in A.3 in Annex 2.

3.3.5 Fault Location Visualization

The fault location visualization is the locating of the fault location in the geographical system information (GIS) diagram. For the visualization process, the folium package is used in the python [18]. The Folium package in Python is a powerful tool used for

creating interactive maps [19]. It provides an easy interface for generating maps using Leaflet.js, a popular JavaScript library for interactive maps. Folium allows you to overlay data such as markers, polygons, and choropleths on maps, making it a great choice for visualizing geospatial data in Python.

The fault point obtained from running the fault localization algorithm is represented in terms of the locations of virtual buses. From these virtual buses, the GIS coordinates are determined. If the fault occurs at a bus, the GIS coordinates of that bus are used, as they are included in the system modeling. However, since the fault could occur anywhere along the line, the virtual buses are used to determine which of the two buses the fault is closer to. Once identified, the distance between the buses is calculated using the formula explained below.

If two buses namely Bus1 and Bus2, having following coordinates:

- Latitude: lat1 for Bus1 and lat2 for Bus2
- Longitude: long1 for Bus1 and long2 for Bus2

The interpolation for the latitude of N intermediate buses between Bus1 and Bus2 is given by equation 21.

$$lat_i = lat_1 + \left(\frac{i}{N+1}\right) * (lat_2 - lat_1) \qquad 21$$

For i = 1,2,3, ……. N

Where:

- $lat_i \; is \; the \; lattitude \; of \; i^{th} \; intermediate \; bus$
- N is the number of intermediate buses

The interpolation for the longitude of N intermediate buses between Bus1 and Bus2 is given by equation 22.

$$long_i = long_1 + \left(\frac{i}{N+1}\right) * (long_2 - long_1) \qquad 22$$

For i = 1,2,3, ……. N

Where:

- $long_i$ *is the longitude of* i^{th} *intermediate bus*
- N is the number of intermediate buses

The equations (21) and (22) are used for finding the GIS coordinate of intermediate buses which have no GIS coordinate during system modeling.

3.4 Test System

The proposed methodology is validated through simulations in three distribution systems. It is first applied to the IEEE 33-bus distribution feeder, a standard radial distribution system. Figure 9 illustrates the single-line diagram of the IEEE 33-bus distribution feeder, which includes a substation at node 1. The active and reactive power demands of the feeder are 3.715 MW and 2.3 MVAr, respectively. Detailed branch and load data can be found in Table 37 and Table 38 of A.1 in Annex 1.

The second test system is a practical Nepalese distribution feeder, the Solati distribution feeder, originating from the Brahathawa substation of the 33/11 kV feeder. This feeder is located in the Sarlahi district of Province 2, Nepal. Figure 10 illustrates the GIS diagram of the Solati distribution feeder, which consists of 36 nodes. The total length of the distribution feeder is 25.58 km, with the longest branch extending 17 km from the substation to the terminal node. Detailed GIS coordinates of the nodes, branch data, and load data are provided in Table 39, Table 40, and Table 41 of A.2 in Annex 2.

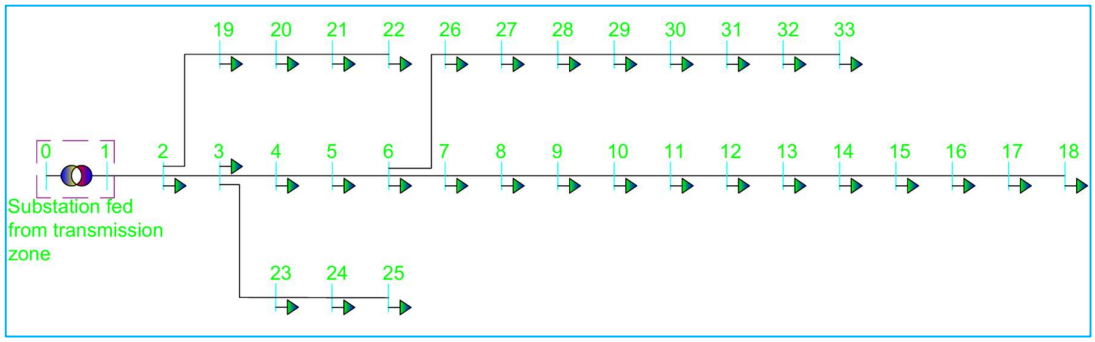

Figure 9: IEEE33 bus test feeder

The third test distribution feeder is the practical Nepalese distribution feeder, the Chapagaun distribution feeder, originated from Patan grid substation of the 66/11 kV feeder. Figure 11 illustrates the GIS diagram of Chapagaun distribution feeder, which consists of 156 nodes. The total length of the distribution feeder is 70 km, with the

longest branch extending 37.43 km from the substation to the terminal node. Detailed GIS coordinates of the nodes, branch data, and load data are provided in Table 42, Table 43, and Table 44 of A.3 in Annex 2.

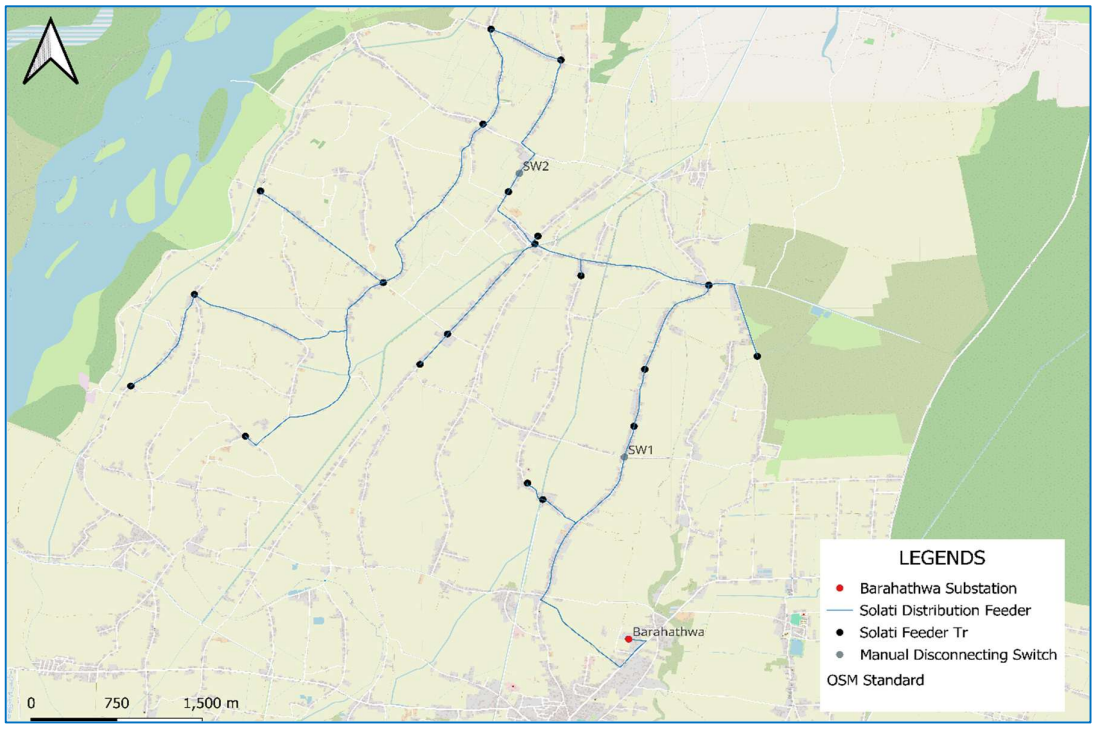

Figure 10: Solati distribution feeder

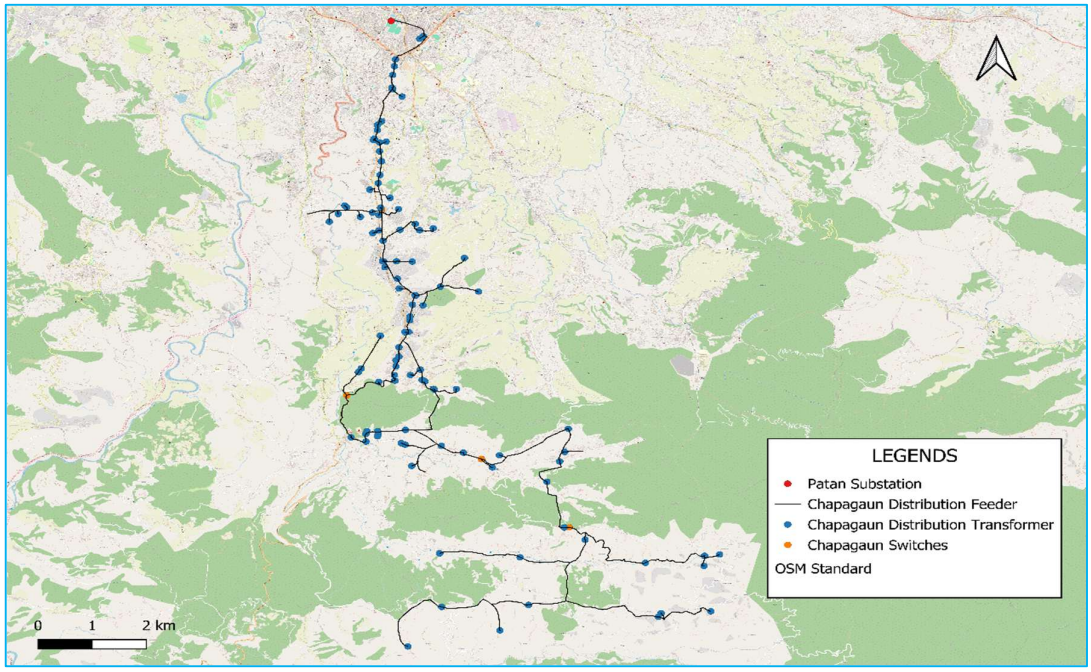

Figure 11: Chapagaun distribution feeder

3.5 Software and Tools

For the modeling of the distribution network, OpenDSS software is used. OpenDSS is an electric distribution system simulator (DSS) developed to facilitate the integration of distributed energy resources (DERs) and support grid modernization. It provides engineers with a versatile, customizable, and user-friendly platform for performing complex analyses, addressing both current needs and future challenges in distribution systems. OpenDSS serves as a foundation for understanding and integrating emerging technologies. It is also being increasingly utilized for distribution automation in modern grids.

The OpenDSS has the following solution capabilities:

a) Unbalanced multiphase power flow
b) Quasi-static time series analysis
c) Fault analysis
d) Harmonic analysis
e) Linear and Non-linear analysis
f) Stray voltage/current analysis
g) Flicker analysis
h) Dynamic analysis

Pycharm is a powerful integrated development specially designed for Python development. It is packed with features that can help in writing better code and faster execution time. Some of the key features of Pycharm include Intelligent code completion, code inspections, on-the-fly error highlighting, quick fixes, and web development. This software is broadly available in two editions. Community edition and professional edition. The community edition is free and open-source software, while the professional edition is paid software. The professional edition has more features than the community edition such as a graphical debugger, a built-in tester, and support for remote development.

The impact full use of Pycharm in the field of electrical engineering is as follows:

a) Power system modeling and simulation: It provides a flexible interface with different power system modeling libraries for performing steady-state analysis as well as transient analysis. These libraries may be PyPSA, OpenDSS, etc.
b) Communication protocol for IoT in smart grid: It provides a flexible library based on protocol IEC 61850, IEC 60870, HTTP, MQTT, and Modbus for communicating with intelligent electronic devices. These devices may be smart meters, sectionalizing switches, or some other type of sensors that can transmit data to locally installed servers.
c) Data visualization: It provides various libraries such as matplotlib for plotting an interactive graph of different data, and Folium for plotting systems in the Geographical Information system.

3.6 Report Writing

The project report is prepared using Microsoft Word 2021. Flowcharts are created using draw.io, an open online software. For the creation of a single-line diagram, AutoCAD Electrical is utilized. Excel is used for chart creation, analysis, and data management.

CHAPTER FOUR: RESULT AND DISCUSSION

4.1 IEEE 33 Bus Simulated Result

The IEEE 33-bus system is modeled using OpenDSS and Python, with a dynamic program developed for fault localization and classification within the Python environment. A total of 640 simulations are conducted for each fault scenario. Since all lines in the standard system have equal lengths, the developed algorithm is tested by simulating 20 faults per line section. This results in 640 simulations for each fault type—LLLG, LL, or LG. The accuracy of fault distance estimation is analyzed by determining how often the predicted location matches the exact fault distance or falls within various error intervals. The simulations are performed on an HP Envy x360 PC with 16 GB of RAM.

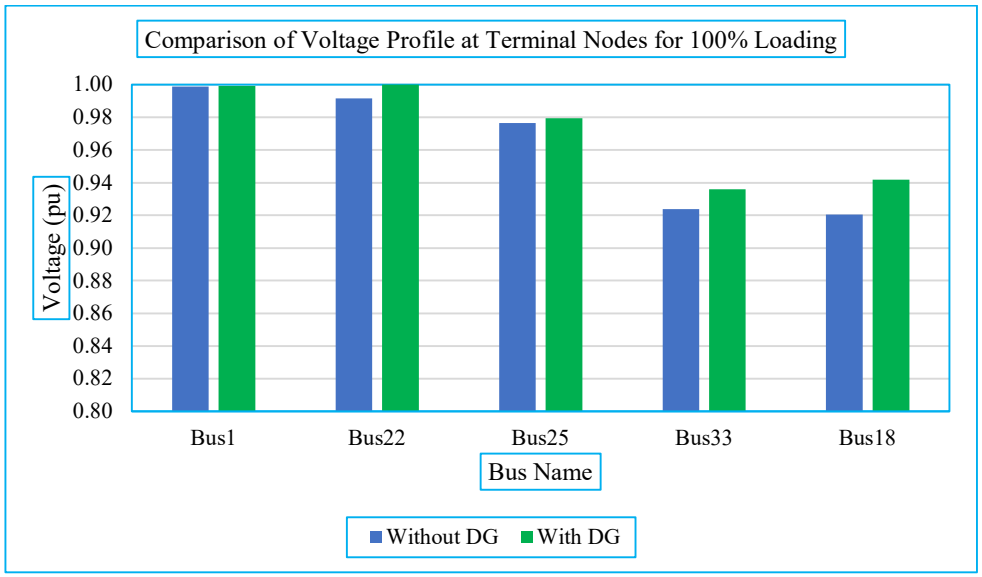

Figure 12: Comparison of voltage profile at terminal nodes with 100 % loading in IEEE33 bus system

Figure 12 illustrates a comparative analysis of voltage profiles in the IEEE 33-bus test system with and without distributed generation (DG). Table 9 provides the specifications for the installed DG units. The voltage profile shows 1.00 p.u. at the substation (Bus1) and 0.92 p.u. at the farthest node (Bus18) in the absence of DG. As the system maintains balanced three-phase conditions, the results are presented as per-phase voltage values. Bus18 is located 18 km from the substation.

With DG integration, the voltage profile shows marginal improvement at terminal nodes, with a maximum increase of 0.02 p.u. Since DG integration yields only marginal voltage improvements (maximum 0.02 p.u.), the voltage sag characteristics presented in following sections exclude DG participation.

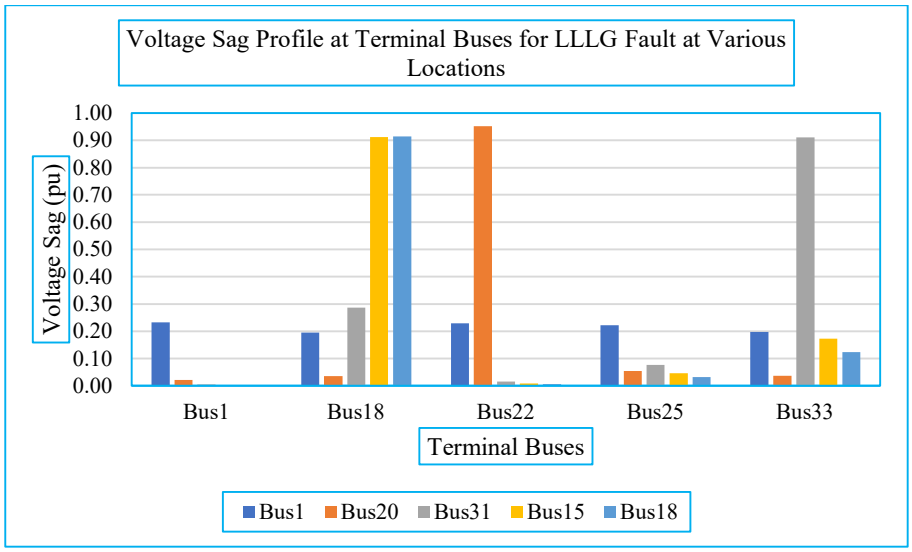

Figure 13: Voltage sag profile at terminal buses for LLLG fault at various locations in IEEE33 bus system

Figure 13 illustrates the voltage sag profile at terminal buses for an LLLG fault at different locations with a fault resistance of 0.1 Ω. When the fault occurs at the substation buses, the voltage sag measures 0.23 pu at the substation and 0.20 pu at the farthest terminal bus (Bus18). This significant voltage sag occurs because the fault current flowing to ground at the substation node is much larger than the load current. Conversely, when the fault occurs at the farthest terminal node (Bus18), the substation experiences only a 0.01 pu voltage sag due to the high line impedance between the substation and fault location. Meanwhile, the faulted terminal node (Bus18) shows the highest sag of 0.91 pu. The profile clearly demonstrates that voltage sags are more severe at nodes closer to the fault location.

Figure 14 illustrates the voltage sag profile at terminal buses for an LG fault at different locations with a fault resistance of 0.1 Ω. When the fault occurs at the substation buses, the voltage sag measures 0.23 pu at the substation and 0.22 pu at the farthest terminal bus (Bus18). This significant voltage sag occurs because the fault current flowing to ground at the substation node is much larger than the load current. Conversely, when

the fault occurs at the farthest terminal node (Bus18), the substation experiences only a 0.03 pu voltage sag due to the high line impedance between the substation and fault location. Meanwhile, the faulted terminal node (Bus18) shows the highest sag of 0.91 pu. The profile clearly demonstrates that voltage sags are more severe at nodes closer to the fault location. The voltage sag characteristics of the faulted phase in LG faults exhibit a similar distribution pattern to those seen in terminal buses during LLLG faults.

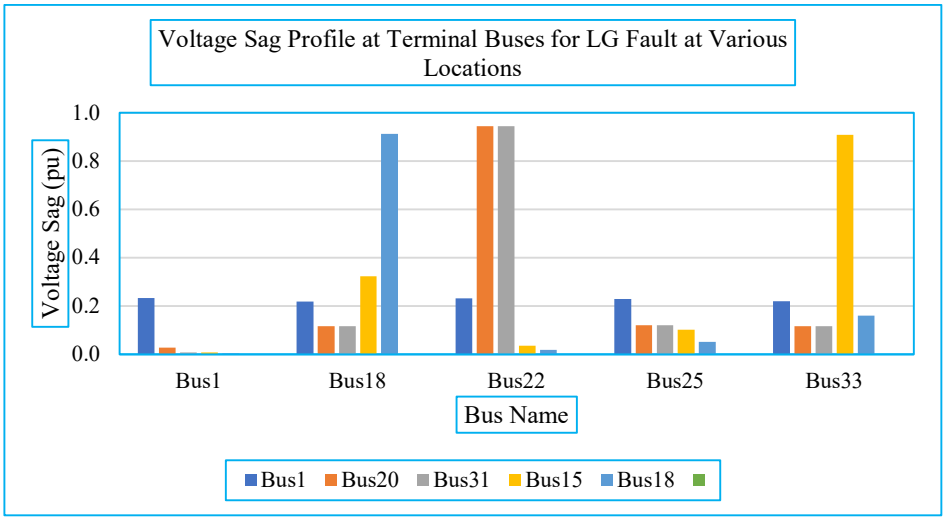

Figure 14: Voltage sag profile at terminal buses for LG fault at various locations in IEEE33 Bus

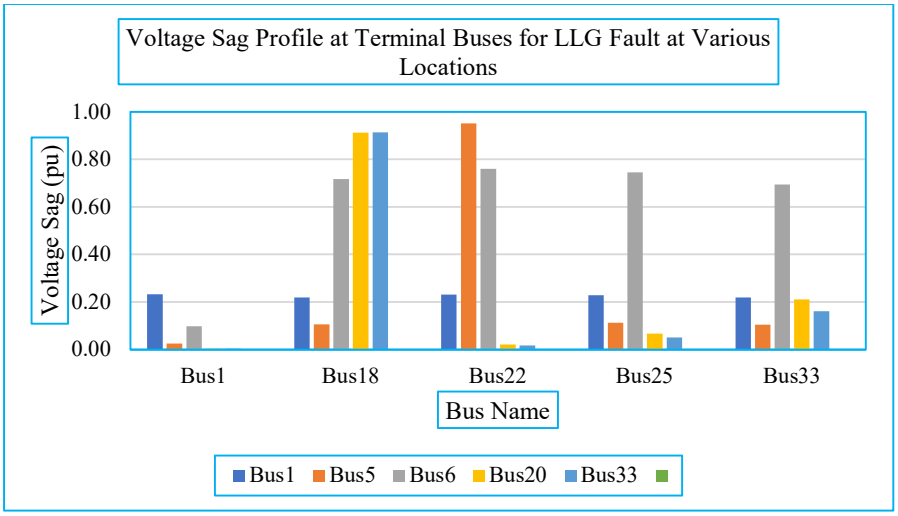

Figure 15: Voltage sag profile at terminal buses for LG fault at various locations in IEEE33 Bus

Figure 15 illustrates the voltage sag profile at terminal buses for an LLG fault at different locations with a fault resistance of 0.1 Ω. When the fault occurs at the

substation buses, the voltage sag measures 0.23 pu at the substation and 0.22 pu at the farthest terminal bus (Bus18). This significant voltage sag occurs because the fault current flowing to ground at the substation node is much larger than the load current. Conversely, when the fault occurs at the farthest terminal node (Bus18), the substation experiences only a 0.00 pu voltage sag due to the high line impedance between the substation and fault location. Meanwhile, the faulted terminal node (Bus18) shows the highest sag of 0.91 pu. The profile clearly demonstrates that voltage sags are more severe at nodes closer to the fault location. The voltage sag characteristics of the faulted phase in LLG faults exhibit a similar distribution pattern to those seen in terminal buses during LLLG and LG faults.

4.1.1 IEEE 33 Bus Fault Localization

Table 6 reports the fault localization results for different fault types under varying fault resistances, ranging from 0.1Ω to 100Ω. The results indicate that in some cases, the identified fault location matches the actual location exactly, while in others, there is a deviation. Additionally, it is observed that the accuracy of fault localization is not dependent on the fault type.

Table 6: Fault localization result at varying fault resistance and fault type in IEEE33 bus system

S. N.	Simulated Distance (km)	Calculated Fault Distance (km)											
		LLLG Fault			LL Fault			LLG Fault			LG Fault		
		R=0.1Ω	R=50Ω	R=100Ω	R=0.1Ω	R=50Ω	R=100Ω	R=0.1Ω	R=50Ω	R=100Ω	R=0.1Ω	R=50Ω	R=100Ω
1.00	15.75	15.75	15.95	15.95	15.75	15.95	15.95	15.75	15.95	15.95	15.75	15.95	15.95
2.00	16.95	16.95	16.95	16.95	16.95	16.95	16.95	16.95	16.95	16.95	16.95	16.95	16.95
3.00	8.8	8.85	8.85	8.85	8.85	8.85	8.85	8.85	8.85	8.85	8.85	8.85	8.85
4.00	8.8	8.85	8.85	8.85	8.85	8.85	8.85	8.85	8.85	8.85	8.85	8.85	8.85
5.00	8.9	8.95	8.95	8.95	8.95	8.95	8.95	8.95	8.95	8.95	8.95	8.95	8.95
6.00	10.05	10.1	10.1	10.1	10.1	10.1	10.1	10.1	10.1	10.1	10.1	10.1	10.1
7.00	10.15	10.2	10.2	10.2	10.2	10.2	10.2	10.2	10.2	10.2	10.2	10.2	10.2
8.00	12.3	12.45	12.45	12.45	12.45	12.45	12.45	12.45	12.45	12.45	12.45	12.45	12.45

9.00	12.35	12.5	12.5	12.5	12.5	12.5	12.5	12.5	12.5	12.5	12.5	12.5	12.5
10.00	12.4	12.55	12.55	12.55	12.55	12.55	12.55	12.55	12.55	12.55	12.55	12.55	12.55
11.00	12.45	12.6	12.6	12.6	12.6	12.6	12.6	12.6	12.6	12.6	12.6	12.6	12.6
12.00	12.5	12.65	12.65	12.65	12.65	12.65	12.65	12.65	12.65	12.65	12.65	12.65	12.65
13.00	12.55	12.7	12.7	12.7	12.7	12.7	12.7	12.7	12.7	12.7	12.7	12.7	12.7

4.1.2 Fault Localization Error Analysis

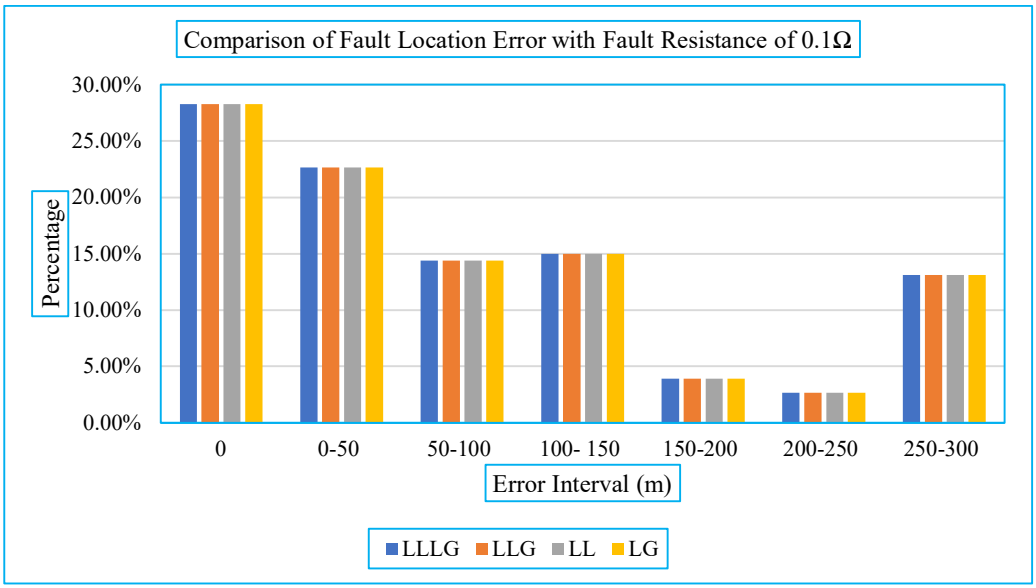

Figure 16: Comparison of fault location error with fault resistance of 0.1 ohm in IEEE 33 bus system

Figure 16 illustrates the fault location error for 640 simulated fault cases of a single fault type with a fault resistance of 0.1Ω. The results show that in 28.28% of cases, the exact fault location is identified. Additionally, the error intervals are distributed as follows: 22.66% of cases fall within 0–50 meters, 14.38% within 50–100 meters, 15.00% within 100–150 meters, 3.91% within 150–200 meters, 2.66% within 200–250 meters, and 13.13% within 250–300 meters. The maximum observed error in fault localization is 300 meters, while the method is also capable of pinpointing the exact fault location in several instances. The error arises due to slight variations in voltage

drop between adjacent nodes, particularly in sections with shorter branch lengths. The localization error is independent of fault type.

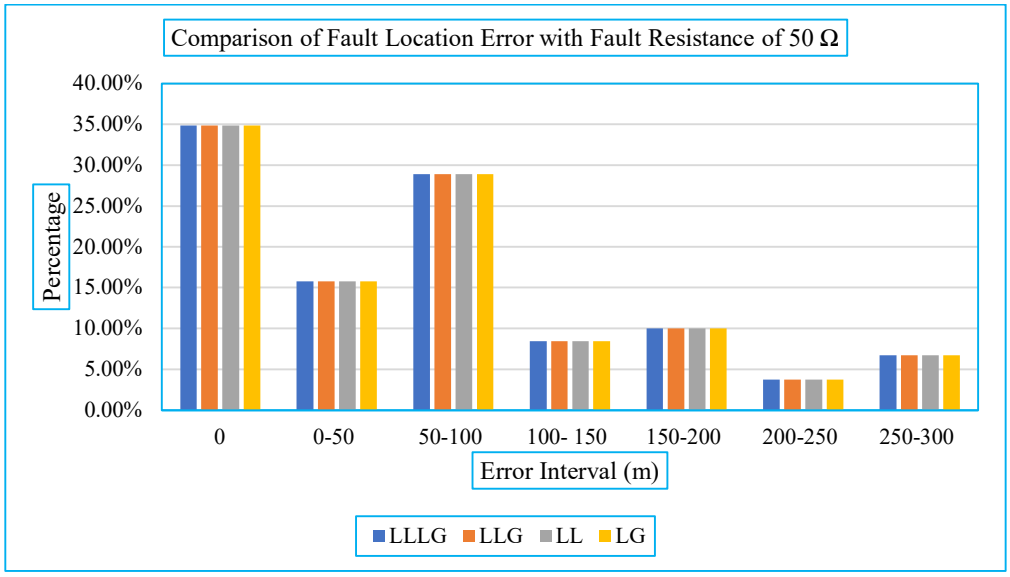

Figure 17: Comparison of fault location error with fault resistance of 50 ohm in IEEE 33 bus system

Figure 17 illustrates the fault location error for 640 simulated fault cases of a single fault type with a fault resistance of 50Ω. The results show that in 34.84% of cases, the exact fault location is identified. Additionally, the error intervals are distributed as follows: 15.78% of cases fall within 0–50 meters, 28.91% within 50–100 meters, 8.44% within 100–150 meters, 10.00% within 150–200 meters, 3.75% within 200–250 meters, and 6.72% within 250–300 meters. The maximum observed error in fault localization is 300 meters, while the method is also capable of pinpointing the exact fault location in several instances. The error arises due to slight variations in voltage drop between adjacent nodes, particularly in sections with shorter branch lengths. The localization error is independent of fault type.

Figure 18 illustrates the fault location error for 640 simulated fault cases of a single fault type with a fault resistance of 100Ω. The results show that in 34.84% of cases, the exact fault location is identified. Additionally, the error intervals are distributed as follows: 28.13% of cases fall within 0–50 meters, 15.63% within 50–100 meters, 8.44% within 100–150 meters, 3.75% within 150–200 meters, 4.84% within 200–250 meters, and 4.84% within 250–300 meters. The maximum observed error in fault localization is 300 meters, while the method is also capable of pinpointing the exact fault location

in several instances. The error arises due to slight variations in voltage drop between adjacent nodes, particularly in sections with shorter branch lengths. The localization error is independent of fault type.

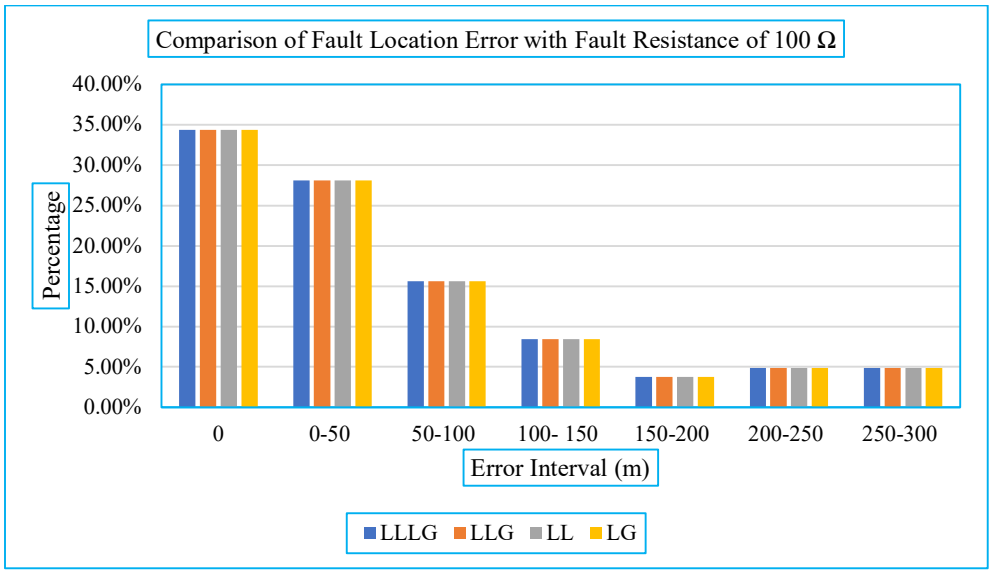

Figure 18: Comparison of fault location error with fault resistance of 100 ohm in IEEE 33 bus system

4.1.3 Impact of Load Variation on Fault Localization Accuracy

Table 7: Effect of load variation on fault localization accuracy for LG fault in IEEE 33 bus system

Error (m)	R=0.1Ω		R=50Ω		R=100Ω	
	70% Loading	100% Loading	70% Loading	100% Loading	70% Loading	100% Loading
0	34.53%	28.28%	35.00%	34.84%	35.16%	34.84%
0-50	19.53%	22.66%	18.75%	15.78%	18.91%	15.78%
50-100	15.31%	14.38%	15.31%	28.91%	15.31%	28.91%
100-150	10.00%	15.00%	9.69%	8.44%	9.84%	8.44%
150-200	9.53%	3.91%	7.19%	10.00%	7.19%	10.00%
200-250	7.34%	2.66%	6.41%	3.75%	6.41%	3.75%
250-300	3.75%	13.13%	7.66%	6.72%	7.19%	6.72%

The effect of load variation is also analyzed by considering 100% loading as the base load and reducing it by 30% to assess its impact. Additionally, three fault resistance

values—R = 0.1Ω, R = 50Ω, and R = 100Ω—are taken into account. Despite the load variation, the maximum error in fault localization remains 300 meters. The results indicate that load variation has no significant impact on localization accuracy. Since line-to-ground (LG) faults are the most common fault type in distribution systems, the simulations primarily focus on this fault scenario. The result is reported in Table 7.

4.1.4 Impact of Line Impedance Measurement on Fault Localization Error

Some sections of the impedance are considered as modeling errors, which may arise due to factors such as improper conductor joints, temperature variations, and measurement errors in GIS data. The changes in impedance for certain sections during the simulation are reported in Table 8.

Table 8: Variation of impedance of sections in IEEE 33 bus system

Section	Impedance Change Percentage
Line 1-2	5%
Line 7-8	-5%
Line 10-11	5%
Line 11-12	-5%
Line 17-18	5%
Line 20-21	5%
Line 24-25	-5%
Line 27-28	5%
Line 30-31	-5%

Figure 19 illustrates the fault location error for 640 simulated fault cases of a single fault type with a fault resistance of 100Ω and variation in the line impedance. The results show that in 34.84% of cases, the exact fault location is identified. Additionally, the error intervals are distributed as follows: 28.13% of cases fall within 0–50 meters, 15.63% within 50–100 meters, 8.44% within 100–150 meters, 3.75% within 150–200 meters, 4.84% within 200–250 meters, and 4.84% within 250–300 meters. The maximum observed error in fault localization is 300 meters, while the method is also capable of pinpointing the exact fault location in several instances. The error arises due to slight variations in voltage drop between adjacent nodes, particularly in sections with shorter branch lengths. The localization error is independent of line impedance variation of ±5%.

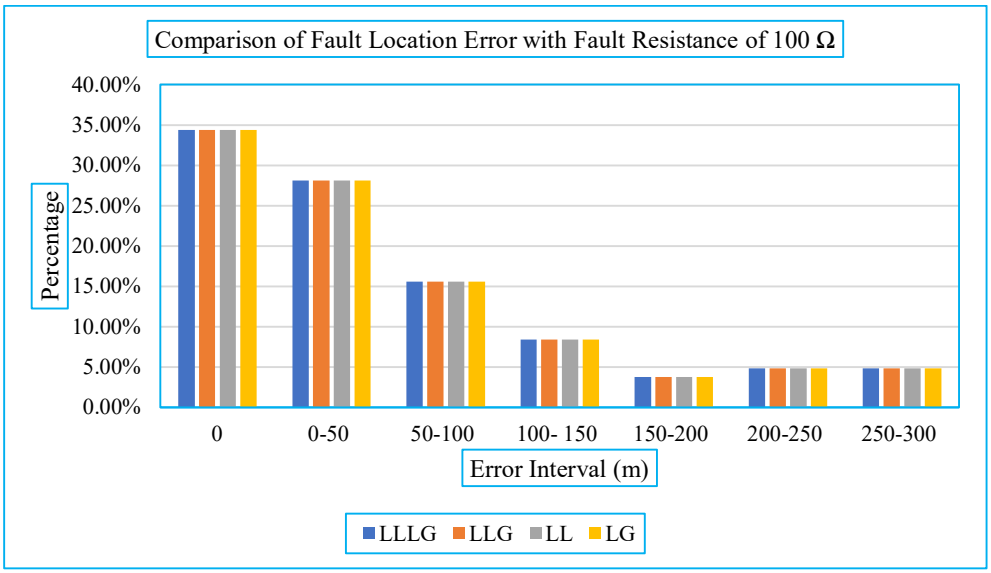

Figure 19:Comparison of fault location error with variation of line impedance in IEEE 33 bus system

4.1.5 Impact of DG Penetration on Fault Localization Accuracy

With the increasing trend of DG penetration in distribution systems, the performance of the algorithm is also evaluated under DG integration. Two types of DGs are considered: three photovoltaic (PV) units and three synchronous generators. The location and size of these DGs are randomly assigned. The details of the DG configurations are reported in the Table 9.

Table 9: Detail of simulated distributed generation for performance evaluation in IEEE 33 bus system

S.N.	Bus Number	Type of DG	Rating (kVA)	Power Factor	Voltage Rating (kV)
1	5	Photovoltaic	250	1	12.66
2	12	Photovoltaic	550	1	12.66
3	18	Photovoltaic	100	1	12.66
4	19	Synchronous	300	0.8	12.66
5	20	Synchronous	500	0.8	12.66
6	32	Synchronous	100	0.8	12.66

The impact of DG penetration on the system is reported in Table 10. It is observed that integrating DG increases the fault localization error. Before DG penetration, the maximum error in fault location was 300 meters, whereas after DG integration, it

increased to 600 meters—an additional 300 meters. This increase in error is attributed to the alteration of voltage sag characteristics caused by DG integration.

Table 10: Impact of the DG penetration in fault localization accuracy in IEEE 33 bus system

Error Interval (m)	Number of Times			Percentage		
	R=0.1Ω	R=50Ω	R=100Ω	R=0.1Ω	R=50Ω	R=100Ω
0	125	125	126	19.53%	19.53%	19.69%
0-50	193	135	134	30.16%	21.09%	20.94%
50-100	85	38	39	13.28%	5.94%	6.09%
100- 150	22	67	70	3.44%	10.47%	10.94%
150-200	24	95	93	3.75%	14.84%	14.53%
200-250	21	45	43	3.28%	7.03%	6.72%
250-300	31	4	4	4.84%	0.63%	0.63%
300-350	30	6	7	4.69%	0.94%	1.09%
350-400	26	21	22	4.06%	3.28%	3.44%
400-450	19	12	10	2.97%	1.88%	1.56%
450-500	18	24	31	2.81%	3.75%	4.84%
500-550	31	26	20	4.84%	4.06%	3.13%
550-600	15	42	41	2.34%	6.56%	6.41%

4.1.6 Fault Classification in IEEE 33 Bus

Table 11: Fault classification result in IEEE 33 bus system

Subjected Fault Types	Simulated Number	Accurately Detected Number	Presence of DG
LLLG	640	640	No
LLG (Phase A & B)	640	640	No
LLG (Phase B & C)	640	640	No
LLG (Phase C & A)	640	640	No
LL (Phase A & B)	640	640	No
LL (Phase B & C)	640	640	No
LL (Phase C & A)	640	640	No
LG (Phase A)	640	640	No
LG (Phase B)	640	640	No
LG (Phase C)	640	640	No
LLLG	640	640	Yes
LLG (Phase A & B)	640	640	Yes
LLG (Phase B & C)	640	640	Yes
LLG (Phase C & A)	640	640	Yes
LL (Phase A & B)	640	640	Yes
LL (Phase B & C)	640	640	Yes
LL (Phase C & A)	640	640	Yes

LG (Phase A)	640	640	Yes
LG (Phase B)	640	640	Yes
LG (Phase C)	640	640	Yes

The developed fault classification approach is also tested in the IEEE 33 bus system, and the results are reported in Table 11 . The method is evaluated both with and without DG integration. The findings indicate that the proposed methodology accurately classifies faults in the IEEE 33-bus feeder. Additionally, the approach effectively identifies the specific phase(s) involved in the fault.

4.1.7 Fault Localization Result Comparison with Paper [16]

For the result comparison with paper [16], the simulations run at two positions along the line: 33% and 67% of the line length from the starting side. Since the base paper also conducts simulations at the same locations, this work follows the same approach for consistency.

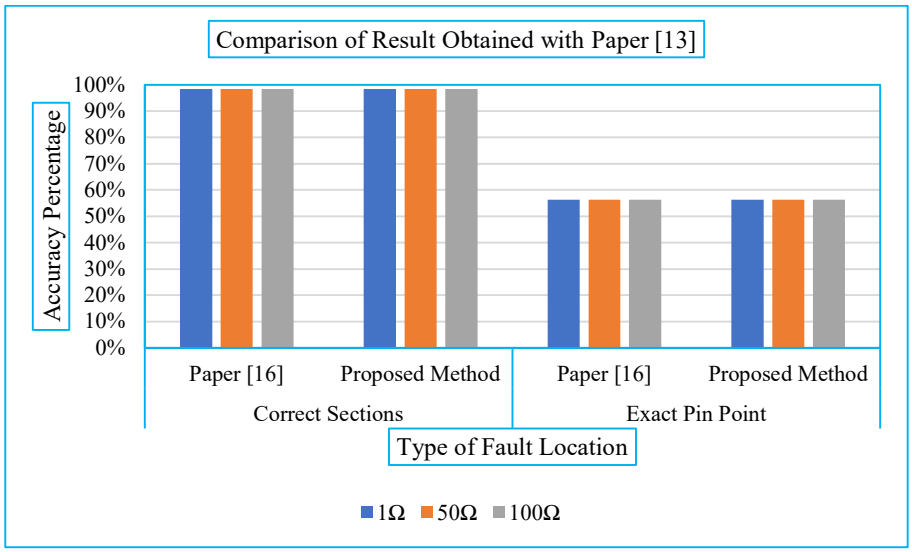

Figure 20: Comparison of result with paper [16] under varying fault resistance in IEEE33 bus system

Figure 20 compares the results with the base paper in two key aspects: identifying the fault section and precisely locating the fault position. If the fault location finds within ≤44% of the bus length from the starting side, it lies in the first half of the sections. Conversely, if the fault location is ≥56%, it falls in the second half.

The comparison bar chart shows that the correct section identification accuracy is 98.44% in both cases, while the exact fault location detection rate is 56.25%. Additionally, the impact of fault resistance variation (tested at 1Ω, 50Ω, and 100Ω) is evaluated. The simulations use an LG fault type, and the results confirm that the fault localization error remains independent of fault resistance.

Figure 21 illustrates a comparative analysis with the base paper, evaluating performance under varying line impedance conditions as detailed in Table 18, along with different fault types. The results demonstrate a 96.88% accuracy rate for correct section identification in both the base paper and this simulation. For exact fault localization, the system achieves 37.50% accuracy for LG faults and 25.00% for LLL faults. These simulation outcomes show excellent agreement with the base paper's findings, confirming consistent performance across varying line impedances and fault conditions. The study validates that the proposed method maintains reliability regardless of these operational variations.

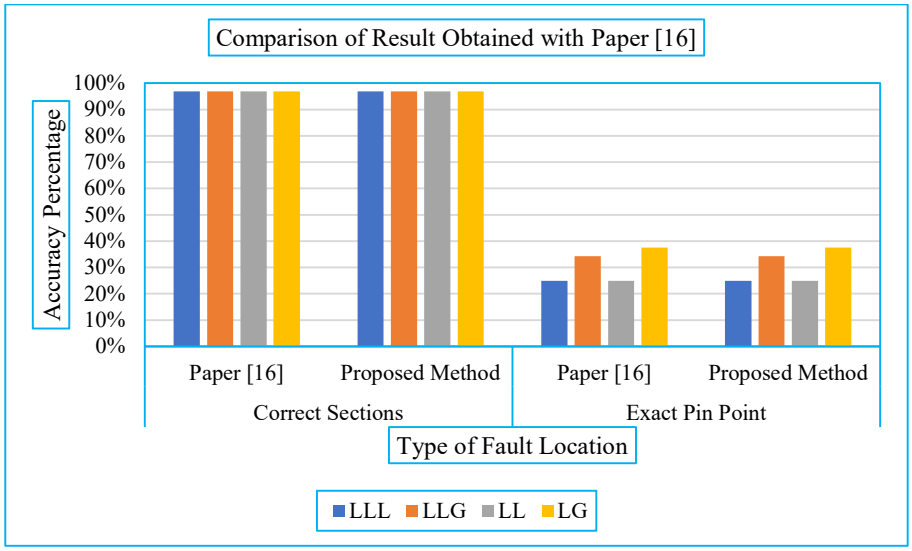

Figure 21: Comparison of result with paper [16] under varying line impedance in IEEE33 bus system

Figure 22 illustrates the comparative performance analysis under varying DG penetration levels. The results demonstrate that the proposed method maintains high accuracy even with significant DG integration. For the most common LG fault scenario, the system achieves 98.44% accuracy in correct section identification and 34.38% precision in exact fault localization. In more challenging cases, the method maintains

90.63% accuracy for LL fault section identification, while the most demanding LLG fault scenario shows 17.19% precision in exact location detection. These findings confirm the method's robustness across different DG penetration conditions and fault types.

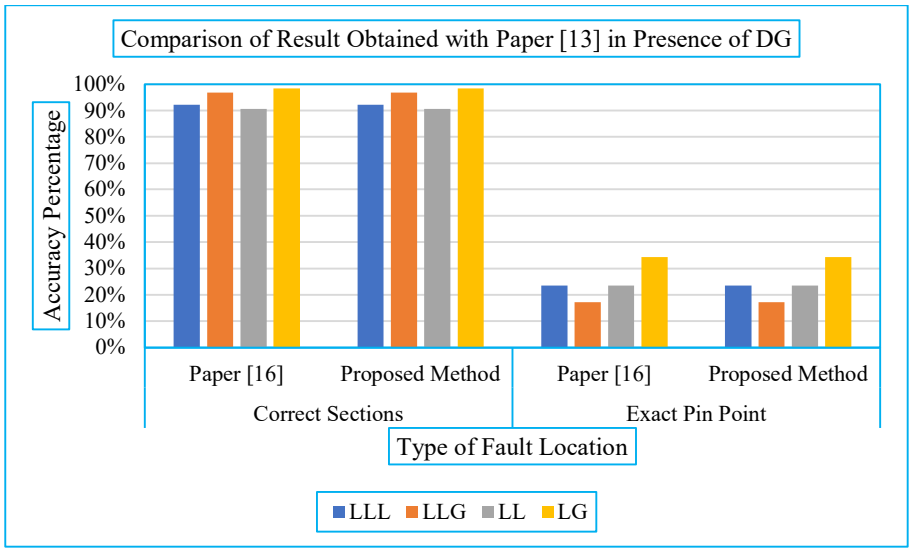

Figure 22: Comparison of result with paper [16] under presence of DG in IEEE33 bus system

4.2 Solati Distribution Feeder Simulated Result

The Solati distribution feeder is modeled using OpenDSS and Python, with a dynamic program developed for fault localization and classification within the Python environment. A total of 200 simulations are conducted for each fault scenario. Fault is created at random length in the line. This results in 200 simulations for each fault type—LLLG, LLG, LL, or LG.

Figure 23 illustrates the voltage profile of terminal nodes equipped with IEDs under 100% loading conditions, comparing scenarios with and without distributed generation (DG) integration. In the base case (without DG), Bus1 (substation node) maintains 1 pu voltage, while the farthest node (Bus36, 16.41 km away) records 0.92 pu, demonstrating characteristic voltage drop with increasing distance from the substation. The balanced system allows representation using R-phase voltage (pu) for all three phases. When photovoltaic DG units (randomly located with capacities specified in Table 16) are integrated at 700 kW total penetration (70% nominal irradiance), the voltage profile shows marginal improvement across the feeder compared to the base case. Because of

marginal improvement in voltage profile, further voltage sag analysis presents in this report is without presence of DG.

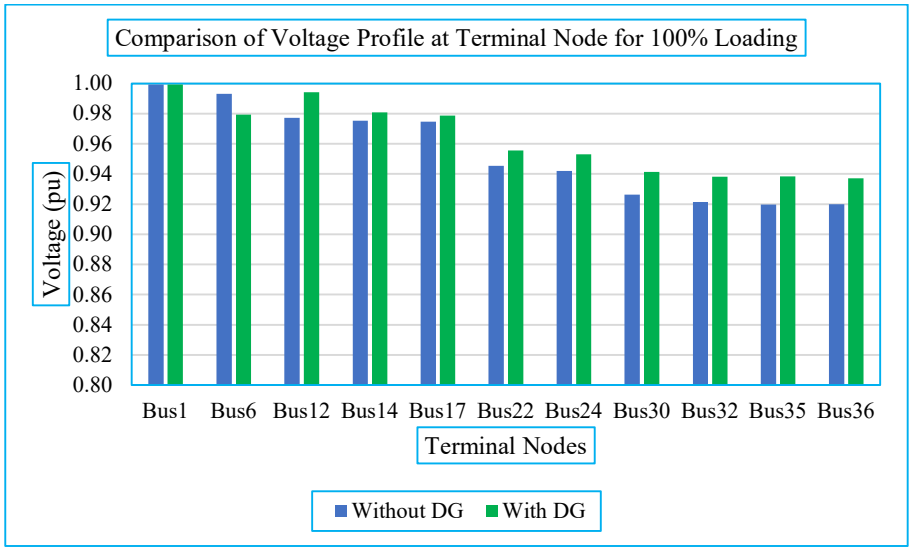

Figure 23: Comparison of voltage profile at terminal nodes with 100% loading in Solati feeder

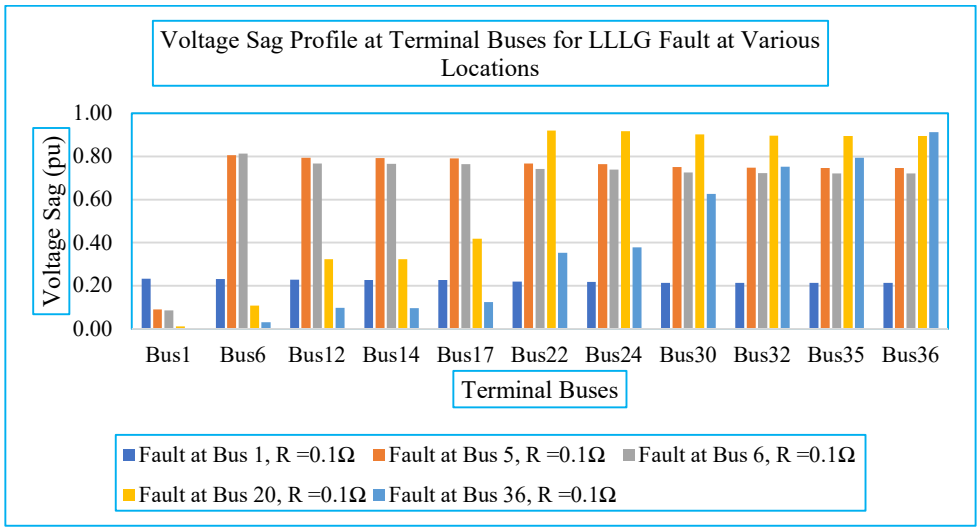

Figure 24: Voltage sag profile at terminal buses for LLLG fault at various locations in Solati feeder

Figure 24 illustrates the voltage sag profile at terminal buses for an LLLG fault at different locations with a fault resistance of 0.1 Ω. When the fault occurs at the substation buses, the voltage sag measures 0.23 pu at the substation and 0.22 pu at the farthest terminal bus (Bus36). This significant voltage sag occurs because the fault current flowing to ground at the substation node is much larger than the load current.

Conversely, when the fault occurs at the farthest terminal node (Bus36), the substation experiences only a 0.03 pu voltage sag due to the high line impedance between the substation and fault location. Meanwhile, the faulted terminal node (Bus36) shows the highest sag of 0.92 pu. The profile clearly demonstrates that voltage sags are more severe at nodes closer to the fault location.

Figure 25 illustrates the voltage sag profile at terminal buses for an LG fault at different locations with a fault resistance of 0.1 Ω. When the fault occurs at the substation buses, the voltage sag measures 0.23 pu at the substation and 0.22 pu at the farthest terminal bus (Bus36). This significant voltage sag occurs because the fault current flowing to ground at the substation node is much larger than the load current. Conversely, when the fault occurs at the farthest terminal node (Bus36), the substation experiences only a 0.03 pu voltage sag due to the high line impedance between the substation and fault location. Meanwhile, the faulted terminal node (Bus36) shows the highest sag of 0.92 pu. The profile clearly demonstrates that voltage sags are more severe at nodes closer to the fault location. The voltage sag characteristics of the faulted phase in LG faults exhibit a similar distribution pattern to those seen in terminal buses during LLLG faults.

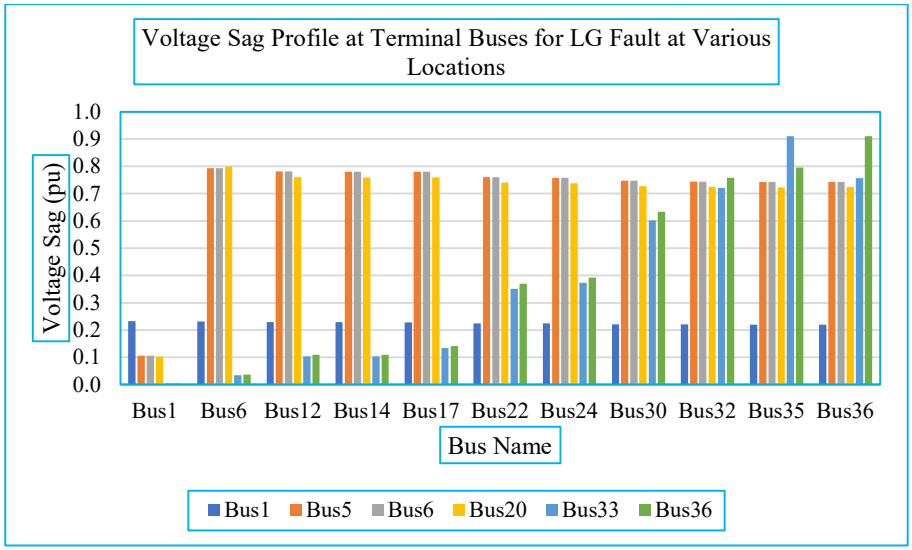

Figure 25: Voltage sag profile at terminal buses for LG fault at various locations in Solati feeder

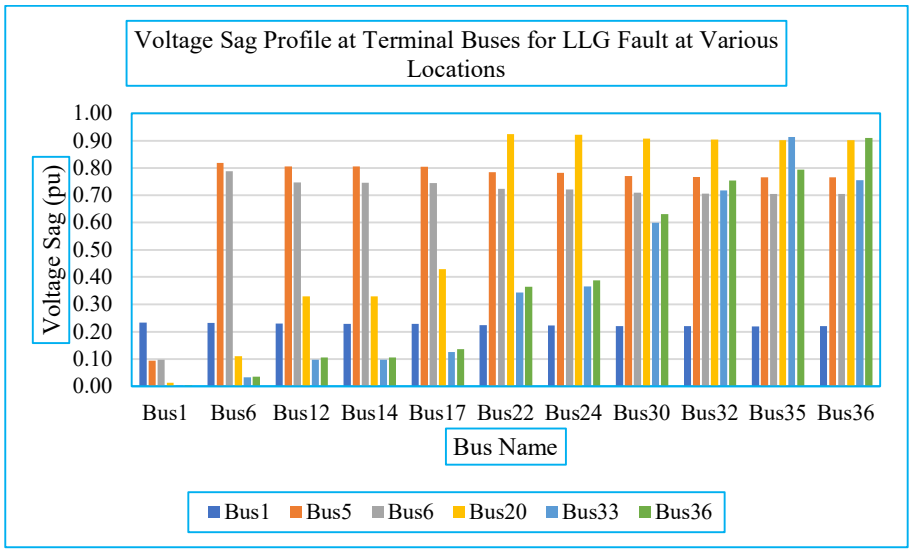

Figure 26: Voltage sag profile at terminal buses for LLG fault at various locations in Solati feeder

Figure 26 illustrates the voltage sag profile at terminal buses for an LLG fault at different locations with a fault resistance of 0.1 Ω. When the fault occurs at the substation buses, the voltage sag measures 0.23 pu at the substation and 0.22 pu at the farthest terminal bus (Bus36). This significant voltage sag occurs because the fault current flowing to ground at the substation node is much larger than the load current. Conversely, when the fault occurs at the farthest terminal node (Bus36), the substation experiences only a 0.00 pu voltage sag due to the high line impedance between the substation and fault location. Meanwhile, the faulted terminal node (Bus36) shows the highest sag of 0.91 pu. The profile clearly demonstrates that voltage sags are more severe at nodes closer to the fault location. The voltage sag characteristics of the faulted phase in LLG faults exhibit a similar distribution pattern to those seen in terminal buses during LLLG and LG faults.

4.2.1 Solati Distribution Feeder Fault Location Visualization

The fault location visualization on OpenStreetMap has been developed to display the simulation timestamp, simulated fault point, and calculated fault point, along with their distance from the substation. This HTML file can be opened in Google Chrome, Microsoft Edge, or other web browsers. Figure 27 and Figure 28 illustrate the fault location visualization—one showing an accurate result and the other with a slight deviation respectively.

Figure 27: Fault location visualization in case of pinpoint in Solati distribution feeder

In Figure 28, the simulated fault location and the calculated fault location differ, making it evident that the two fault-indicated points are distinct—where the red marker represents the simulated fault node, and the blue marker represents the calculated fault node. In contrast Figure 27 both locations coincide, causing the markers to overlap.

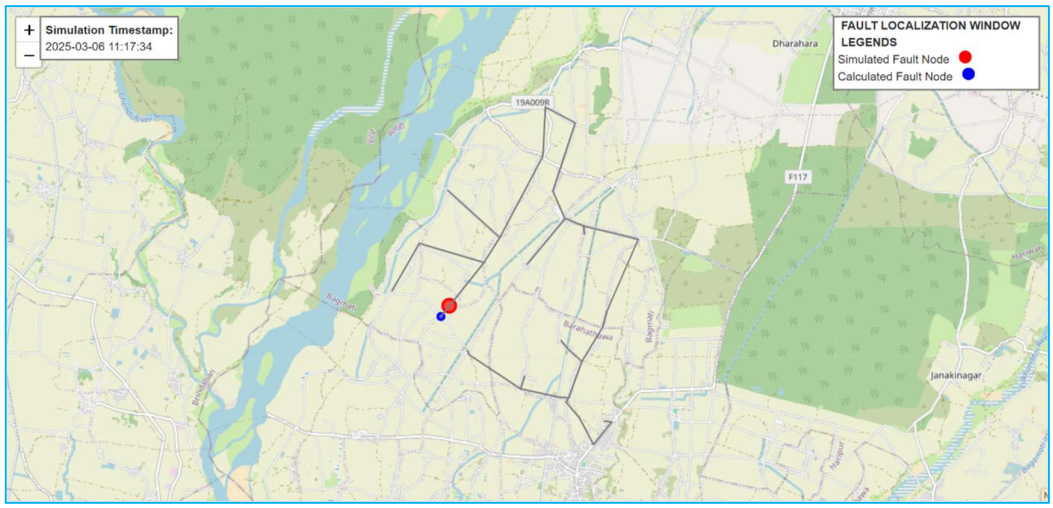

Figure 28: Fault location visualization in case of deviation in Solati distribution feeder

4.2.2 Solati Distribution Feeder Fault Location Analysis

Table 12: Impact of fault resistance in fault location in Solati distribution feeder

Type of	Simulated Number	R=0.1Ω			R=50Ω			R=100Ω		
		Number of	Average	Maximum Distan	Number of	Average	Maximum Distan	Number of	Average	Maximum Distan

Fault		Time Pin Point	Error (m)	ce Error (m)	Time Pin Point	Error (m)	ce Error (m)	Time Pin Point	Error (m)	ce Error (m)
LLLG	200	175	34.55	370	189	10.91	270	189	10.91	270
LLG	200	175	34.55	370	189	10.91	270	189	10.91	270
LL	200	175	34.55	370	189	10.91	270	189	10.91	270
LG	200	175	34.55	370	189	10.91	270	189	10.91	270

A total of 200 faults are simulated for each fault type, with varying fault resistances of R = 0.1Ω, R = 50Ω, and R = 100Ω. The results are reported in Table 12. For bolted faults, the fault location is accurately pinpointed 175 times out of 200, with an average localization error of 34.55 meters and a maximum error of 370 meters. For faults with higher resistance values (R = 50Ω and R = 100Ω), the fault location is pinpointed 189 times out of 200, with a lower average error of 10.91 meters and a maximum error of 270 meters. These results indicate that higher fault resistance leads to lower localization errors. Additionally, fault location accuracy in this case remains independent of fault type.

4.2.3 Impact of Load Variation on Fault Localization Accuracy

Table 13: Impact of load variation on fault localization error in Solati feeder

Type of Fault	Simulated Number	R=0.1Ω, 70% Loading			R=0.1Ω, 100% Loading			R=0.1Ω, 120% Loading		
		Number of Time Pin Point	Average Error (m)	Maximum Distance Error (m)	Number of Time Pin Point	Average Error (m)	Maximum Distance Error (m)	Number of Time Pin Point	Average Error (m)	Maximum Distance Error (m)
LLLG	200	175	34.55	370	175	34.55	370	175	34.55	370
LLG	200	175	34.55	370	175	34.55	370	175	34.55	370
LL	200	175	34.55	370	175	34.55	370	175	34.55	370
LG	200	175	34.55	370	175	34.55	370	175	34.55	370

The Table 13 presents the impact of load variation on fault localization accuracy for different fault types under varying loading conditions (70%, 100%, and 120%). Each fault type, including LLLG, LLG, LL, and LG, is simulated 200 times, and the results are analyzed based on the number of times the fault location is pinpointed, the average localization error (in meters), and the maximum error distance (in meters). For all fault types and loading conditions, the fault location is accurately pinpointed 175 times out of 200, with an average localization error of 34.55 meters and a maximum error of 370 meters. These values remain constant across all loading conditions, indicating that load variation does not affect fault localization accuracy when R = 0.1Ω. This result suggests that, in this case, fault localization accuracy is independent of system loading, as there is no observed impact on the pinpointing accuracy, average error, or maximum error distance.

4.2.4 Impact of Line Impedance Measurement on Fault Localization Error

Some sections of the impedance are considered as modeling errors, which may arise due to factors such as improper conductor joints, temperature variations, and measurement errors in GIS data. The changes in impedance for certain sections during the simulation are reported in Table 14.

Table 14: Variation of impedance of sections in Solati feeder

Section	Impedance Change Percentage
Line 3-4	5%
Line 10-11	-5%
Line 20-21	5%
Line 26-27	-5%
Line 33-34	5%

Table 15: Comparison of variation of line impedance with base cases with fault resistance of 0.1Ω in Solati distribution feeder

Type of Fault	Simulated Number	Base Case			Impedance Variation Case		
		Number of Time Pin Point	Average Error (m)	Maximum Distance Error (m)	Number of Time Pin Point	Average Error (m)	Maximum Distance Error (m)

LLL G	200	175	34.55	370	145	45.273	370
LLG	200	175	34.55	370	145	45.273	370
LL	200	175	34.55	370	145	45.273	370
LG	200	175	34.55	370	145	45.273	370

Table 15 compares fault localization accuracy for different fault types under two scenarios: the Base Case (no impedance variation) and the Impedance Variation Case. In the Base Case, a total of 200 faults are simulated for each fault type, and the fault location is accurately pinpointed 175 times out of 200. The average localization error remains 34.55 meters, and the maximum distance error is 370 meters across all fault types. In the Impedance Variation Case, the fault location is correctly identified 145 times out of 200 for each fault type, indicating a decrease in fault localization accuracy compared to the Base Case. The average error increases to 45.273 meters, showing that impedance variations lead to higher localization errors. Despite these changes, the maximum distance error remains the same at 370 meters. This suggests that impedance variation results in a higher average error and fewer successful fault localizations, but it does not affect the maximum observed error distance.

4.2.5 Impact of DG Penetration on Fault Localization Accuracy

With the increasing trend of DG penetration in distribution systems, the performance of the algorithm is also evaluated under DG integration. The location of the four photovoltaic (PV) units are taken randomly as well as their sizes. The detail of the DG configurations is reported in the Table 16.

Table 16: Detail of simulated distributed generation for performance evaluation in Solati distribution feeder

S.N.	Bus Number	Type of DG	Rating (kW)	Power Factor	Voltage Rating (kV)
1	10	Photovoltaic	100	1	11
2	17	Photovoltaic	150	1	11
3	26	Photovoltaic	200	1	11
4	34	Photovoltaic	250	1	11

Table 17: Impact of DG penetration in Solati distribution feeder with fault resistance of 0.1 ohm

Type of Fault	Simulated Number	Base Case			DG Penetration		
		Number of Time Pin Point	Average Error (m)	Maximum Distance Error (m)	Number of Time Pin Point	Average Error (m)	Maximum Distance Error (m)
LLLG	200	175	34.55	370	149	47.81818	370
LLG	200	175	34.55	370	149	47.81818	370
LL	200	175	34.55	370	149	47.81818	370
LG	200	175	34.55	370	149	47.81818	370

Table 17 compares fault localization accuracy for different fault types under two scenarios: the Base Case (no Distributed Generation (DG) penetration) and the DG Penetration Case (with DG penetration), with a fault resistance of 0.1Ω. In the Base Case, a total of 200 faults are simulated for each fault type, and the fault location is accurately pinpointed 175 times out of 200. The average localization error is 34.55 meters, and the maximum distance error is 370 meters across all fault types. In the DG Penetration Case, the fault location is correctly identified 149 times out of 200 for each fault type, showing a decrease in fault localization accuracy compared to the Base Case. The average error increases to 47.82 meters, indicating that the presence of DG penetration increases the localization error. Despite this, the maximum distance error remains the same at 370 meters, meaning that although the overall fault localization accuracy worsens with DG penetration, the worst-case error does not change.

Table 18: Impact of DG penetration in Solati distribution feeder with fault resistance of 50 ohm

Type of Fault	Simulated Number	Base Case			DG Penetration		
		Number of Time Pin Point	Average Error (m)	Maximum Distance Error (m)	Number of Time Pin Point	Average Error (m)	Maximum Distance Error (m)
LLLG	200	189	10.91	270	145	53.63636	370

LLG	200	189	10.91	270	145	53.63636	370
LL	200	189	10.91	270	145	53.63636	370
LG	200	189	10.91	270	145	53.63636	370

Table 18 reports fault localization accuracy under two conditions: the Base Case (without Distributed Generation (DG) penetration) and the DG Penetration Case (with DG penetration), considering a fault resistance of 50.0Ω. Each fault type—LLLG, LLG, LL, and LG—is simulated 200 times, and the results are analyzed based on the number of times the fault is pinpointed correctly, the average localization error, and the maximum error distance. In the Base Case, fault localization performs well, with the fault being accurately pinpointed 189 times out of 200 for all fault types. The average localization error remains 10.91 meters, and the maximum distance error is 270 meters, indicating a high level of accuracy in fault identification. However, in the DG Penetration Case, fault localization accuracy decreases significantly. The number of times the fault is correctly pinpointed drops to 145 out of 200, showing a reduction in accuracy compared to the Base Case. The average localization error increases significantly to 53.64 meters, suggesting that the presence of DG introduces disturbances that impact fault localization precision. Additionally, the maximum error distance increases to 370 meters, indicating a higher risk of incorrect fault identification with DG penetration.

Table 19: Impact of DG penetration in Solati distribution feeder with fault resistance of 100 ohm

Type of Fault	Simulated Number	Base Case			DG Penetration		
		Number of Time Pin Point	Average Error (m)	Maximum Distance Error (m)	Number of Time Pin Point	Average Error (m)	Maximum Distance Error (m)
LLLG	200	189	10.91	270	145	53.6364	370
LLG	200	189	10.91	270	145	53.6364	370
LL	200	189	10.91	270	145	53.6364	370
LG	200	189	10.91	270	145	53.6364	370

Table 19 reports the impact of Distributed Generation (DG) penetration on fault localization accuracy, considering a fault resistance of 100Ω. The comparison is made between the Base Case (without DG) and the DG Penetration Case across different fault types (LLLG, LLG, LL, and LG) based on 200 simulated faults. In the Base Case, the fault location is correctly pinpointed 189 times out of 200, showing a high accuracy rate. The average localization error is 10.91 meters, and the maximum distance error is 270 meters, indicating that the method is highly effective under normal conditions. However, in the DG Penetration Case, the accuracy decreases notably. The fault is correctly pinpointed only 145 times out of 200, a significant drop from the Base Case. The average localization error increases to 53.64 meters, indicating a reduced precision in fault location detection. Additionally, the maximum distance error increases to 370 meters, suggesting that DG penetration introduces additional complexities that lead to greater deviations in fault location estimation.

Overall, the results suggest that DG penetration negatively impacts fault localization accuracy, leading to higher errors and a lower number of correctly identified fault locations compared to the Base Case.

The results indicate that while the average distance error increases with DG penetration, the maximum distance error remains unchanged at 370 meters. This suggests that DG penetration introduces inconsistencies in fault localization, leading to a higher overall error, but it does not necessarily worsen the worst-case scenario. The increase in average error implies that fault location estimations are becoming less precise overall, likely due to the influence of DG on network conditions. However, since the maximum error remains the same, it indicates that the most extreme fault localization deviations are not significantly affected by DG penetration.

4.2.6 Fault Classification in Solati Distribution Feeder

Table 20: Fault classification result in Solati distribution feeder

Subjected Fault Types	Simulated Number	Accurately Detected Number	Presence of DG
LLLG	200	200	No
LLG (Phase A & B)	200	200	No
LLG (Phase B & C)	200	200	No
LLG (Phase C & A)	200	200	No
LL (Phase A & B)	200	200	No

LL (Phase B & C)	200	200	No
LL (Phase C & A)	200	200	No
LG (Phase A)	200	200	No
LG (Phase B)	200	200	No
LG (Phase C)	200	200	No
LLLG	200	200	Yes
LLG (Phase A & B)	200	200	Yes
LLG (Phase B & C)	200	200	Yes
LLG (Phase C & A)	200	200	Yes
LL (Phase A & B)	200	200	Yes
LL (Phase B & C)	200	200	Yes
LL (Phase C & A)	200	200	Yes
LG (Phase A)	200	200	Yes
LG (Phase B)	200	200	Yes
LG (Phase C)	200	200	Yes

The developed fault classification approach is also tested in the Solati distribution feeder, and the results are reported in Table 20. The method is evaluated both with and without DG integration. The findings indicate that the proposed methodology accurately classifies faults in the Solati distribution feeder. Additionally, the approach effectively identifies the specific phase(s) involved in the fault.

4.3 Chapagaun Distribution Feeder Simulated Result

The Chapagaun distribution feeder is modeled using OpenDSS and Python, with a dynamic program developed for fault localization and classification within the Python environment. A total of 314 simulations are conducted for each fault scenario. Fault is created at random length in the line. This results in 314 simulations for each fault type—LLLG, LLG, LL, or LG.

4.3.1 Chapagaun Distribution Feeder Fault Location Visualization

The fault location visualization on OpenStreetMap has been developed to display the simulation timestamp, simulated fault point, and calculated fault point, along with their distance from the substation. This HTML file can be opened in Google Chrome, Microsoft Edge, or other web browsers. Figure 29 and Figure 30 illustrate the fault location visualization—one showing an accurate result and the other with a slight deviation respectively.

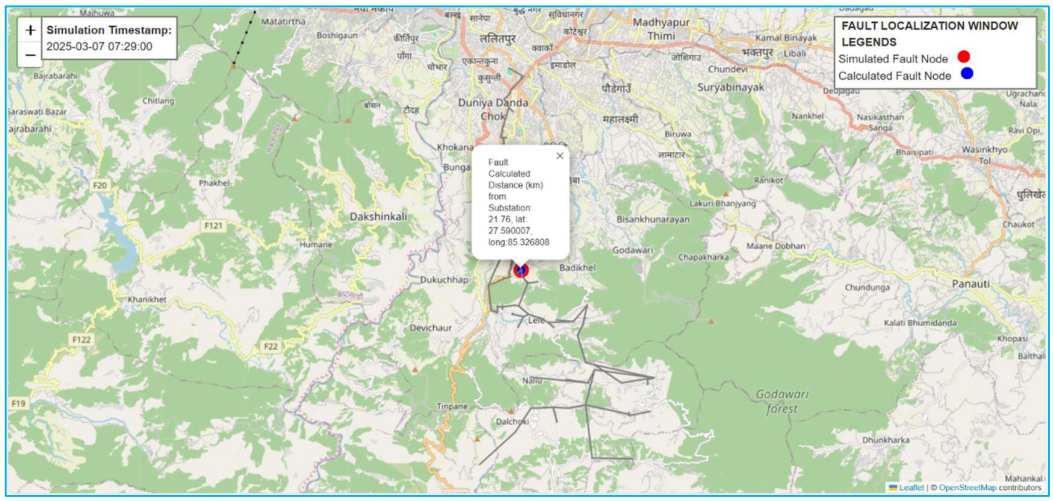

Figure 29: Fault location visualization in case of pinpoint in Chapagaun distribution feeder

In Figure 30, the simulated fault location and the calculated fault location differ, making it evident that the two fault-indicated points are distinct—where the red marker represents the simulated fault node, and the blue marker represents the calculated fault node. In contrast Figure 29 both locations coincide, causing the markers to overlap.

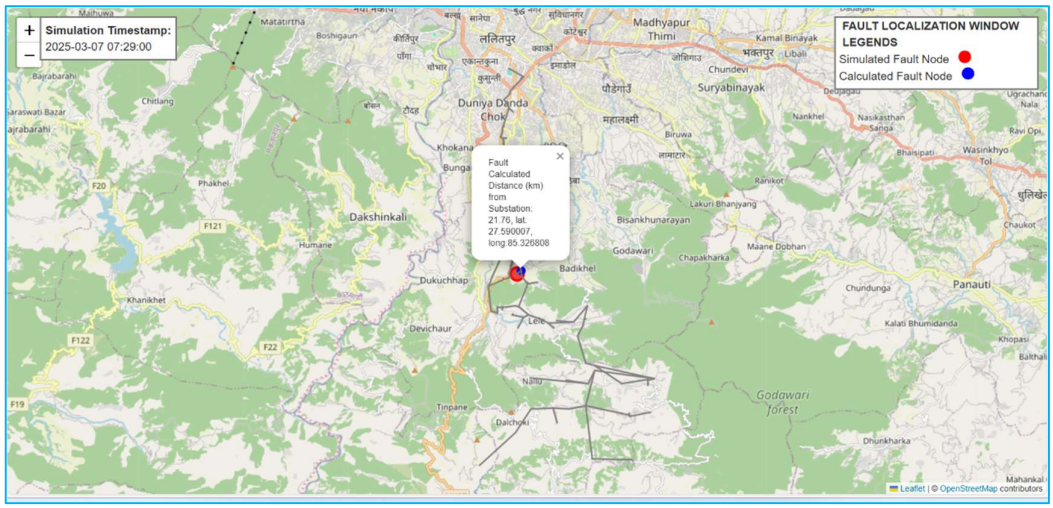

Figure 30: Fault location visualization in case of deviation in Chapagaun distribution feeder

4.3.2 Chapagaun Distribution Feeder Fault Location Analysis

A total of 314 faults are simulated for each fault type, with varying fault resistances of R = 0.1Ω, R = 50Ω, and R = 100Ω. The results are reported in Table 21. For bolted faults, the fault location is accurately pinpointed 260 times out of 314, with an average

localization error of 82.35 meters and a maximum error of 550 meters. For faults with higher resistance values (R = 50Ω and R = 100Ω), the fault location is pinpointed 270 times out of 314, with a lower average error of 65.78 meters and a maximum error of 450 meters. These results indicate that higher fault resistance leads to lower localization errors. Additionally, fault location accuracy in this case remains independent of fault type.

Table 21: Impact of fault resistance in fault location in Chapagaun distribution feeder

Type of Fault	Simulated Number	R=0.1Ω			R=50Ω			R=100Ω		
		Number of Time Pin Point	Average Error (m)	Maximum Distance Error (m)	Number of Time Pin Point	Average Error (m)	Maximum Distance Error (m)	Number of Time Pin Point	Average Error (m)	Maximum Distance Error (m)
LLLG	314	260	82.35	550	270	65.78	450	270	65.78	450
LLG	314	260	82.35	550	270	65.78	450	270	65.78	450
LL	314	260	82.35	550	270	65.78	450	270	65.78	450
LG	314	260	82.35	550	270	65.78	450	270	65.78	450

4.3.3 Impact of Load Variation on Fault Localization Accuracy

Table 22: Impact of load variation on fault localization error in Chapagaun distribution feeder

Type of Fault	Simulated Number	R=0.1Ω, 30% Loading			R=0.1Ω, 50% Loading			R=0.1Ω, 70% Loading		
		Number of Time Pin Point	Average Error (m)	Maximum Distance Error (m)	Number of Time Pin Point	Average Error (m)	Maximum Distance Error (m)	Number of Time Pin Point	Average Error (m)	Maximum Distance Error (m)
LLLG	314	260	82.35	550	260	82.35	550	260	82.35	550
LLG	314	260	82.35	550	260	82.35	550	260	82.35	550

LL	314	260	82.35	550	260	82.35	550	260	82.35	550
LG	314	260	82.35	550	260	82.35	550	260	82.35	550

The Table 22 presents the impact of load variation on fault localization accuracy for different fault types under varying loading conditions (30%, 50%, and 70%). Each fault type, including LLLG, LLG, LL, and LG, is simulated 314 times, and the results are analyzed based on the number of times the fault location is pinpointed, the average localization error (in meters), and the maximum error distance (in meters). For all fault types and loading conditions, the fault location is accurately pinpointed 260 times out of 314, with an average localization error of 80 meters and a maximum error of 550 meters. These values remain constant across all loading conditions, indicating that load variation does not affect fault localization accuracy when R = 0.1Ω. This result suggests that, in this case, fault localization accuracy is independent of system loading, as there is no observed impact on the pinpointing accuracy, average error, or maximum error distance.

4.3.4 Impact of Line Impedance Measurement on Fault Localization Error

Some sections of the impedance are considered as modeling errors, which may arise due to factors such as improper conductor joints, temperature variations, and measurement errors in GIS data. The changes in impedance for certain sections during the simulation are reported in Table 23.

Table 23: Variation of impedance of sections in Chapagaun distribution feeder

Section	Impedance Change Percentage
Line 3-4	5%
Line 10-11	-5%
Line 20-21	5%
Line 26-27	-5%
Line 33-34	5%

Table 24 compares fault localization accuracy for different fault types under two scenarios: the Base Case (no impedance variation) and the Impedance Variation Case. In the Base Case, a total of 314 faults are simulated for each fault type, and the fault

location is accurately pinpointed 260 times out of 314. The average localization error remains 82.35 meters, and the maximum distance error is 550 meters across all fault types. In the Impedance Variation Case, the fault location is correctly identified 213 times out of 314 for each fault type, indicating a decrease in fault localization accuracy compared to the Base Case. The average error increases to 103.78 meters, showing that impedance variations lead to higher localization errors. Despite these changes, the maximum distance error remains the same at 550 meters. This suggests that impedance variation results in a higher average error and fewer successful fault localizations, but it does not affect the maximum observed error distance.

Table 24: Comparison of variation of line impedance with base cases with fault resistance of 0.1Ω in Chapagaun distribution feeder

Type of Fault	Simulated Number	Base Case			Impedance Variation Case		
		Number of Time Pin Point	Average Error (m)	Maximum Distance Error (m)	Number of Time Pin Point	Average Error (m)	Maximum Distance Error (m)
LLLG	314	260	82.35	550	213	103.78	550
LLG	314	260	82.35	550	213	103.78	550
LL	314	260	82.35	550	213	103.78	550
LG	314	260	82.35	550	213	103.78	550

4.3.5 Impact of DG Penetration on Fault Localization Accuracy

With the increasing trend of DG penetration in distribution systems, the performance of the algorithm is also evaluated under DG integration. The location of the four photovoltaic (PV) units are taken randomly as well as their sizes. The detail of the DG configurations is reported in Table 25.

Table 25: Detail of simulated distributed generation for performance evaluation in Chapagaun distribution feeder

S.N.	Bus Number	Type of DG	Rating (kVA)	Power Factor	Voltage Rating (kV)
1	10	Photovoltaic	350	1	11
2	30	Photovoltaic	300	1	11

3	50	Photovoltaic	250	1	11
4	99	Photovoltaic	400	1	11

Table 26: Impact of DG penetration in Chapagaun distribution feeder with fault resistance of 0.1 ohm

Type of Fault	Simulated Number	Base Case			DG Penetration		
		Number of Time Pin Point	Average Error (m)	Maximum Distance Error (m)	Number of Time Pin Point	Average Error (m)	Maximum Distance Error (m)
LLLG	314	260	82.35	550	220	97.65	550
LLG	314	260	82.35	550	220	97.65	550
LL	314	260	82.35	550	220	97.65	550
LG	314	260	82.35	550	220	97.65	550

Table 26 compares fault localization accuracy for different fault types under two scenarios: the Base Case (no Distributed Generation (DG) penetration) and the DG Penetration Case (with DG penetration), with a fault resistance of 0.1Ω. In the Base Case, a total of 314 faults are simulated for each fault type, and the fault location is accurately pinpointed 260 times out of 314. The average localization error is 82.35 meters, and the maximum distance error is 550 meters across all fault types. In the DG Penetration Case, the fault location is correctly identified 220 times out of 314 for each fault type, showing a decrease in fault localization accuracy compared to the Base Case. The average error increases to 97.65 meters, indicating that the presence of DG penetration increases the localization error. Despite this, the maximum distance error remains the same at 550 meters, meaning that although the overall fault localization accuracy worsens with DG penetration, the worst-case error does not change.

Table 27 reports fault localization accuracy under two conditions: the Base Case (without Distributed Generation (DG) penetration) and the DG Penetration Case (with DG penetration), considering a fault resistance of 50.0Ω. Each fault type—LLLG, LLG, LL, and LG—is simulated 314 times, and the results are analyzed based on the number of times the fault is pinpointed correctly, the average localization error, and the

maximum error distance. In the Base Case, fault localization performs well, with the fault being accurately pinpointed 270 times out of 314 for all fault types. The average localization error remains 65.78 meters, and the maximum distance error is 450 meters, indicating a high level of accuracy in fault identification. However, in the DG Penetration Case, fault localization accuracy decreases significantly. The number of times the fault is correctly pinpointed drops to 230 out of 314, showing a reduction in accuracy compared to the Base Case. The average localization error increases significantly to 87.25 meters, suggesting that the presence of DG introduces disturbances that impact fault localization precision. Additionally, the maximum error distance remains to same as 450 meters.

Table 27: Impact of DG penetration in Chapagaun distribution feeder with fault resistance of 50 ohm

Type of Fault	Simulated Number	Base Case			DG Penetration		
		Number of Time Pin Point	Average Error (m)	Maximum Distance Error (m)	Number of Time Pin Point	Average Error (m)	Maximum Distance Error (m)
LLLG	314	270	65.78	450	230	87.25	450
LLG	314	270	65.78	450	230	87.25	450
LL	314	270	65.78	450	230	87.25	450
LG	314	270	65.78	450	230	87.25	450

Table 28 reports the impact of Distributed Generation (DG) penetration on fault localization accuracy, considering a fault resistance of 100Ω. The comparison is made between the Base Case (without DG) and the DG Penetration Case across different fault types (LLLG, LLG, LL, and LG) based on 314 simulated faults. In the Base Case, the fault location is correctly pinpointed 270 times out of 314, showing a high accuracy rate. The average localization error is 65.78 meters, and the maximum distance error is 550 meters, indicating that the method is highly effective under normal conditions. However, in the DG Penetration Case, the accuracy decreases notably. The fault is correctly pinpointed only 230 times out of 314, a significant drop from the Base Case. The average localization error increases to 87.25 meters, indicating a reduced precision

in fault location detection. Additionally, the maximum distance error increases to 370 meters.

Table 28: Impact of DG penetration in Chapagaun distribution feeder with fault resistance of 100 ohm

Type of Fault	Simulated Number	Base Case			DG Penetration		
		Number of Time Pin Point	Average Error (m)	Maximum Distance Error (m)	Number of Time Pin Point	Average Error (m)	Maximum Distance Error (m)
LLLG	314	270	65.78	450	230	87.25	450
LLG	314	270	65.78	450	230	87.25	450
LL	314	270	65.78	450	230	87.25	450
LG	314	270	65.78	450	230	87.25	450

Overall, the results suggest that DG penetration negatively impacts fault localization accuracy, leading to higher errors and a lower number of correctly identified fault locations compared to the Base Case.

The results indicate that while the average distance error increases with DG penetration, the maximum distance error remains unchanged at 550 meters. This suggests that DG penetration introduces inconsistencies in fault localization, leading to a higher overall error, but it does not necessarily worsen the worst-case scenario. The increase in average error implies that fault location estimations are becoming less precise overall, likely due to the influence of DG on network conditions. However, since the maximum error remains the same, it indicates that the most extreme fault localization deviations are not significantly affected by DG penetration.

4.3.6 Fault Classification in Chapagaun Distribution Feeder

The developed fault classification approach is also tested in the Solati distribution feeder, and the results are reported in Table 29. The method is evaluated both with and without DG integration. The findings indicate that the proposed methodology accurately classifies faults in the Solati distribution feeder. Additionally, the approach effectively identifies the specific phase(s) involved in the fault.

Table 29: Fault classification result in chapagaun distribution feeder

Subjected Fault Types	Simulated Number	Accurately Detected Number	Presence of DG
LLLG	314	314	No
LLG (Phase A & B)	314	314	No
LLG (Phase B & C)	314	314	No
LLG (Phase C & A)	314	314	No
LL (Phase A & B)	314	314	No
LL (Phase B & C)	314	314	No
LL (Phase C & A)	314	314	No
LG (Phase A)	314	314	No
LG (Phase B)	314	314	No
LG (Phase C)	314	314	No
LLLG	314	314	Yes
LLG (Phase A & B)	314	314	Yes
LLG (Phase B & C)	314	314	Yes
LLG (Phase C & A)	314	314	Yes
LL (Phase A & B)	314	314	Yes
LL (Phase B & C)	314	314	Yes
LL (Phase C & A)	314	314	Yes
LG (Phase A)	314	314	Yes
LG (Phase B)	314	314	Yes
LG (Phase C)	314	314	Yes

4.4 Underground Distribution Feeder Simulation

To validate the proposed methodology for underground distribution systems, the study modifies the Solati distribution feeder by converting it from overhead to underground configuration while preserving the original feeder length and loading conditions. The overhead conductors (rabbit and dog type) are systematically replaced with 11 kV, 120 mm^2 XLPE cables in each section, featuring characteristic parameters of 0.35 Ω/km resistance, 0.10 Ω/km reactance, 0.32 μF/km capacitance, and 220 A current carrying capacity as per IEC 60502-2 standards. This underground cable conversion maintains identical analysis conditions for direct performance comparison with the overhead system, with detailed results presented in subsequent sections. The modification enables comprehensive evaluation of the methodology's effectiveness in underground distribution networks while ensuring consistency in all other operational parameters.

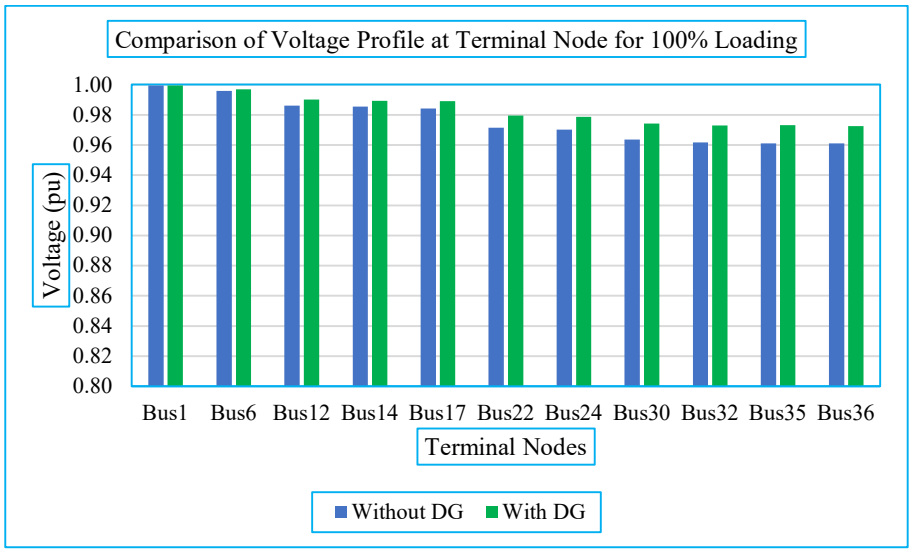

Figure 31: Comparison of voltage profile at terminal nodes with 100% loading in underground distribution feeder

Figure 31 illustrates the voltage profile of terminal nodes equipped with IEDs under 100% loading conditions, comparing scenarios with and without distributed generation (DG) integration. In the base case (without DG), Bus1 (substation node) maintains 1 pu voltage, while the farthest node (Bus36, 16.41 km away) records 0.96 pu, demonstrating characteristic voltage drop with increasing distance from the substation. The balanced system allows representation using R-phase voltage (pu) for all three phases. When photovoltaic DG units (randomly located with capacities specified in Table 16) are integrated at 700 kW total penetration (70% nominal irradiance), the voltage profile shows marginal improvement across the feeder compared to the base case. Because of marginal improvement in voltage profile, further voltage sag analysis presents in this report is without presence of DG.

Figure 32 illustrates the voltage sag profile at terminal buses for an LLLG fault at different locations with a fault resistance of 0.1 Ω. When the fault occurs at the substation buses, the voltage sag measures 0.23 pu at the substation and 0.22 pu at the farthest terminal bus (Bus36). This significant voltage sag occurs because the fault current flowing to ground at the substation node is much larger than the load current. Conversely, when the fault occurs at the farthest terminal node (Bus36), the substation experiences only a 0.00 pu voltage sag due to the high line impedance between the substation and fault location. Meanwhile, the faulted terminal node (Bus36) shows the

highest sag of 0.94 pu. The profile clearly demonstrates that voltage sags are more severe at nodes closer to the fault location.

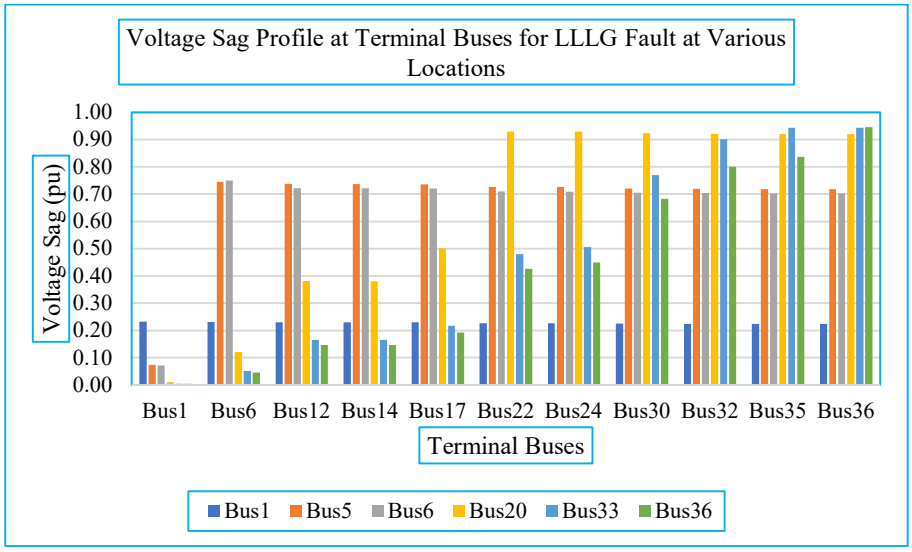

Figure 32: Voltage sag profile at terminal buses for LLLG fault at various locations in underground distribution feeder

Figure 33 illustrates the voltage sag profile at terminal buses for an LG fault at different locations with a fault resistance of 0.1 Ω. When the fault occurs at the substation buses, the voltage sag measures 0.23 pu at the substation and 0.23 pu at the farthest terminal bus (Bus36). This significant voltage sag occurs because the fault current flowing to ground at the substation node is much larger than the load current. Conversely, when the fault occurs at the farthest terminal node (Bus36), the substation experiences only a 0.00 pu voltage sag due to the high line impedance between the substation and fault location. Meanwhile, the faulted terminal node (Bus36) shows the highest sag of 0.94 pu. The profile clearly demonstrates that voltage sags are more severe at nodes closer to the fault location. The voltage sag characteristics of the faulted phase in LG faults exhibit a similar distribution pattern to those seen in terminal buses during LLLG faults.

Figure 34 illustrates the voltage sag profile at terminal buses for an LLG fault at different locations with a fault resistance of 0.1 Ω. When the fault occurs at the substation buses, the voltage sag measures 0.23 pu at the substation and 0.18 pu at the farthest terminal bus (Bus36). This significant voltage sag occurs because the fault current flowing to ground at the substation node is much larger than the load current. Conversely, when the fault occurs at the farthest terminal node (Bus36), the substation

experiences only a 0.00 pu voltage sag due to the high line impedance between the substation and fault location. Meanwhile, the faulted terminal node (Bus36) shows the highest sag of 0.90 pu. The profile clearly demonstrates that voltage sags are more severe at nodes closer to the fault location. The voltage sag characteristics of the faulted phase in LLG faults exhibit a similar distribution pattern to those seen in terminal buses during LLLG and LG faults.

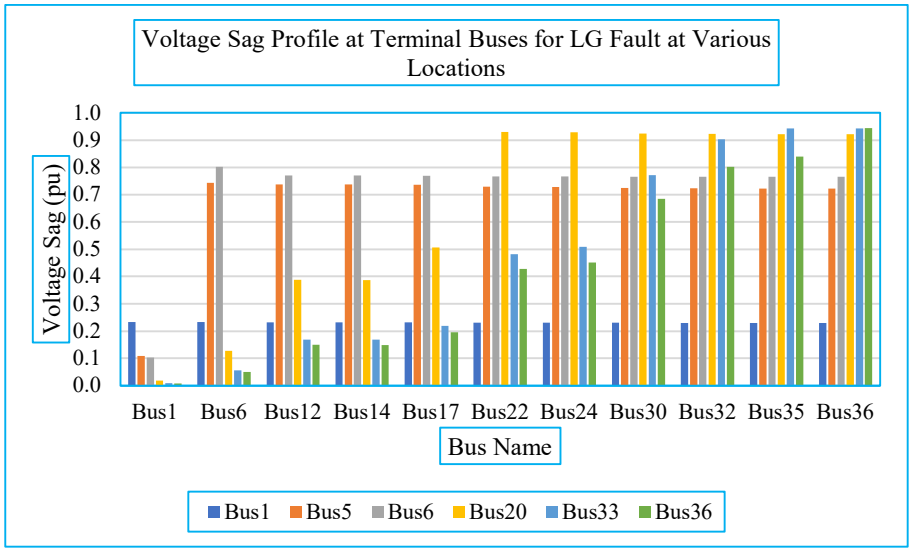

Figure 33: Voltage sag profile at terminal buses for LG fault at various locations in underground distribution feeder

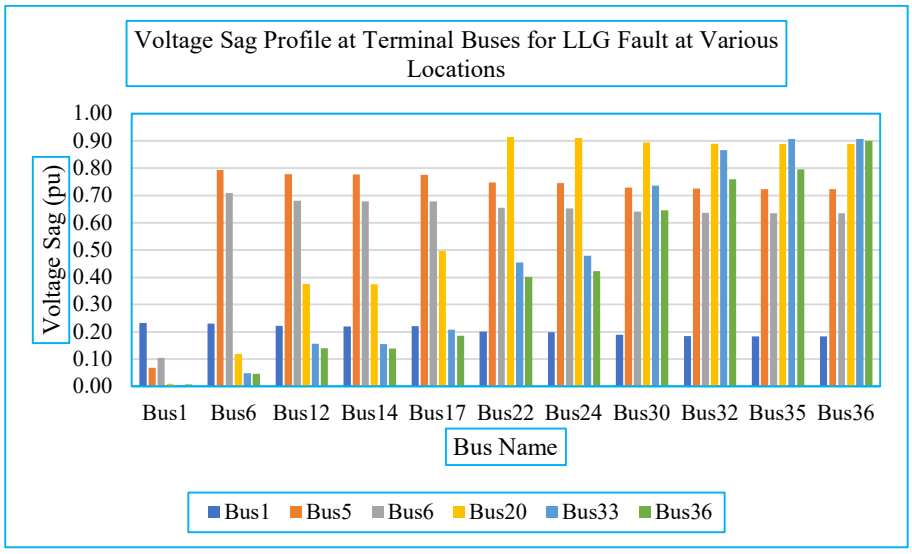

Figure 34: Voltage sag profile at terminal buses for LG fault at various locations in underground distribution feeder

4.4.1 Underground Distribution Feeder Fault Location Analysis

Table 30: Impact of fault resistance in fault location in underground distribution feeder

Type of Fault	Simulated Number	R=0.1Ω			R=50Ω			R=100Ω		
		Number of Time Pin Point	Average Error (m)	Maximum Distance Error (m)	Number of Time Pin Point	Average Error (m)	Maximum Distance Error (m)	Number of Time Pin Point	Average Error (m)	Maximum Distance Error (m)
LLLG	200	160	22.36	370	196	0.55	30	196	0.55	30
LLG	200	156	29.09	370	178	5.82	30	196	0.55	30
LL	200	156	29.09	370	178	5.82	30	196	0.55	30
LG	200	156	29.09	370	196	0.55	30	196	0.55	30

A total of 200 faults are simulated for each fault type, with fault resistances of R = 0.1Ω, R = 50Ω, and R = 100Ω. The results are presented in Table 30. For bolted faults, the fault location is accurately identified 160 times out of 200, with an average localization error of 22.36 meters for LLLG faults. For other fault types, the fault location is accurately determined 156 times out of 200, with an average error of 29.09 meters. However, the maximum localization error remains constant at 370 meters for all fault types with very low resistance. It is observed that as fault resistance increases, both the average and maximum localization errors decrease. For LLLG faults with higher fault resistances of 50Ω and 100Ω, the maximum localization error is 30 meters, which is also the case for LG faults. Additionally, for LLG and LL faults with a resistance of 100Ω, the results remain consistent.

4.4.2 Impact of Load Variation on Fault Localization Accuracy

Table 31 reports the results of fault location accuracy for different fault types under varying loading conditions (70%, 100%, and 120%) while maintaining a fault resistance of R = 0.1Ω. A total of 200 faults are simulated for each fault type, and the number of times the fault is accurately pinpointed remains consistent across all loading conditions. For LLLG faults, the fault is correctly identified 160 times out of 200, with an average localization error of 22.36 meters. The maximum localization error remains at 370 meters, regardless of the loading level. Similarly, for LLG, LL, and LG faults,

the fault is pinpointed correctly 156 times out of 200, with an average error of 29.09 meters and a maximum error of 370 meters.

These results indicate that changes in system loading do not impact fault localization accuracy when the fault resistance is low (0.1Ω). The consistency in both the number of correctly identified faults and the associated errors suggests that the accuracy of fault location estimation is primarily influenced by fault resistance rather than variations in loading conditions.

Table 31: Impact of load variation on fault localization error in underground distribution feeder

Type of Fault	Simulated Number	R=0.1Ω, 70% Loading			R=0.1Ω, 100% Loading			R=0.1Ω, 120% Loading		
		Number of Time Pin Point	Average Error (m)	Maximum Distance Error (m)	Number of Time Pin Point	Average Error (m)	Maximum Distance Error (m)	Number of Time Pin Point	Average Error (m)	Maximum Distance Error (m)
LLLG	200	160	22.36	370	160	22.36	370	160	22.36	370
LLG	200	156	29.09	370	156	29.09	370	156	29.09	370
LL	200	156	29.09	370	156	29.09	370	156	29.09	370
LG	200	156	29.09	370	156	29.09	370	156	29.09	370

4.4.3 Impact of Line Impedance Measurement on Fault Localization Error

The changes in impedance for certain sections during the simulation are reported in Table 14. Table 32 reports the results of fault location accuracy under two different cases: the Base Case and the Impedance Variation Case. A total of 200 faults are simulated for each fault type (LLLG, LLG, LL, and LG), and the number of times the fault is accurately pinpointed, along with the average and maximum localization errors, is recorded for both cases. In the Base Case, for LLLG faults, the fault is correctly identified 160 times out of 200, with an average localization error of 22.36 meters and a maximum error of 370 meters. For LLG, LL, and LG faults, the fault is pinpointed accurately 156 times out of 200, with an average error of 29.09 meters and the same maximum error of 370 meters.

Table 32: Comparison of variation of line impedance with base case with fault resistance of 0.1Ω in underground distribution feeder

Type of Fault	Simulated Number	Base Case			Impedance Variation Case		
		Number of Time Pin Point	Average Error (m)	Maximum Distance Error (m)	Number of Time Pin Point	Average Error (m)	Maximum Distance Error (m)
LLLG	200	160	22.36	370	133	29.31	370
LLG	200	156	29.09	370	129	38.12	370
LL	200	156	29.09	370	129	38.12	370
LG	200	156	29.09	370	129	38.12	370

In the Impedance Variation Case, the number of correctly pinpointed faults decreases for all fault types. For LLLG faults, the fault is accurately identified 133 times, with an increased average localization error of 29.31 meters, while the maximum error remains at 370 meters. Similarly, for LLG, LL, and LG faults, the fault is pinpointed correctly 129 times, with an even higher average localization error of 38.12 meters, though the maximum error remains unchanged at 370 meters.

These results suggest that variations in impedance negatively impact fault localization accuracy, reducing the number of correctly identified fault locations and increasing the average localization error. However, the maximum localization error remains the same across both cases, indicating that impedance variations primarily affect the precision of fault identification rather than the worst-case error scenario.

4.4.4 Impact of DG Penetration on Fault Localization Accuracy

Table 33 presents the impact of Distributed Generation (DG) penetration on fault location accuracy for a fault resistance of 1Ω. The results compare the Base Case (without DG) and the DG Penetration Case, analyzing the number of correctly pinpointed faults, the average localization error, and the maximum localization error. A total of 200 faults are simulated for each fault type (LLLG, LLG, LL, and LG).

In the Base Case, for LLLG faults, the fault is accurately pinpointed 160 times out of 200, with an average localization error of 22.36 meters and a maximum error of 370 meters. For LLG, LL, and LG faults, the fault is correctly identified 156 times out of

200, with an average localization error of 29.09 meters and a maximum error of 370 meters.

With DG Penetration, fault localization improves significantly. For LLLG, LLG, and LL faults, the number of correctly pinpointed faults increases to 171 out of 200, while the average localization error decreases to just 7.45 meters, and the maximum error is reduced to 60 meters. For LG faults, the accuracy also improves, with the fault pinpointed 167 times out of 200, an average localization error of 9.09 meters, and a maximum error of 90 meters.

Table 33: Impact of DG Penetration in underground distribution feeder with fault resistance of 0.1 Ω

Type of Fault	Simulated Number	Base Case			DG Penetration		
		Number of Time Pin Point	Average Error (m)	Maximum Distance Error (m)	Number of Time Pin Point	Average Error (m)	Maximum Distance Error (m)
LLLG	200	160	22.36	370	171	7.45	60
LLG	200	156	29.09	370	171	7.45	60
LL	200	156	29.09	370	171	7.45	60
LG	200	156	29.09	370	167	9.09	90

Table 34 presents the impact of Distributed Generation (DG) penetration on fault location accuracy for a fault resistance of 50Ω. The results are compared between the Base Case (without DG) and the DG Penetration Case. A total of 200 faults are simulated for each fault type (LLLG, LLG, LL, and LG), and the accuracy of fault localization is assessed in terms of the number of correctly pinpointed faults, the average localization error, and the maximum error.

In the Base Case, for LLLG faults, the fault is correctly identified 160 times out of 200, with an average localization error of 22.36 meters and a maximum error of 370 meters. Similarly, for LLG, LL, and LG faults, the fault is pinpointed 156 times out of 200, with an average localization error of 29.09 meters and the same maximum error of 370 meters. With DG Penetration, fault localization accuracy improves significantly. For LLLG, LLG, and LL faults, the number of correctly pinpointed faults increases to 171

out of 200, while the average localization error decreases drastically to 7.45 meters. Additionally, the maximum localization error reduces to 60 meters, showing a substantial improvement in precision. For LG faults, the number of correctly pinpointed faults also increases to 167, with an average error of 9.09 meters and a maximum error of 90 meters.

Table 34: Impact of DG penetration in underground distribution feeder with fault resistance of 50 Ω

Type of Fault	Simulated Number	Base Case			DG Penetration		
		Number of Time Pin Point	Average Error (m)	Maximum Distance Error (m)	Number of Time Pin Point	Average Error (m)	Maximum Distance Error (m)
LLLG	200	196	0.55	30	175	6.91	60
LLG	200	178	5.82	30	175	6.91	60
LL	200	178	5.82	30	175	6.91	60
LG	200	196	0.55	30	175	6.91	60

Table 35 presents the impact of Distributed Generation (DG) penetration on fault location accuracy for a fault resistance of 100Ω. The results compare the Base Case (without DG) and the DG Penetration Case, analyzing the number of correctly pinpointed faults, the average localization error, and the maximum localization error. A total of 200 faults are simulated for each fault type (LLLG, LLG, LL, and LG).

In the Base Case, for LLLG faults, the fault is accurately identified 175 times out of 200, with an average localization error of 6.91 meters and a maximum error of 60 meters. For LLG, LL, and LG faults, the accuracy is significantly higher, with the fault pinpointed 196 times out of 200, and the average localization error reduced to just 0.55 meters, while the maximum error is only 30 meters.

With DG Penetration, the accuracy remains exceptionally high across all fault types. For LLLG faults, the number of correctly pinpointed faults increases further to 196 out of 200, while the average error is reduced to just 0.55 meters, and the maximum error drops to 30 meters. For LLG, LL, and LG faults, the results remain unchanged,

maintaining an average localization error of 0.55 meters and a maximum error of 30 meters, with 196 faults accurately pinpointed.

Table 35: Impact of DG penetration in underground distribution feeder with fault resistance of 100 Ω

Type of Fault	Simulated Number	Base Case			DG Penetration		
		Number of Time Pin Point	Average Error (m)	Maximum Distance Error (m)	Number of Time Pin Point	Average Error (m)	Maximum Distance Error (m)
LLLG	200	175	6.91	60	196	0.55	30
LLG	200	196	0.55	30	196	0.55	30
LL	200	196	0.55	30	196	0.55	30
LG	200	196	0.55	30	196	0.55	30

These results indicate that at higher fault resistance (100Ω), fault localization accuracy significantly improves, even in the base case. The addition of DG penetration further enhances accuracy, ensuring minimal error in fault location identification. The low average and maximum localization errors demonstrate that high-resistance faults are easier to localize accurately in the presence of DG. This improvement is likely due to better voltage profile stabilization and enhanced fault current contribution from DG units, leading to more distinct fault signatures that improve fault localization performance.

4.4.5 Fault Classification in Underground Distribution Feeder

The developed fault classification approach is also tested in the underground distribution feeder, and the results are reported in Table 36. The method is evaluated both with and without DG integration. The findings indicate that the proposed methodology accurately classifies faults in the Solati distribution feeder. Additionally, the approach effectively identifies the specific phase(s) involved in the fault.

Table 36: Fault classification result in underground distribution feeder

Subjected Fault Types	Simulated Number	Accurately Detected Number	Presence of DG
LLLG	200	200	No

LLG (Phase A & B)	200	200	No
LLG (Phase B & C)	200	200	No
LLG (Phase C & A)	200	200	No
LL (Phase A & B)	200	200	No
LL (Phase B & C)	200	200	No
LL (Phase C & A)	200	200	No
LG (Phase A)	200	200	No
LG (Phase B)	200	200	No
LG (Phase C)	200	200	No
LLLG	200	200	Yes
LLG (Phase A & B)	200	200	Yes
LLG (Phase B & C)	200	200	Yes
LLG (Phase C & A)	200	200	Yes
LL (Phase A & B)	200	200	Yes
LL (Phase B & C)	200	200	Yes
LL (Phase C & A)	200	200	Yes
LG (Phase A)	200	200	Yes
LG (Phase B)	200	200	Yes
LG (Phase C)	200	200	Yes

4.5 Comparative Result Analysis of Nepalese Distribution Feeder

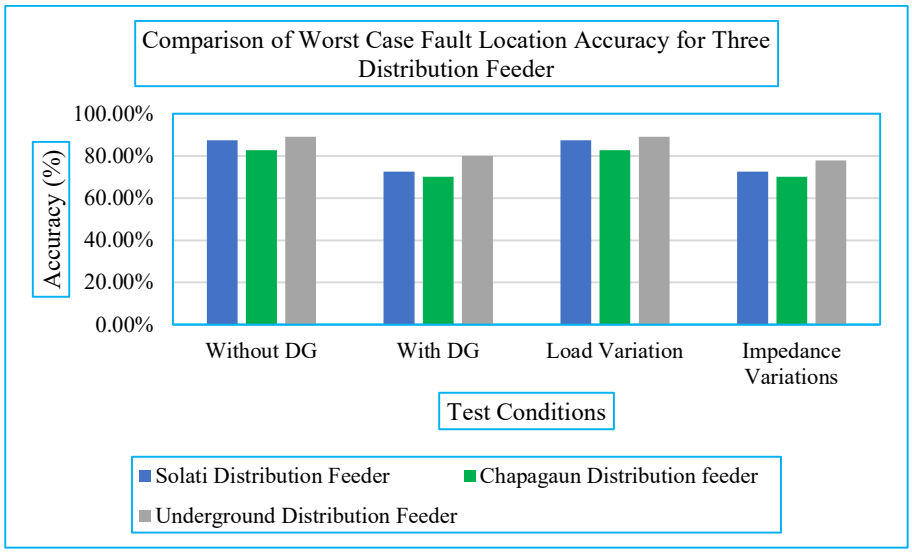

Figure 35: Comparative analysis of worst-case fault location accuracy in Nepalese distribution feeders

Figure 35 compares the worst-case fault location accuracy across three different distribution feeders under varying test conditions. The feeders analyzed include the Solti Distribution Feeder (25.41 km), Chapagaun Distribution Feeder (70 km), and an

Underground Distribution Feeder (25.41 km). The study evaluates the impact of Distributed Generation (DG), load variation, and impedance variation on fault localization accuracy.

Without DG scenario, fault location accuracy is relatively high for all three feeders. The Solti feeder achieves 87.50% accuracy, while the Chapagaun feeder records a slightly lower accuracy of 82.80%. The Underground feeder performs best, achieving 89% accuracy.

When DG is introduced, fault localization accuracy declines across all feeders. The accuracy for Solti feeder drops to 72.50%, while the Chapagaun feeder decreases to 70.06%. The Underground feeder also experiences a decline, but it maintains the highest accuracy at 80%. For the Load Variation scenario, the accuracy remains unchanged compared to the Without DG case. The Solti feeder and Chapagaun feeder maintain their accuracy at 87.50% and 82.80%, respectively, while the Underground feeder retains its highest accuracy of 89%. This indicates that changes in system loading do not significantly affect fault detection performance, suggesting that the system is well-adapted to handle varying load conditions.

Under Impedance Variation, fault location accuracy drops similarly to the With DG scenario. The Solti feeder experiences a decline to 72.50%, while the Chapagaun feeder decreases to 70.06%. The Underground feeder's accuracy reduces to 78%, showing that impedance variations impact fault detection, particularly in underground networks where cable impedance fluctuations alter fault characteristics.

Overall, the Underground feeder consistently shows the highest accuracy across all scenarios, likely due to its more predictable impedance and fault characteristics compared to overhead feeders.

Figure 36 illustrates the average fault location error for three distribution feeders. Under normal conditions, the worst-case average fault location errors for the Solti, Chapagaun, and Underground distribution feeders are 34.55 m, 82.35 m, and 29.09 m, respectively. This indicates that the fault location algorithm performs better in underground distribution feeders compared to overhead distribution lines.

With the penetration of Distributed Generation (DG), the average error increases in overhead distribution lines, whereas in underground distribution lines, the average error remains unchanged. Under varying loading conditions, the performance impact remains consistent, showing that load variations do not significantly affect fault localization accuracy.

However, in the case of distribution line modeling, if line impedance is incorrectly represented for certain sections, the average error increases significantly for all cases. This highlights the importance of accurate impedance modeling in improving fault location precision.

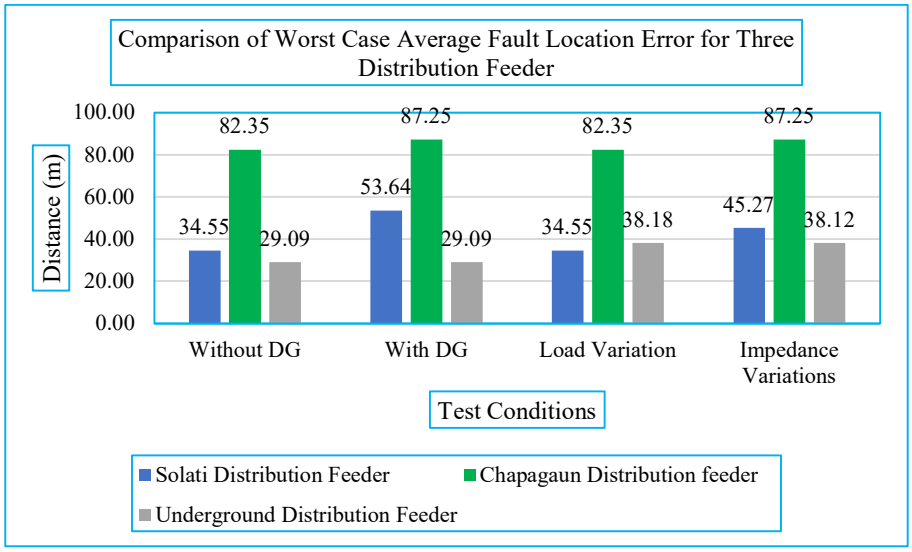

Figure 36: Comparative analysis of worst-case average fault location error in Nepalese distribution feeders

CHAPTER FIVE: CONCLUSION AND RECOMMENDATION

This thesis proposed fault localization and novel classification methodology for distribution feeders using voltage sag data and circuit analysis. The proposed approach integrates OpenDSS and Python to achieve fault type detection while minimizing the need for extensive sensor networks. Additionally, the incorporation of Geographic Information Systems (GIS) enhances fault visualization, aiding in efficient fault restoration.

The methodology is validated using the IEEE 33-bus test system, along with two practical Nepalese distribution feeders—Solati and Chapagaun—and an underground distribution feeder.

The following conclusions have been drawn from the simulation results:

- The developed fault classification approach demonstrates high accuracy under diverse test conditions, effectively classifying fault types and identifying the faulty phase in the network, even with variations in load, distributed generation (DG) penetration, errors in line impedance measurements, and changing fault resistance.
- The fault localization accuracy remains consistent under varying loading conditions.
- Inaccurate impedance measurement data during the modeling of the distribution line negatively impacts the accuracy of fault location.
- The penetration of distributed generation slightly affects the precision of fault location, but both the average and maximum errors remain unchanged. Additionally, fault location accuracy is higher in underground distribution feeders compared to overhead feeders.

The research contributes to improving fault management strategies in Nepal's distribution network by providing an efficient, cost-effective alternative to traditional fault localization methods. Future work can focus on expanding the methodology to enhance the resilience of distribution feeders, improving system reliability by enabling the switching of available tie lines during fault conditions, and developing a self-healing distribution system with advanced control and protection mechanisms.

REFERENCES

[1] Łukasik, Zbigniew and Olczykowski, Zbigniew, Quality and reliability of electricity supply, 2020, pp. 1-6.

[2] Chen, Chen and Wang, Jianhui and Qiu, Feng and Zhao, Dongbo, "Resilient distribution system by microgrids formation after natural disasters," *IEEE Transactions on smart grid,* vol. 7, pp. 958--966, 2015.

[3] Billinton, R. and Salvaderi, L. and McCalley, J.D. and Chao, H. and Seitz, T. and Allan, R.N. and Odom, J. and Fallon, C., "Reliability issues in today's electric power utility environment," *IEEE Transactions on Power Systems,* vol. 12, pp. 1708-1714, 1997.

[4] Majidi, Mehrdad and Etezadi-Amoli, Mehdi, "A new fault location technique in smart distribution networks using synchronized/nonsynchronized measurements," *IEEE Transactions on Power Delivery,* vol. 33, pp. 1358--1368, 2017.

[5] Souhe, Felix Ghislain Yem and Boum, Alexandre Teplaira and Ele, Pierre and Mbey, Camille Franklin and Kakeu, Vinny Junior Foba and others, "Fault detection, classification and location in power distribution smart grid using smart meters data," *Journal of Applied Science and Engineering,* vol. 26, pp. 23--24, 2022.

[6] Jamali, Sadegh and Bahmanyar, Alireza and Bompard, Ettore, "Fault location method for distribution networks using smart meters}," *Measurement,* vol. 102, pp. 150-157, 2017.

[7] Lotfifard, Saeed and Kezunovic, Mladen and Mousavi, Mirrasoul J, "Voltage sag data utilization for distribution fault location," *IEEE Transactions on Power Delivery,* vol. 26, pp. 1239--1246, 2011.

[8] Dong, Yimai and Zheng, Ce and Kezunovic, Mladen, "Enhancing accuracy while reducing computation complexity for voltage-sag-based distribution fault location," *IEEE Transactions on Power Delivery,* vol. 28, pp. 1202--1212, 2013.

[9] Chen, Po-Chen and Malbasa, Vuk and Dong, Yimai and Kezunovic, Mladen, "Sensitivity analysis of voltage sag based fault location with distributed generation," *IEEE Transactions on Smart Grid,* vol. 6, pp. 2098--2106, 2015.

[10] Myeon-Song Choi and Seung-Jae Lee and Duck-Su Lee and Bo-Gun Jin, "A new fault location algorithm using direct circuit analysis for distribution systems," *IEEE Transactions on Power Delivery,* vol. 19, pp. 35-41, 2004.

[11] Trindade, Fernanda C. L. and Freitas, Walmir and Vieira, José C. M., "Fault Location in Distribution Systems Based on Smart Feeder Meters," *IEEE Transactions on Power Delivery,* vol. 19, pp. 251-260, 2014.

[12] Majidi, M. and Arabali, A. and Etezadi-Amoli, M., "Fault Location in Distribution Networks by Compressive Sensing," *IEEE Transactions on Power Delivery,* vol. 30, pp. 1761-1769, 2015.

[13] DP Kothari, IJ Nagratha, Modern Power System Analysis, Chennai: McGraw Hill Education (India) Private Limited, 2016.

[14] Sodin, Denis and Smolnikar, Miha and Rude, Urban and ampa, Andrej, "Precise PMU-based localization and classification of short-circuit faults in power distribution systems," vol. 38, pp. 3262--3273, 2023.

[15] Heine, Pirjo and Lehtonen, Matti, "Voltage sag distributions caused by power system faults," *IEEE Transactions on Power Systems,* vol. 18, pp. 1367-1373, 2003.

[16] Buzo, Ricardo Fonseca and Barradas, Henrique Molina and Le{\~a}o, F{\'a}bio Bertequini, "A new method for fault location in distribution networks based on voltage sag measurements," *IEEE Transactions on Power Delivery,* vol. 36, pp. 651--662, 2020.

[17] Kim, Ji-Soo and Kim, Chul-Hwan and Oh, Yun-Sik and Cho, Gyu-Jung and Song, Jin-Sol, "An Islanding Detection Method for Multi-RES Systems Using the Graph Search Method," *IEEE Transactions on Sustainable Energy,* vol. 11, pp. 2722-2731, 2020.

[18] Thakur, Awnish Kumar and Dharel, Sagar and Bhat, Sher Shingh, "Distribution System Voltage Monitoring and Control Using Smart Meters and Tap Changing Transformers," in *2024 IEEE International Conference on Power System Technology (PowerCon)*, Kathmandu, 2024.

[19] Team, Jupyter Development, "Folium: Python data, leaflet.js maps".

APPENDIX A: DISTRIBUTION FEEDER DATA

A.1 IEEE 33 bus system data

Table 37: Data of existing branches of 33-bus test system

From	To	R(Ω)	X(Ω)	Current Capacity (A)
1	2	0.0922	0.0477	500
2	3	0.493	0.2511	500
3	4	0.366	0.1864	500
4	5	0.3811	0.1941	500
5	6	0.819	0.707	500
6	7	0.1872	0.6188	500
7	8	1.7114	1.2351	500
8	9	1.03	0.74	500
9	10	1.04	0.74	500
10	11	0.1966	0.065	500
11	12	0.3744	0.1238	500
12	13	1.468	1.155	500
13	14	0.5416	0.7129	500
14	15	0.591	0.526	500
15	16	0.7463	0.545	500
16	17	1.289	1.721	500
17	18	0.732	0.574	500
2	19	0.164	0.1565	500
19	20	1.5042	1.3554	500
20	21	0.4095	0.4784	500
21	22	0.7089	0.9373	500
3	23	0.4512	0.3083	500
23	24	0.898	0.7091	500
24	25	0.896	0.7011	500
6	26	0.203	0.1043	500
26	27	0.2842	0.1447	500
27	28	1.059	0.9337	500
28	29	0.8042	0.7006	500
29	30	0.5075	0.2585	500
30	31	0.9744	0.963	500
31	32	0.3105	0.3619	500
32	33	0.341	0.5302	500

Table 38: Data of IEEE 33 bus load at node

Bus Number	Active Power (kW)	Reactive Power (kVar)
1	0	0
2	100	60
3	90	40
4	120	80
5	60	30
6	60	20
7	200	100
8	200	100
9	60	20
10	60	20
11	45	30
12	60	35
13	60	35
14	60	80
15	120	10
16	60	20
17	60	20
18	60	40
19	90	40
20	90	40
21	90	40
22	90	40
23	90	40
24	90	50
25	420	200
26	420	200
27	60	25
28	60	25
29	60	20
30	120	70
31	200	600
32	150	70
33	210	100

A.2 Solati Distribution Feeder Data

Table 39: GIS coordinates of bus in Solati distribution feeder

Bus_Name	Longitude	Latitude
1	85.469879	27.008212
2	85.470307	27.008198
3	85.4714412	27.0080378
4	85.4677258	27.0041479
5	85.46756598	27.00399959
6	85.46739768	27.00407702

7	85.46469853	27.0087986
8	85.46201144	27.01170383
9	85.46241096	27.01243916
10	85.46035296	27.01262806
11	85.452472	27.014242
12	85.4533087	27.0164654
13	85.441841	27.020377
14	85.4414838	27.0211372
15	85.4651526	27.0192582
16	85.4622835	27.0214378
17	85.4609306	27.0229896
18	85.469498	27.0254363
19	85.470336	27.02837
20	85.4769581	27.0417353
21	85.4656378	27.0441602
22	85.46566674	27.04263071
23	85.4618592	27.0454912
24	85.45386377	27.03711309
25	85.4616006	27.045629
26	85.4592507	27.050584
27	85.463892	27.063062
28	85.4577076	27.065986
29	85.4571573	27.0569185
30	85.4570047	27.057
31	85.448195	27.041982
32	85.4373395	27.0506587
33	85.4449472	27.037453
34	85.4315002	27.0408707
35	85.425874	27.032184
36	85.43600221	27.0274315

Table 40: Solati feeder branch data

Line_Name	B1	B2	Length	Units	R(Ω)	X(Ω)	Current Capacity (A)	Type of Conductor
L1	1	2	0.043	km	0.7394	0.3548	193	Rabbit
L2	2	3	0.112	km	0.3724	0.3332	300	Dog
L3	3	4	0.569	km	0.3724	0.3332	300	Dog
L4	4	5	0.022	km	0.7394	0.3548	193	Rabbit
L5	5	6	0.025	km	0.7394	0.3548	193	Rabbit
L6	5	7	0.448	km	0.3724	0.3332	300	Dog

L7	7	8	1.234	km	0.3724	0.3332	300	Dog
L8	8	9	0.09	km	0.7394	0.3548	193	Rabbit
L9	9	10	0.23	km	0.7394	0.3548	193	Rabbit
L10	10	11	0.83	km	0.7394	0.3548	193	Rabbit
L11	11	12	0.256	km	0.7394	0.3548	193	Rabbit
L12	11	13	1.479	km	0.7394	0.3548	193	Rabbit
L13	13	14	0.091	km	0.7394	0.3548	193	Rabbit
L14	9	15	0.808	km	0.3724	0.3332	300	Dog
L15	15	16	0.379	km	0.7394	0.3548	193	Rabbit
L16	16	17	0.2447	km	0.7394	0.3548	193	Rabbit
L17	15	18	0.848	km	0.3724	0.3332	300	Dog
L18	18	19	0.345	km	0.7394	0.3548	193	Rabbit
L19	19	20	1.745	km	0.7394	0.3548	193	Rabbit
L20	20	21	1.168	km	0.7394	0.3548	193	Rabbit
L21	21	22	0.172	km	0.7394	0.3548	193	Rabbit
L22	21	23	0.405	km	0.7394	0.3548	193	Rabbit
L23	23	24	1.174	km	0.7394	0.3548	193	Rabbit
L24	23	25	0.028	km	0.7394	0.3548	193	Rabbit
L25	25	26	0.713	km	0.7394	0.3548	193	Rabbit
L26	26	27	1.552	km	0.7394	0.3548	193	Rabbit
L27	27	28	0.702	km	0.7394	0.3548	193	Rabbit
L28	28	29	1.076	km	0.7394	0.3548	193	Rabbit
L29	29	30	0.017	km	0.7394	0.3548	193	Rabbit
L30	29	31	2.02	km	0.7394	0.3548	193	Rabbit

L31	31	32	1.451	km	0.7394	0.3548	193	Rabbit
L32	31	33	0.645	km	0.7394	0.3548	193	Rabbit
L33	33	34	1.43	km	0.7394	0.3548	193	Rabbit
L34	34	35	1.1176	km	0.7394	0.3548	193	Rabbit
L35	33	36	1.841	km	0.7394	0.3548	193	Rabbit

Table 41: Solati feeder load data

Load_Name	Phases	B1	Voltage (kV)	Model	Active Power (kW)	Reactive Power (kVar)
Seller	3	6	11	1	28	21
Pranami_Mandir	3	8	11	1	56	42
Museli_Tole	3	10	11	1	28	21
Hati_Danda	3	12	11	1	56	42
Rajghat_Nemichowk_Samudayik	3	13	11	1	56	42
Rajghat_Samudayik_Nemichowk	3	14	11	1	56	42
Hati_Danda_Khanepani_Tole	3	16	11	1	56	42
Khanepani_Office	3	17	11	1	14	10.5
Shankarpur1	3	19	11	1	14	10.5
Shankarpur2	3	20	11	1	56	42
Shankarpur3	3	22	11	1	56	42
Shankarpur4	3	24	11	1	56	42
Shankarpur5	3	25	11	1	56	42
Shankarpur6	3	26	11	1	56	42
Murli_Chowk_Rajghat1	3	27	11	1	56	42
Bihani_Chowk2	3	28	11	1	56	42
Doodh_Dairy_Chowk3	3	30	11	1	56	42

Khalte_Chowk	3	31	11	1	56	42
Lalbahadur_Chowk	3	32	11	1	28	21
Newar_Tole	3	34	11	1	28	21
Maane_Mela	3	35	11	1	28	21
Khadka_Tole	3	36	11	1	56	42

A.3 Chapagaun Distribution Feeder

Table 42: GIS coordinates of bus in Chapagaun distribution feeder

Bus	Longitude	Latitude
1	85.32146	27.66537
2	85.32756	27.66233
3	85.32738	27.6622
4	85.32668	27.66167
5	85.32219	27.65698
6	85.32193	27.6558
7	85.31963	27.65371
8	85.3217	27.6509
9	85.32152	27.65104
10	85.32158	27.65072
11	85.32161	27.65064
12	85.32336	27.64907
13	85.31914	27.64378
14	85.31953	27.64373
15	85.3189	27.64305
16	85.31881	27.64296
17	85.31876	27.64189
18	85.31802	27.63972
19	85.31819	27.64
20	85.31914	27.6392
21	85.31924	27.63936
22	85.32043	27.63932
23	85.31938	27.63726
24	85.31917	27.63726
25	85.31952	27.63516
26	85.31926	27.63216
27	85.31895	27.6304
28	85.31921	27.62843
29	85.31732	27.62895
30	85.31941	27.6278

31	85.32115	27.62714
32	85.31961	27.62507
33	85.31937	27.62502
34	85.31937	27.62511
35	85.31956	27.62401
36	85.32272	27.62472
37	85.31919	27.62403
38	85.31906	27.62344
39	85.31781	27.62403
40	85.31488	27.62447
41	85.31563	27.62306
42	85.31297	27.62449
43	85.31306	27.62508
44	85.31267	27.62551
45	85.31128	27.62444
46	85.31146	27.62372
47	85.31069	27.62442
48	85.30979	27.62202
49	85.31859	27.62008
50	85.31906	27.62012
51	85.31789	27.61954
52	85.31983	27.61789
53	85.32299	27.62017
54	85.32585	27.62143
55	85.32668	27.62011
56	85.32926	27.62052
57	85.31993	27.6134
58	85.32237	27.61345
59	85.3253	27.61342
60	85.3199	27.61348
61	85.31972	27.61349
62	85.32071	27.61225
63	85.32021	27.61214
64	85.32252	27.6097
65	85.32419	27.60755
66	85.32284	27.60756
67	85.32582	27.60612
68	85.32597	27.6061
69	85.32816	27.60691
70	85.32731	27.60394
71	85.33052	27.60797
72	85.33505	27.61397
73	85.3377	27.60672
74	85.32531	27.60409
75	85.32487	27.60152
76	85.32459	27.59817

77	85.32457	27.59822
78	85.32392	27.59818
79	85.3235	27.59631
80	85.32281	27.59491
81	85.3228	27.59287
82	85.32221	27.59203
83	85.32224	27.59074
84	85.32157	27.58897
85	85.32195	27.58887
86	85.32197	27.5877
87	85.32206	27.58766
88	85.31917	27.58691
89	85.31903	27.58736
90	85.31303	27.58423
91	85.31523	27.58947
92	85.31528	27.58963
93	85.31576	27.5903
94	85.31932	27.59738
95	85.32681	27.59001
96	85.32494	27.58888
97	85.32712	27.58779
98	85.32761	27.58726
99	85.32946	27.58529
100	85.32983	27.58542
101	85.32942	27.58572
102	85.32922	27.58583
103	85.33356	27.58583
104	85.32557	27.57672
105	85.32982	27.57387
106	85.32783	27.57268
107	85.32524	27.56892
108	85.32294	27.57378
109	85.32326	27.5741
110	85.33063	27.5734
111	85.33074	27.57355
112	85.33487	27.57207
113	85.33818	27.57055
114	85.3403	27.56881
115	85.34872	27.57103
116	85.34159	27.57149
117	85.35447	27.57722
118	85.35319	27.57203
119	85.35379	27.57224
120	85.35286	27.57018
121	85.35045	27.56578
122	85.3537	27.55587

123	85.35773	27.55479
124	85.3689	27.54822
125	85.37993	27.54977
126	85.38	27.54926
127	85.37984	27.5474
128	85.38268	27.54989
129	85.38271	27.54999
130	85.35765	27.55311
131	85.35482	27.54822
132	85.34546	27.54942
133	85.33042	27.55026
134	85.35397	27.53979
135	85.3713	27.53645
136	85.37242	27.53594
137	85.37185	27.53726
138	85.38109	27.53765
139	85.34703	27.53878
140	85.34016	27.53912
141	85.34173	27.53346
142	85.33075	27.53857
143	85.32441	27.52991
144	85.3092	27.5178
145	85.35647	27.52002
146	85.37324	27.51985
147	85.32398	27.57694
148	85.31883	27.57649
149	85.31883	27.57671
150	85.3189	27.57606
151	85.31882	27.5756
152	85.31686	27.5764
153	85.31684	27.57672
154	85.3166	27.57611
155	85.31664	27.57447
156	85.31385	27.57539

Table 43: Chapagaun feeder branch data

LineName	Bus1	Bus2	Length	Resistance	Reactance	Current Rating (A)
L1	1	2	1.59	0.7394	0.3598	193
L2	2	3	0.03	0.7394	0.3598	193
L3	3	4	0.098	0.7394	0.3598	193
L4	2	5	1.59	0.7394	0.3598	193
L5	5	6	0.45	0.7394	0.3598	193
L6	6	7	0.45	0.7394	0.3598	193
L7	7	8	0.39	0.7394	0.3598	193

L8	8	9	0.015	0.7394	0.3598	193
L9	9	10	0.01	0.7394	0.3598	193
L10	8	11	0.39	0.7394	0.3598	193
L11	11	12	0.28	0.7394	0.3598	193
L12	11	13	1.47	0.7394	0.3598	193
L13	13	14	0.05	0.7394	0.3598	193
L14	13	15	1.47	0.7394	0.3598	193
L15	15	16	0.02	0.7394	0.3598	193
L16	15	17	1.47	0.7394	0.3598	193
L17	17	18	1.47	0.7394	0.3598	193
L18	18	19	0.01	0.7394	0.3598	193
L19	18	20	1.47	0.7394	0.3598	193
L20	20	21	0.47	0.7394	0.3598	193
L21	21	22	0.02	0.7394	0.3598	193
L22	21	23	0.47	0.7394	0.3598	193
L23	23	24	0.024	0.7394	0.3598	193
L24	23	25	0.47	0.7394	0.3598	193
L25	25	26	2.8	0.7394	0.3598	193
L26	26	27	0.2	0.7394	0.3598	193
L27	27	28	0.21	0.7394	0.3598	193
L28	28	29	0.27	0.7394	0.3598	193
L29	28	30	0.08	0.7394	0.3598	193
L30	30	31	0.25	0.7394	0.3598	193
L31	30	32	0.31	0.7394	0.3598	193
L32	32	33	0.03	0.7394	0.3598	193
L33	33	34	0.01	0.7394	0.3598	193
L34	32	35	0.12	0.7394	0.3598	193
L35	35	36	0.43	0.7394	0.3598	193
L36	35	37	0.04	0.7394	0.3598	193
L37	37	38	0.11	0.7394	0.3598	193
L38	37	39	0.17	0.7394	0.3598	193
L39	39	40	0.27	0.7394	0.3598	193
L40	40	41	0.19	0.7394	0.3598	193
L41	40	42	0.21	0.7394	0.3598	193
L42	42	43	0.04	0.7394	0.3598	193
L43	43	44	0.06	0.7394	0.3598	193
L44	42	45	0.17	0.7394	0.3598	193
L45	45	46	0.09	0.7394	0.3598	193
L46	45	47	0.04	0.7394	0.3598	193
L47	47	48	0.32	0.7394	0.3598	193
L48	35	49	0.43	0.7394	0.3598	193
L49	49	50	0.05	0.7394	0.3598	193
L50	50	51	0.17	0.7394	0.3598	193

L51	49	52	0.25	0.7394	0.3598	193
L52	52	53	0.43	0.7394	0.3598	193
L53	53	54	0.29	0.7394	0.3598	193
L54	54	55	0.286	0.7394	0.3598	193
L55	55	56	0.33	0.7394	0.3598	193
L56	52	57	0.787	0.7394	0.3598	193
L57	57	58	0.25	0.7394	0.3598	193
L58	58	59	0.329	0.7394	0.3598	193
L59	57	60	0.001	0.7394	0.3598	193
L60	60	61	0.024	0.7394	0.3598	193
L61	57	62	0.15	0.7394	0.3598	193
L62	62	63	0.06	0.7394	0.3598	193
L63	62	64	0.36	0.7394	0.3598	193
L64	64	65	0.29	0.7394	0.3598	193
L65	65	66	0.14	0.7394	0.3598	193
L66	65	67	0.235	0.7394	0.3598	193
L67	67	68	0.016	0.7394	0.3598	193
L68	68	69	0.245	0.7394	0.3598	193
L69	69	70	0.345	0.7394	0.3598	193
L70	69	71	0.27	0.7394	0.3598	193
L71	71	72	0.397	0.7394	0.3598	193
L72	71	73	0.752	0.7394	0.3598	193
L73	67	74	0.231	0.7394	0.3598	193
L74	74	75	0.305	0.7394	0.3598	193
L75	75	76	0.308	0.7394	0.3598	193
L76	76	77	0.308	0.7394	0.3598	193
L77	76	78	0.277	0.7394	0.3598	193
L78	78	79	0.002	0.7394	0.3598	193
L79	78	80	0.229	0.7394	0.3598	193
L80	80	81	0.1	0.7394	0.3598	193
L81	81	82	0.07	0.7394	0.3598	193
L82	81	83	0.178	0.7394	0.3598	193
L83	83	84	0.243	0.7394	0.3598	193
L84	84	85	0.05	0.7394	0.3598	193
L85	84	86	0.189	0.7394	0.3598	193
L86	86	87	0.012	0.7394	0.3598	193
L87	86	88	0.454	0.7394	0.3598	193
L88	88	89	0.0525	0.7394	0.3598	193
L89	88	90	0.773	0.7394	0.3598	193
L90	90	91	0.671	0.7394	0.3598	193
L91	91	92	0.017	0.7394	0.3598	193
L92	92	93	0.092	0.7394	0.3598	193
L93	93	94	0.861	0.7394	0.3598	193

L94	78	95	0.799	0.7394	0.3598	193
L95	95	96	0.252	0.7394	0.3598	193
L96	95	97	0.252	0.7394	0.3598	193
L97	97	98	0.41	0.7394	0.3598	193
L98	98	99	0.01	0.7394	0.3598	193
L99	99	100	0.05	0.7394	0.3598	193
L100	100	101	0.06	0.7394	0.3598	193
L101	101	102	0.03	0.7394	0.3598	193
L102	100	103	0.474	0.7394	0.3598	193
L103	99	104	1.305	0.7394	0.3598	193
L104	104	105	0.542	0.7394	0.3598	193
L105	105	106	0.263	0.7394	0.3598	193
L106	106	107	0.582	0.7394	0.3598	193
L107	106	108	0.453	0.7394	0.3598	193
L108	108	109	0.088	0.7394	0.3598	193
L109	105	110	0.125	0.7394	0.3598	193
L110	110	111	0.025	0.7394	0.3598	193
L111	110	112	0.507	0.7394	0.3598	193
L112	112	113	0.444	0.7394	0.3598	193
L113	113	114	0.334	0.7394	0.3598	193
L114	113	115	0.661	0.7394	0.3598	193
L115	115	116	0.154	0.7394	0.3598	193
L116	115	117	1.538	0.7394	0.3598	193
L117	117	118	0.691	0.7394	0.3598	193
L118	118	119	0.071	0.7394	0.3598	193
L119	118	120	0.245	0.7394	0.3598	193
L120	120	121	0.954	0.7394	0.3598	193
L121	121	122	1.474	0.7394	0.3598	193
L122	122	123	0.39	0.7394	0.3598	193
L123	123	124	1.73	0.7394	0.3598	193
L124	124	125	1.47	0.7394	0.3598	193
L125	125	126	0.03	0.7394	0.3598	193
L126	126	127	0.25	0.7394	0.3598	193
L127	126	128	0.27	0.7394	0.3598	193
L128	123	129	0.78	0.7394	0.3598	193
L129	129	130	0.04	0.7394	0.3598	193
L130	130	131	0.89	0.7394	0.3598	193
L131	131	132	0.05	0.7394	0.3598	193
L132	131	133	1.64	0.7394	0.3598	193
L133	130	134	0.96	0.7394	0.3598	193
L134	134	135	1.84	0.7394	0.3598	193
L135	135	136	0.19	0.7394	0.3598	193
L136	136	137	0.13	0.7394	0.3598	193

L137	136	138	1.1	0.7394	0.3598	193
L138	134	139	0.72	0.7394	0.3598	193
L139	139	140	0.7	0.7394	0.3598	193
L140	140	141	0.6	0.7394	0.3598	193
L141	140	142	1.19	0.7394	0.3598	193
L142	142	143	1.3	0.7394	0.3598	193
L143	143	144	0.43	0.7394	0.3598	193
L144	134	145	1.4	0.7394	0.3598	193
L145	145	146	0.3	0.7394	0.3598	193
L146	104	147	0.179	0.7394	0.3598	193
L147	147	148	0.586	0.7394	0.3598	193
L148	148	149	0.038	0.7394	0.3598	193
L149	148	150	0.055	0.7394	0.3598	193
L150	150	151	0.06	0.7394	0.3598	193
L151	148	152	0.219	0.7394	0.3598	193
L152	152	153	0.042	0.7394	0.3598	193
L153	152	154	0.044	0.7394	0.3598	193
L154	154	155	0.189	0.7394	0.3598	193
L155	155	156	0.322	0.7394	0.3598	193

Table 44: Chapagaun distribution feeder load data

Name	Phases	Bus	kV	kW	kVar	Model
Accountant	3	3	11	104.85	78.64	1
Dhalout_Karyasala	3	4	11	26.21	19.66	1
Safa_Charging_Services	3	5	11	10.48	7.86	1
Tutepani	3	6	11	31.45	23.59	1
Laproshay	3	7	11	20.97	15.73	1
a	3	9	11	26.21	19.66	1
Ullens	3	10	11	10.48	7.86	1
Ullens_Agadi	3	11	11	10.48	7.86	1
Shushil_Nepal	3	12	11	10.48	7.86	1
Meat_Product	3	14	11	10.48	7.86	1
Good_Life	3	16	11	10.48	7.86	1
Sarma_ko_Pasal	3	17	11	5.24	3.93	1
Mahalakshmi_Trade	3	19	11	10.48	7.86	1
Dohalhity_Ukalo	3	18	11	20.97	15.73	1
Dohalhity_Bari	3	20	11	5.24	3.93	1
b	3	22	11	20.97	15.73	1
National_Food_Product	3	24	11	10.48	7.86	1
Simiko1	3	25	11	10.48	7.86	1
Simiko2	3	25	11	20.97	15.73	1
Aare	3	26	11	20.97	15.73	1

Balkumari	3	27	11	10.48	7.86	1
Valley_Home	3	29	11	20.97	15.73	1
Wokhat	3	31	11	10.48	7.86	1
Bangedhara	3	33	11	16.78	12.58	1
OmFood	3	34	11	20.97	15.73	1
Okhat	3	36	11	10.48	7.86	1
Techo	3	38	11	10.48	7.86	1
Suman_Academi	3	39	11	2.62	1.97	1
Techo_Housing_Muni	3	41	11	10.48	7.86	1
Nakhukhola	3	43	11	5.24	3.93	1
China_Long_Food	3	44	11	15.73	11.80	1
Dhalekshwor_Mahadeb	3	46	11	52.42	39.32	1
Appolo_Precast	3	48	11	15.73	11.80	1
Techo_Health	3	50	11	10.48	7.86	1
Bethegal	3	51	11	10.48	7.86	1
Dhapakhel_Chowk	3	52	11	20.97	15.73	1
Add_New1	3	53	11	10.48	7.86	1
Boldaya_School	3	54	11	10.48	7.86	1
New_ADD	3	55	11	20.97	15.73	1
Bethegal2	3	56	11	10.48	7.86	1
Guhe_Tole	3	60	11	20.97	15.73	1
Guhe_Tole1	3	61	11	10.48	7.86	1
Sarswati_School	3	58	11	10.48	7.86	1
Durikhel_Mandir	3	59	11	10.48	7.86	1
Mandir_Agadi	3	63	11	20.97	15.73	1
Kuwar_Gau	3	64	11	10.48	7.86	1
Ticho_Chapagaun_Road	3	66	11	20.97	15.73	1
Pode_Tole	3	67	11	15.73	11.80	1
Pode_Tole1	3	68	11	10.48	7.86	1
Bajara_Bahari_Mandir	3	70	11	10.48	7.86	1
Bajara_Bahari_Pokhari	3	71	11	10.48	7.86	1
Dhusufat	3	72	11	10.48	7.86	1
Pokhari_Tar	3	73	11	10.48	7.86	1
Bulu_Sectionalizer	3	74	11	2.62	1.97	1
Bulu_Danda	3	75	11	10.48	7.86	1
Tel_Mill	3	75	11	10.48	7.86	1
Unknown	3	77	11	20.97	15.73	1
Pyangaun	3	76	11	10.48	7.86	1
Takhel_Samudayik	3	79	11	10.48	7.86	1
c	3	80	11	20.97	15.73	1
Private_Biscuit	3	82	11	10.48	7.86	1
Takhel	3	83	11	15.73	11.80	1
Nav_Pravat	3	85	11	104.85	78.64	1

Takhel_KhanePani	3	86	11	10.48	7.86	1
Kukl	3	87	11	10.48	7.86	1
Subha_Road	3	89	11	10.48	7.86	1
Kathmandu_Khanepani	3	91	11	2.62	1.97	1
Charghar_Serafat	3	92	11	5.24	3.93	1
Prakritu_Jadibuti	3	93	11	10.48	7.86	1
Serafat	3	94	11	10.48	7.86	1
Jivnashwor	3	95	11	10.48	7.86	1
Takhel1	3	96	11	10.48	7.86	1
Purano_Road_Dhunga	3	97	11	10.48	7.86	1
Khajuriko_Nepal	3	98	11	62.91	47.18	1
Khanepani_Pump_House	3	101	11	10.48	7.86	1
Mundola_KhanePani	3	102	11	2.62	1.97	1
Mundol	3	103	11	5.24	3.93	1
Dugdha_Bikash	3	105	11	5.24	3.93	1
Thapagaun	3	107	11	10.48	7.86	1
NEA_Chinese	3	108	11	31.45	23.59	1
Attax_PVT	3	109	11	15.73	11.80	1
Lele_Bazar	3	112	11	20.97	15.73	1
Tileshwor_Mahadeb	3	114	11	5.24	3.93	1
Nepal_Telecome	3	116	11	2.62	1.97	1
Mahal_Gau	3	117	11	10.48	7.86	1
Kavre_Gau	3	119	11	5.24	3.93	1
Lele_Kavre	3	120	11	10.48	7.86	1
Sauraha_Bhayang	3	121	11	10.48	7.86	1
Nallu_Bhayang	3	122	11	5.24	3.93	1
Suire	3	124	11	5.24	3.93	1
Bhardeu_Bhalukhola	3	125	11	2.62	1.97	1
Loepakha	3	127	11	2.62	1.97	1
Pauwachaur	3	128	11	2.62	1.97	1
Konjyosom	3	128	11	5.24	3.93	1
SundarPani	3	129	11	2.62	1.97	1
Devisthan	3	132	11	10.48	7.86	1
Tallo_Nallu	3	133	11	2.62	1.97	1
Bhagh_Bhairab	3	135	11	2.62	1.97	1
Deurali	3	135	11	2.62	1.97	1
Ncell	3	137	11	2.62	1.97	1
SimbalBhanjyang	3	138	11	2.62	1.97	1
Chaughare_Sir_Danda	3	139	11	1.57	1.18	1
Siru_Danda	3	141	11	2.62	1.97	1
Dalchoki	3	142	11	2.62	1.97	1
Bhot_Danda	3	143	11	2.62	1.97	1
Kholmchaur	3	144	11	2.62	1.97	1

Thosne_Khola	3	146	11	2.62	1.97	1
Foidal_Nea	3	147	11	10.48	7.86	1
Himalyan_Road_Udhyog	3	149	11	16.78	12.58	1
Fulchowki_Chun_Dhunga	3	150	11	26.21	19.66	1
National_Biotech	3	151	11	10.48	7.86	1
Shree_Krishna_Oxygen	3	153	11	52.42	39.32	1
Leprosy_Hospital	3	154	11	10.48	7.86	1
Hospital_Gate_Lele	3	155	11	10.48	7.86	1
Tika_Bhairav_Bazar	3	156	11	10.48	7.86	1

APPENDIX B: PYTHON PROGRAM FOR SYSTEM MODELING

A.1 Python Code for System Modeling

```
import py_dss_interface
import pandas as pd
# Creating variable for storing operational parameter data
busdata = pd.read_excel(r"D:\Academic\0.MSc_Thesis_Awnish\4. Simulation_File\2.
Solatte_Distribution_Feeder\Solati_Feeder\0.
SOLTI_FEEDER_SYSTEM_DATA.xlsx", sheet_name='Bus_Coord')
loaddata = pd.read_excel(r"D:\Academic\0.MSc_Thesis_Awnish\4.
Simulation_File\2. Solatte_Distribution_Feeder\Solati_Feeder\0.
SOLTI_FEEDER_SYSTEM_DATA.xlsx", sheet_name='Load_Data')
linedata = pd.read_excel(r"D:\Academic\0.MSc_Thesis_Awnish\4. Simulation_File\2.
Solatte_Distribution_Feeder\Solati_Feeder\0.
SOLTI_FEEDER_SYSTEM_DATA.xlsx", sheet_name='Line_Data')
# Interfacing with OpenDSS
dss = py_dss_interface.DSSDLL()
dss_file = r"D:\Academic\0.MSc_Thesis_Awnish\4. Simulation_File\2.
Solatte_Distribution_Feeder\Solati_Feeder\01complete_system.dss"
# New Generator.DG1 phases = 3 bus1 = 35 kW = 640 kVAr = 480 pf=0.8
# Main file coding
runfile_content = f"""
clear
New Circuit.Solati_Feeder BasekV=11 Bus1=1 Phases=3 pu=1.0 R1=0.01 X1=0.03
R0=0.01 X0=0.03
Redirect 02complete_system_line.dss
Redirect 03complete_system_load.dss
New EnergyMeter.Feeder Line.L1 terminal=1
set voltagebase=11
CalcVoltagebases
Set Mode=Dyanamic
BusCoords Bus_Coord.CSV
"""
```

```
with open(dss_file, 'w') as f:
    f.write(runfile_content)
# Defining Load at different buses
Load_Commands = []
for _, row in loaddata.iterrows():
    Load_Commands.append(f"new Load.{row['Load_Name']} "
                         f"Phases={row['Phases']} "
                         f"Bus1={row['B1']} "
                         f"kV={row['Voltage (kV)']} "
                         f"Model={row['Model']} "
                         f"kw={row['Active Power (kW)']} "
                         f"kvar={row['Reactive Power (kVar)']} ")
with open(r"D:\Academic\0.MSc_Thesis_Awnish\4. Simulation_File\2.
Solatte_Distribution_Feeder\Solati_Feeder\03complete_system_load.dss", 'w') as f:
    f.write('\n'.join(Load_Commands))
# Defining Line between different buses
Line_Commands = []
for _, row in linedata.iterrows():
    Line_Commands.append(f"new Line.{row['Line_Name']} "
                         f"Bus1 = {row['B1']} "
                         f"Bus2 = {row['B2']} "
                         f"length = {row['Length']} "
                         f"units = {row['Units']} "
                         f"r = {row['R(Ω)']} "
                         f"x = {row['X(Ω)']} "
                         f"emergamp = {row['Current Capacity (A)']} ")
with open(r"D:\Academic\0.MSc_Thesis_Awnish\4. Simulation_File\2.
Solatte_Distribution_Feeder\Solati_Feeder\02complete_system_line.dss", 'w') as f:
    f.write('\n'.join(Line_Commands))
# Compiling main file
dss.text(f"compile [{dss_file}]")
dss.text('solve')
```

A.2 Python Code for Formation of Subsystem

```
import win32com.client
from collections import defaultdict, deque
import os
# Initializing OpenDSS
dssObj = win32com.client.Dispatch("OpenDSSEngine.DSS")
if not dssObj.Start(0):
    print("Unable to start the OpenDSS engine.")
    exit()
# Define command objects
dsstext = dssObj.Text
dsscircuit = dssObj.ActiveCircuit
dsssolution = dsscircuit.Solution
dssbus = dsscircuit.ActiveBus
dssline = dsscircuit.Lines
# Main file loading program
circuit_file = r"D:\Academic\0.MSc_Thesis_Awnish\4. Simulation_File\2.
Solatte_Distribution_Feeder\Solati_Feeder\01complete_system.dss"
# Redirect to main.dss
dsstext.Command = f'Redirect "{circuit_file}"'
# Solve the circuit
dsssolution.Solve()
if dsssolution.Converged:
    print("Load flow analysis completed successfully!")
else:
    print("Load flow analysis did not converge.")
# Extract bus connections
bus_connections = defaultdict(set)
line_data = {}
dssline.First
while True:
    bus1 = dssline.Bus1.split(".")[0]
    bus2 = dssline.Bus2.split(".")[0]
```

```
    bus_connections[bus1].add(bus2)
    bus_connections[bus2].add(bus1)
    line_data[(bus1,bus2)] = f"New Line.{dssline.Name} Bus1={bus1} Bus2={bus2}
Length={dssline.Length} R1={dssline.R1} X1={dssline.X1}"
    line_data[(bus2, bus1)] = line_data[(bus1, bus2)]
    if not dssline.Next:
        break
root_node = str(1)
print(f"Root Node: {root_node}")
# Extract leaf nodes and convert to integers
leaf_nodes = sorted({int(bus) for bus, connections in bus_connections.items() if
len(connections) == 1})
# Remove root_node (ensure it is treated as an integer)
leaf_nodes = [bus for bus in leaf_nodes if bus != int(root_node)]
# Convert back to string for OpenDSS
leaf_nodes = [str(bus) for bus in leaf_nodes]
print("Last nodes of all branches (leaf buses):", leaf_nodes)
# Function to find the shortest path using BFS
def shortest_path(start, end):
    queue = deque([[start]])
    visited = set()
    while queue:
        path = queue.popleft()
        node = path[-1]
        if node == end:
            return path
        if node not in visited:
            visited.add(node)
            for neighbor in bus_connections[node]:
                new_path = list(path)
                new_path.append(neighbor)
                queue.append(new_path)
    return []
```

```
# Create subsystems
output_dir = r"D:\Academic\0.MSc_Thesis_Awnish\4. Simulation_File\2.
Solatte_Distribution_Feeder\Solati_Feeder"
os.makedirs(output_dir, exist_ok=True)
for i, last_node in enumerate(leaf_nodes):
    path = shortest_path(root_node, last_node)
    if not path:
        print(f"Warning: No path found from {root_node} to {last_node}")
        continue
    sub_lines = []
    for j in range(len(path) - 1):
        bus1, bus2 = path[j], path[j + 1]
        if (bus1, bus2) in line_data:
            sub_lines.append(line_data[(bus1, bus2)])
    sub_file = os.path.join(output_dir, f"Subsystem{i}_line.dss")
    with open(sub_file, "w") as f:
        for line in sub_lines:
            f.write(line + "\n")
print("All subsystems created successfully!")
```

A.3 Python Code for Fault Localization and Classifications

```
import win32com.client
import matplotlib.pyplot as plt
import numpy as np
from math import  *
import pandas as pd
from openpyxl import load_workbook
from datetime import datetime
import subprocess
import time
import folium
from folium.plugins import AntPath
```

```
from folium.plugins import PolyLineTextPath
from folium import PolyLine
subprocess.run(["Python","Full_System_Creation.py"])
subprocess.run(["Python","Subsystem_Creation.py"])
dssObj = win32com.client.Dispatch("OpenDSSEngine.DSS")
if not dssObj.Start(0):
   print("Unable to start the Opendss engine.")
   exit()
dsstext = dssObj.Text
dsscircuit = dssObj.ActiveCircuit
dsssolution = dsscircuit.Solution
dsselm = dsscircuit.ActiveCktElement
dssbus = dsscircuit.ActiveBus
dssline = dsscircuit.Lines
subsystem_lines = []
subsystem_ymatrix = []
subsystem_zmatrix = []
subsystem_bus_names = []
number_of_subsystem = 10
total_start_time = time.time()
fault_data = []
def get_system_matirx():
   Y_tuple = dsscircuit.SystemY
   num_buses = np.asarray(dsscircuit.NumBuses)
   All_buses = np.array(dsscircuit.AllBusNames)
   Y_matrix = np.zeros((num_buses*3, num_buses*3), dtype=complex)
   index_count = 0
   for i in range(num_buses*3):
      for j in range(num_buses*3):
         Y_matrix[i, j] = complex(Y_tuple[index_count], Y_tuple[index_count+1])
         index_count += 2
   Z_matrix = np.linalg.inv(Y_matrix)
   return Y_matrix, Z_matrix, All_buses
```

```
def Calcualte_systembusvoltage ():
    systembus_voltage = []
    for i in range(len(subsystem_bus_names)):
        bus_voltage = []
        for j in range(len(subsystem_bus_names[i])):
            bus_voltage_phase = np.zeros((3,1), dtype=complex)
            dsscircuit.SetActiveBus(subsystem_bus_names[i][j])
            Voltage = dssbus.Voltages
            lc = 0
            for k in range (3):
                bus_voltage_phase[k]= complex(Voltage[lc], Voltage[lc+1])
                lc += 2
            bus_voltage.append(bus_voltage_phase)
        systembus_voltage.append(bus_voltage)
    return systembus_voltage
def Calculate_voltage_diff(pref, during_fault):
    volt_del = []
    for i in range (len(pref)):
        v_delta = []
        for j in range (len(pref[i])):
            voltage_diff = pref[i][j] - during_fault[i][j]
            v_delta.append(voltage_diff)
        volt_del.append (v_delta)
    return volt_del
# Defining function for calculating lines connected to faulted buses:
def find_lines_connected_to_bus(bus_name):
    connected_lines = []
    dssline.First # Start iterating over lines
    while True:
        line_name = dssline.Name  # Get the current line name
        bus1 = dssline.Bus1.split('.')[0]
        bus2 = dssline.Bus2.split('.')[0]
        if bus_name in [bus1, bus2]:  # Check if the bus is connected
            connected_lines.append(line_name)
```

```
        if not dssline.Next:  # Move to the next line; exit if no more lines
            break
    return connected_lines
# Obtain the y matrix of subsystem 0 ( the one with pmu)
dsstext.command = r"compile 'Subsystem_main.dss'"
dsstext.command = r"Redirect subsystem0_2portequivalent.dss"
dsssolution.Solve()
system_matrix = get_system_matirx()
Y_matrix_two_port_equivalent = system_matrix [0]
for iter in range(number_of_subsystem):
    dsstext.command = r"compile 'Subsystem_main.dss'"
    dsstext.command = r"Redirect subsystem"+str(iter)+"_line.dss"
    dsssolution.Solve()
    system_matrix = get_system_matirx()
    [Y_matrix, Z_matrix, allbuses] = system_matrix
    subsystem_ymatrix.append(Y_matrix)
    subsystem_zmatrix.append(Z_matrix)
    subsystem_bus_names.append(allbuses)
print('Z bus calculation finished')
# Function for Finding Fault Classification Approach
def classify_fault(IAP, IBP, ICP):
    # Fault classification logic
    if IAP < 1e-5 and IBP < 1e-5 and ICP < 1e-5:
        print("Classification: Three-Phase to Ground Fault (LLLG)")
    elif abs(IAP - (IBP + ICP)) < 1e-6 and IAP > 1.5:
        print("Classification: Single Line-to-Ground Fault (Phase A)")
    elif abs(IBP - (IAP + ICP)) < 1e-6 and IBP > 1.5:
        print("Classification: Single Line-to-Ground Fault (Phase B)")
    elif abs(ICP - (IAP + IBP)) < 1e-6 and ICP > 1.5:
        print("Classification: Single Line-to-Ground Fault (Phase C)")
    elif IAP > 0.95 or IBP > 0.95 or ICP > 0.95:
        if IAP > 0.95:
            print("Classification: Double Line Fault (Phases B and C)")
```

```
        elif IBP > 0.95:
            print("Classification: Double Line Fault (Phases A and C)")
        elif ICP > 0.95:
            print("Classification: Double Line Fault (Phases A and B)")
    else:
        print("Classification: No Fault Detected")
    print("=" * 60 + "\n")
def print_fault_summary(actual_bus, calculated_bus, faulted_subsystem,
iteration_time, faulted_bus_distance):
    print("\n" + "=" * 60)
    print("Fault Localization Summary")
    print("=" * 60)
    print(f"{'Fault Simulated Node:':<25} {actual_bus}")
    print(f"{'Fault Calculated Node:':<25} {calculated_bus}")
    print(f"{'Faulted Subsystem:':<25} {faulted_subsystem}")
    print(f"{'Fault Localization Time:':<25} {iteration_time:.4f} seconds")
    print(f"{'Calculated Distance from Substation (km):':<25}
{faulted_bus_distance}")
    print("=" * 60 + "\n")
# Get the during Pre-fault voltage of the buses
dsstext.command = r"compile '01complete_system.dss'"
dsssolution.Solve()
complete_system_all_buses = np.array(dsscircuit.AllBusNames)
Prefault_systembusvoltage = Calcualte_systembusvoltage()
# Load bus coordinates from Excel file
bus_coords = pd.read_csv(r"D:\Academic\0.MSc_Thesis_Awnish\4.
Simulation_File\2. Solatte_Distribution_Feeder\Solati_Feeder\Bus_Coord.csv")
# Load line shapefiles
line_data = pd.read_excel(r"D:\Academic\0.MSc_Thesis_Awnish\4.
Simulation_File\2. Solatte_Distribution_Feeder\Solati_Feeder\Line_Data.xlsx")
line_data = line_data.merge(bus_coords[['Bus_Name', 'Lattitude', 'Longitude']],
how='left', left_on='Bus_1', right_on='Bus_Name')
line_data = line_data.rename(columns={'Latitude': 'Latitude_bus1', 'Longitude':
'Longitude_bus1'})
```

```
line_data = line_data.merge(bus_coords[['Bus_Name', 'Lattitude', 'Longitude']],
how='left', left_on='Bus_2', right_on='Bus_Name')
line_data = line_data.rename(columns={'Latitude': 'Latitude_bus2', 'Longitude':
'Longitude_bus2'})
# Defining colour to faulted buses
def bus_to_color(bus, faulted_bus):
    try:
        bus = int(float(bus))
        faulted_bus = int(float(faulted_bus))  # Convert faulted bus to int
    except ValueError:
        bus = str(bus).strip()  # Handle non-numeric cases
        faulted_bus = str(faulted_bus).strip()
    if bus == faulted_bus:
        return "red"  # Faulted bus color
    else:
        return "white"
distances = {}
for bus in dsscircuit.AllBusNames:
    dsscircuit.SetActiveBus(bus)
    distance = dssbus.Distance
    distances[bus] = round(distance,2)
df = pd.DataFrame(list(distances.items()), columns=["Bus Name", "Distance (km)"])
df.to_excel("Bus_Distance.xlsx", index=False, sheet_name="Bus Distances")
for senerio in complete_system_all_buses:
    iteration_start_time = time.time()
    dsstext.command = r"compile '01complete_system.dss'"
    dsstext.command = r"New Fault.F1 Bus1 = " + str(senerio) + " phases = 1 r=100.0"
    dsssolution.Solve()
    faulted_systembusvoltage = Calcualte_systembusvoltage()
    delta_voltage = Calculate_voltage_diff(Prefault_systembusvoltage,
faulted_systembusvoltage)
    arranged_voltage = np.zeros((3*len(subsystem_bus_names[0]), 1), dtype =
complex)
    arranged_count = 0
```

```
    for i in range(len(delta_voltage[0])):
        for j in range(len(delta_voltage[0][i])):
            arranged_voltage[arranged_count] = delta_voltage[0][i][j]
            arranged_count += 1
    fault_del_v = np.zeros((6,1), dtype=complex)
    for i in range(int(len(fault_del_v)/2)):
        fault_del_v[i] = arranged_voltage[i]
        fault_del_v[len(fault_del_v)-i-1] = arranged_voltage[len(arranged_voltage)-1-i]
    current = Y_matrix_two_port_equivalent @ fault_del_v
    fault_current = np.zeros((3,1),dtype=complex)
    for i in range(int(len(current)/2)):
        fault_current[i] = current[i] + current[i+3]
    Phase_A_Current = abs(fault_current[0])
    Phase_B_Current = abs(fault_current[1])
    Phase_C_Current = abs(fault_current[2])
    Mean_Current_Ampere =
(Phase_A_Current+Phase_B_Current+Phase_C_Current)/3
    IAP = abs(((Phase_A_Current - Mean_Current_Ampere)/Mean_Current_Ampere))
    IBP = abs(((Phase_B_Current - Mean_Current_Ampere) /
Mean_Current_Ampere))
    ICP = abs(((Phase_C_Current - Mean_Current_Ampere) /
Mean_Current_Ampere))
    error_matrix = []
    for a in range(number_of_subsystem):
        cc=0
        calc_v_diff = np.zeros((len(subsystem_bus_names[a]), 1))
        for i in range(len(subsystem_bus_names[a])):
            temp_current = np.zeros((len(subsystem_bus_names[a])*3, 1),
dtype=complex)
            temp_current[cc] = fault_current[0]
            temp_current[cc+1] = fault_current[1]
            temp_current[cc+2] = fault_current[2]
            calc_v = subsystem_zmatrix[a] @  temp_current
            cc += 3
```

```
            ad = abs(abs(delta_voltage[a][len(subsystem_bus_names[a])-1][0]) -
abs(calc_v[-3]))
            ad1 = abs(abs(delta_voltage[a][len(subsystem_bus_names[a])-1][1]) -
abs(calc_v[-2]))
            ad2 = abs(abs(delta_voltage[a][len(subsystem_bus_names[a])-1][2]) -
abs(calc_v[-1]))
            calc_v_diff[i] = (ad + ad1 + ad2)
        error_matrix.append(calc_v_diff)
    # Formulation of vector 'X'
    X = []
    for i in range(number_of_subsystem):
        min_index = np.argmin(error_matrix[i])
        X.append(subsystem_bus_names[i][min_index])
    # Formulation of vector 'Y'
    Y = []
    for i in X:
        duplication_number = 0
        for j in subsystem_bus_names:
            for k in j:
                if k == i:
                    duplication_number += 1
        Y.append(duplication_number)
    # Formulation of vector 'J'
    J = []
    for i in X:
        occurance = X.count(i)
        J.append(occurance)
    # Formulation of vector 'W'
    W = np.divide(J,Y)
    # Get the candidate faulted bus
    Faulted_subsystem = np.argmax(W)
    Faulted_bus = X[Faulted_subsystem]
    Faulted_bus_distance = distances[Faulted_bus]
    Simulated_bus_distance = distances[senerio]
```

```
    # Store fault information in a list
    timestamp = datetime.now().strftime("%Y-%m-%d %H:%M:%S")
    iteration_time = time.time() - iteration_start_time
    fault_data.append([timestamp, senerio, Faulted_bus, Faulted_subsystem,
iteration_time, Simulated_bus_distance, Faulted_bus_distance])
    print_fault_summary(senerio, Faulted_bus, Faulted_subsystem, iteration_time,
Faulted_bus_distance)
    classify_fault(IAP, IBP, ICP)
    subsystems_with_faulted_bus = set()
    for i in range (number_of_subsystem):
        if Faulted_bus in subsystem_bus_names[i]:
            subsystems_with_faulted_bus.add(i)
    m = folium.Map(location=[bus_coords['Lattitude'].mean(),
bus_coords['Longitude'].mean()], zoom_start=13.48,
                   width='100%', height='120%')
    fault_given_row = bus_coords[bus_coords["Bus_Name"] == float(senerio)]
    fault_calculated_row = bus_coords[bus_coords["Bus_Name"] ==
float(Faulted_bus)]
    fault_given_lat = fault_given_row.iloc[0]["Lattitude"]
    fault_given_lon = fault_given_row.iloc[0]["Longitude"]
    fault_calculated_lat = fault_calculated_row.iloc[0]["Lattitude"]
    fault_calculated_lon = fault_calculated_row.iloc[0]["Longitude"]
    folium.CircleMarker(location=(fault_given_lat, fault_given_lon),
                        radius=8,
                        color="red",
                        fill=True,
                        fill_color="red",
                        fill_opacity=0.7,
                        popup=folium.Popup(f"Fault Simulated Distance (km) from
Substation: {Simulated_bus_distance}", parse_html=True)
                        ).add_to(m)
    # Plot Fault Calculated Node
    folium.CircleMarker(location=(fault_calculated_lat, fault_calculated_lon),
                        radius=4,
```

```
                color="blue",
                fill=True,
                fill_color="blue",
                fill_opacity=0.7,
                popup=folium.Popup(f"Fault Calculated Distance (km) from
Substation: {Faulted_bus_distance}", parse_html=True)
                ).add_to(m)
    # Plot the lines
    for _, row in line_data.iterrows():
        line = PolyLine(locations=[(row['Lattitude_x'], row['Longitude_bus1']),
(row['Lattitude_y'], row['Longitude_bus2'])],
            color='gray',
            weight=2,
            tooltip=row['Line_Name']
        )
        line.add_to(m)
    legend_html = f'''
        <div style="position: fixed;
                top: 10px; left: 40px; width: auto; padding: 5px;
                border:2px solid grey; z-index:9999; font-size:14px;
                background-color: white;">
            <b>Simulation Timestamp:</b> <br>
            {timestamp}
        </div>
        <div style="position: fixed;
                top: 10px; right: 10px; width: 250px; height: 90px;
                border:2px solid grey; z-index:9999; font-size:14px;
                background-color: white;">
              <b> FAULT LOCALIZATION WINDOW </b> <br>
              <b> LEGENDS </b> <br>
             Simulated Fault Node   <span style="display: inline-block;
width: 15px; height: 15px; background-color: red; border-radius: 50%;"></span><br>
             Calculated Fault Node   <span style="display: inline-block;
width: 15px; height: 15px; background-color: blue; border-radius: 50%;"></span>
```

```
        </div>
    '''
    m.get_root().html.add_child(folium.Element(legend_html))
    # Save the map as an HTML file
    m.save(f'Fault_Visualization_{senerio}.html')
# Save the fault data to an Excel file
fault_df = pd.DataFrame(fault_data, columns=["Timestamp", "Fault Simulated Node", "Fault Calculated Node", "Faulted Subsystem", "Execution_Time","Simulated Distance (km)","Calculated Distance (km)"])
fault_df.to_excel("Fault_Information.xlsx", index=False)
```

APPENDIX C: PUBLICATION


[IOEGC16] Editor Decision Inbox x

Suwarna Lingden <conference-noreply@ioe.edu.np> Sun 6 Apr, 02:01

to me

Awnish Kumar Thakur Thakur:

We are pleased to inform you that your manuscript titled "A Robust Method of Fault Classification and Localization in Nepalese Distribution System" submitted to 16th IOE Graduate Conference is **Accepted** for presentation in the Conference as well as inclusion in the Peer-Reviewed Proceedings. Please note that inclusion in hard copy proceedings is contingent upon your timely response to further edits, if any, during the publication process.

With Warm Regards,
IOEGC-16 Editorial Team

Figure 37: Confirmation email of paper acceptance

APPENDIX D: PLAGRISM TEST REPORT

Awnish Kumar Thakur

Fault Localization and Classification in Distribution Feeder Utilizing Voltage Sag Data

Tribhuvan University

Document Details

Submission ID
trn:oid:::3117:445492746

Submission Date
Apr 4, 2025, 12:34 AM GMT+5:45

Download Date
Apr 21, 2025, 9:40 PM GMT+5:45

File Name
MSc_Thesis_Awnish.docx

File Size
5.9 MB

100 Pages

24,393 Words

128,745 Characters

10% Overall Similarity

The combined total of all matches, including overlapping sources, for each database.

Match Groups

- **227** Not Cited or Quoted 9%
  Matches with neither in-text citation nor quotation marks
- **4** Missing Quotations 0%
  Matches that are still very similar to source material
- **11** Missing Citation 1%
  Matches that have quotation marks, but no in-text citation
- **10** Cited and Quoted 0%
  Matches with in-text citation present, but no quotation marks

Top Sources

7% Internet sources
8% Publications
0% Submitted works (Student Papers)

Integrity Flags

0 Integrity Flags for Review

No suspicious text manipulations found.

Our system's algorithms look deeply at a document for any inconsistencies that would set it apart from a normal submission. If we notice something strange, we flag it for you to review.

A Flag is not necessarily an indicator of a problem. However, we'd recommend you focus your attention there for further review.

Match Groups

- 227 Not Cited or Quoted 9%
  Matches with neither in-text citation nor quotation marks
- 4 Missing Quotations 0%
  Matches that are still very similar to source material
- 11 Missing Citation 1%
  Matches that have quotation marks, but no in-text citation
- 10 Cited and Quoted 0%
  Matches with in-text citation present, but no quotation marks

Top Sources

- 7% Internet sources
- 8% Publications
- 0% Submitted works (Student Papers)

Top Sources

The sources with the highest number of matches within the submission. Overlapping sources will not be displayed.

1	Internet	www.torontomu.ca <1%
2	Internet	webfiles.portal.chalmers.se <1%
3	Publication	Shamina Hossain, Hao Zhu, Thomas Overbye. "Distribution high impedance fault ... <1%
4	Internet	www.mdpi.com <1%
5	Internet	keep.lib.asu.edu <1%
6	Internet	repositorio.unesp.br <1%
7	Internet	nottingham-repository.worktribe.com <1%
8	Publication	Júlia S. Paul, Edison A. C. Aranha Neto. "Evaluation of Brazilian regulatory parame... <1%
9	Internet	arxiv.org <1%
10	Internet	www.researchgate.net <1%

11	Publication	"Proceedings of PURPLE MOUNTAIN FORUM 2019-International Forum on Smart ... <1%
12	Internet	core.ac.uk <1%
13	Internet	spiral.imperial.ac.uk <1%
14	Publication	Xiu, Wanjing, and Yuan Liao. "Optimal Fault-location Estimation in Distribution Sy... <1%
15	Publication	Lotfifard, Saeed, Mladen Kezunovic, and Mirrasoul J. Mousavi. "Voltage Sag Data ... <1%
16	Internet	mpce.info <1%
17	Internet	www.rspublication.com <1%
18	Internet	vdoc.pub <1%
19	Internet	ilcphys.kek.jp <1%
20	Internet	slidetodoc.com <1%
21	Internet	www.lib.ncsu.edu <1%
22	Publication	Ganjkhani, Mehdi. "Analytical and Machine Learning Solutions for Cyber Security ... <1%
23	Publication	Jisoo Kim, Jean Mahseredjian. "Development of coordinated control method base... <1%
24	Internet	stars.library.ucf.edu <1%

25 Publication
Mehrdad Majidi, Mehdi Etezadi-Amoli. "A New Fault Location Technique in Smart ... <1%

26 Internet
www.semanticscholar.org <1%

27 Publication
"Application of Smart Technologies in Power System and Smart Grid", Springer Sc... <1%

28 Internet
nainfo.nb.rs <1%

29 Publication
Sadegh Jamali, Alireza Bahmanyar, Ettore Bompard. "Fault location method for di... <1%

30 Internet
real-j.mtak.hu <1%

31 Publication
Christos Apostolopoulos, Charalampos Arsoniadis, Pavlos Georgilakis, Vassilis Nik... <1%

32 Publication
Felix Ghislain Yem Souhe, Alexandre Teplaira Boum, Pierre Ele, Camille Franklin ... <1%

33 Publication
Rahman Dashti, Mohammad Daisy, Hamid Mirshekali, Hamid Reza Shaker, Mahm... <1%

34 Publication
Sanjeevikumar Padmanaban, Hassan Haes Alhelou, Om Prakash Mahela, S. Rajku... <1%

35 Internet
www.ipstconf.org <1%

36 Publication
Wael Al Hanaineh, Jose Matas, Josep M. Guerrero, Mostafa Bakkar. "A Secure Dual... <1%

37 Publication
Yuxuan Guo, Xuan Pei, Xiaolin Luo, Hongjie Liu, Tao Tang, Taogang Hou. "A Partic... <1%

38 Publication
Denis Sodin, Miha Smolnikar, Urban Rudež, Andrej Čampa. "Precise PMU-Based L... <1%

39 Publication
Ricardo Fonseca Buzo, Henrique Molina Barradas, Fabio Bertequini Leao. "A New ... <1%

40 Internet
research.aalto.fi <1%

41 Publication
Farshad, Mohammad, and Javad Sadeh. "A Novel Fault-Location Method for HVDC... <1%

42 Publication
Komal A. Sonagra, Bhargav Y. Vyas. "A Review: Methods of Fault Detection, Identi... <1%

43 Publication
Po-Chen Chen, Vuk Malbasa, Yimai Dong, Mladen Kezunovic. "Sensitivity Analysis ... <1%

44 Publication
Tang, Yingying. "Distribution System Modeling, Analysis and Design with High Pe... <1%

45 Internet
layarkacafilm21.net <1%

46 Publication
Ramar, K, and E E Ngu. "A new impedance-based fault location method for radial ... <1%

47 Publication
Maysoun Alshrouf, Cajetan M. Akujuobi, Emad Awada. "Discrete Wavelet Transfor... <1%

48 Internet
www.frontiersin.org <1%

49 Publication
"Medical Image Computing and Computer Assisted Intervention – MICCAI 2020", ... <1%

50 Internet
upcommons.upc.edu <1%

51 Publication
Ke Jia, Bin Yang, Tianshu Bi, Liming Zheng. "An Improved Sparse-Measurement B... <1%

52 Publication
XiaoFu Xiong, JinXin Ouyang, Jing Jin. "Calculation of steady-state short-circuit cur... <1%

53 Publication
Ying Zhang, Jianhui Wang, Mohammad E. Khodayar. "Graph-based Faulted Line Id... <1%

54 Internet
www.gei-journal.com <1%

55 Publication
Chavan, Mukesh R, S R Paraskar, and S S Jadhao. "A signal processing based overc... <1%

56 Publication
E. EspinosaJuarez, A. Hernandez. "An Analytical Approach for Stochastic Assessme... <1%

57 Internet
m.moam.info <1%

58 Internet
opus.lib.uts.edu.au <1%

59 Publication
Md Shafiullah, Mohammad Ali Abido. "A Review on Distribution Grid Fault Locatio... <1%

60 Publication
Honghua Cao, Xiaoyan Yan, Yan Li. "SLFNs interpolation fingerprint particle filter-... <1%

61 Publication
Mohammadi, M., and Mehdi Nafar. "Optimal placement of multitypes DG as inde... <1%

62 Internet
ajbasweb.com <1%

63 Internet
discovery.researcher.life <1%

64 Publication
Stuart Borlase. "Smart Grids - Advanced Technologies and Solutions", CRC Press, ... <1%

65 Publication
T. A. Short. "Electric Power Distribution Handbook", CRC Press, 2018 <1%

66 Internet
synodus.com <1%

67 Publication
Dong, Yimai, Ce Zheng, and Mladen Kezunovic. "Enhancing Accuracy While Reduci... <1%

68 Publication
Simelane, Mxolisi Irvin. "Investigation into Harmonic Compliance with Respect to ... <1%

69 Publication
Wang, Jianhong, Yongqiang Ye, and YangQuan Chen. "Fraction Phase Lead Repeti... <1%

70 Publication
Xu, Yan, and Ping Han. "Research on Flow Transferring Identification Method Bas... <1%

71 Internet
www.coursehero.com <1%

72 Internet
www.fayoum.edu.eg <1%

73 Publication
Yikui Liu, Lei Wu, Jie Li. "D-PMU based applications for emerging active distributio... <1%

74 Internet
blog.interact911.com <1%

75 Internet
journals.sagepub.com <1%

76 Internet
www.hindawi.com <1%

77 Publication
M. Garcia-Gracia. "Travelling waves distance protection in a distribution network... <1%

78 Publication
"Handbook of Position Location", Wiley, 2011 <1%

79 Publication
Fernanda C. L. Trindade, Walmir Freitas. "Low Voltage Zones to Support Fault Loc... <1%

80 Publication
Jatinder Kumar, Rishabh Gupta, Deepika Saxena, Ashutosh Kumar Singh. "Power ... <1%

81 Publication
Paulo A.H. Cavalcante, Madson C. de Almeida. "Fault location approach for distrib... <1%

82 Internet
backend.orbit.dtu.dk <1%

83 Internet
emeral.ut.ac.ir <1%

84 Internet
hdl.handle.net <1%

85 Internet
ieee-pes.org <1%

86 Internet
ltu.diva-portal.org <1%

87 Internet
repositories.lib.utexas.edu <1%

88 Internet
tel.archives-ouvertes.fr <1%

89 Internet
www.acarindex.com <1%

90 Internet
www.ncc.gov.ng <1%

91 Internet
www.repositorio.unicamp.br <1%

92 Publication
Ahad Esmaeilian, Mladen Kezunovic. "An impedance based fault location algorith... <1%

93 Publication
Himadri Lala, Subrata Karmakar, Sanjib Ganguly. "Detection and localization of fa... <1%

94 Publication
Karunakar Gampa. "Errors in fault analysis of power distribution systems using s... <1%

95 Publication
Lipsa Priyadarshini, P. K. Dash. "Detection of islanding and non-islanding fault dis... <1%

96 Publication
M. Majidi, M. Etezadi-Amoli, M. Sami Fadali. "A Novel Method for Single and Simul... <1%

97 Publication
Majid Jamil, Rajveer Singh, Sanjeev Kumar Sharma. "Fault identification in electric... <1%

98 Publication
Pengpeng Chen, Fen Liu, Shouwan Gao, Peihao Li, Xu Yang, Qiang Niu. "Smartpho... <1%

99 Publication
Ranjbar, Ali Mohammad, and Ahmad Salehi-Dobakhshari. "Application of synchro... <1%

100 Publication
Ritu Singh, Smruti Rekha Pattanaik, Anshuman Bhuyan, Basanta K. Panigrahi, Jyo... <1%

101 Publication
Shu Zhang, Sheng Lin, Zhengyou He, Wei-jen Lee. "Ground fault location in radial ... <1%

102 Publication
Studies in Fuzziness and Soft Computing, 2015. <1%

103 Publication
T.S. Sidhu, M. Bajpai, J. Burnworth, A. Darlington et al. "Bibliography of Relay Liter... <1%

104 Publication
Teke Gush, Syed Basit Ali Bukhari, Raza Haider, Samuel Admasie, Yun-Sik Oh, Gyu... <1%

105 Publication
Trindade, Fernanda C. L., Walmir Freitas, and Jose C. M. Vieira. "Fault Location in ... <1%

106 Publication
Tzu-Chiao Lin, Zhi-Ren Xu, Faouzi Brice Ouedraogo, Yu-Ju Lee. "A new fault locatio... <1%

107 Publication
Xiangyu Kong, Yong Xu, Zaibin Jiao, Delong Dong, Xiaoxiao Yuan, Shupeng Li. "Fa... <1%

108 Publication
Yanxia Zhang, Ting Li, Jian Wang, Haidong Wang, Yuqing Chang. "Fault location fo... <1%

109 Internet
era.library.ualberta.ca <1%

110 Internet
mafiadoc.com <1%

111 Internet
merl.com <1%

112 Internet
sfitlibrary.blogspot.com <1%

113 Internet
smartgridcenter.tamu.edu <1%

114 Internet
starbiz.net <1%

115 Internet
vbn.aau.dk <1%

116 Publication
Alireza Bahmanyar, Abouzar Estebsari. "A Practical Integrated Fault Location Met... <1%

117 Publication
Chongyu Wang, Kaiyuan Pang, Yan Xu, Fushuan Wen, Ivo Palu, Changsen Feng. "... <1%

118 Publication
El Halabi, Nabil, Miguel Garc&#65533;a-Gracia, Diego L&#65533;pez And&#65533;a, and Marta Abad. "N... <1%

119 Publication
A. Bahmanyar, S. Jamali, A. Estebsari, E. Bompard. "A comparison framework for ... <1%

120 Publication
Alireza Bahmanyar, Abouzar Estebsari, Enrico Pons, Edoardo Patti, Sadegh Jamali,... <1%

121 Publication
Gajanand Sharma, Om Prakash Mahela, Mahendra Kumar, Neeraj Kumar. "Detect... <1%

122 Publication
Haotian Sun, Hao Yi, Fang Zhuo, Xiaotong Du, Guangyu Yang. "Precise Fault Locat... <1%

IOE Graduate Conference
[Placeholder for Publication Information]

A Robust Method of Fault Classification and Localization in Nepalese Distribution System

Awnish Kumar Thakur [a], Anil Kumar Panjiyar [b], Basanta Kumar Gautam, PhD [c]

[a,b,c] *Department of Electrical Engineering, Pulchowk Campus, IOE, Tribhuvan University, Nepal*
[a] 079mspse004.awnish@pcampus.edu.np , [b] anil.panjiyar@pcampus.edu.np , [c] basanta.gautam@pcampus.edu.np

Abstract
Ensuring an uninterrupted power supply in developing countries like Nepal is challenging due to factors such as geographical terrain, vegetation, aging infrastructure, manual fault clearing, long feeder lengths with limited switch deployment, and the use of bare conductors. This paper introduces a robust method for fault localization in Nepalese distribution systems along with a novel approach to fault classification. The proposed fault classification method requires only two synchronized time measurement units, positioned at the start and end of a lateral. For fault localization, smart meters are needed at the end of all laterals. By utilizing voltage sag data from synchronized time measurement units, a two-nodal current source is calculated and injected at each node, then compared with the system's actual voltage sag. The effectiveness of the proposed method is validated using OpenDSS and Python on the Solati distribution feeder.

Keywords
Fault Classification, OpenDSS, Python, Synchronized Time Measurement, Voltage Sag, Fault Localization

1. Introduction

Electric utilities face numerous reliability issues in distribution systems, which directly impact consumers through power outages and utilities through revenue losses. The power systems in many developing countries were originally designed to serve basic lighting and limited industrial loads. However, with improving economic conditions and increasing load demand, these systems are now under significant strain. One of the primary causes of poor reliability is aging infrastructure, including outdated transformers and inadequate distribution line capacity [1].

Numerous research studies and algorithms have been developed for fault localization in transmission lines. However, fault localization in distribution systems remains a critical process for electric utilities, involving the identification of precise fault locations. Accurate fault localization is essential for minimizing downtime, reducing repair costs, and restoring service efficiently [2]. Traditional fault localization methods often rely on manual inspection, which can be time-consuming, particularly in large or remote areas. However, modern system employs advanced technologies such as smart meter grids, sensors, phasor measurement units (PMUs), and fault indicators to detect anomalies in voltage, current, or impedance.

The electric distribution network in Nevada experienced approximately 50,000 customers outage hours that affected 40,000 customers due to sustained fault in year of 2016 AD [3].

1.1 Type of Short Circuit Faults

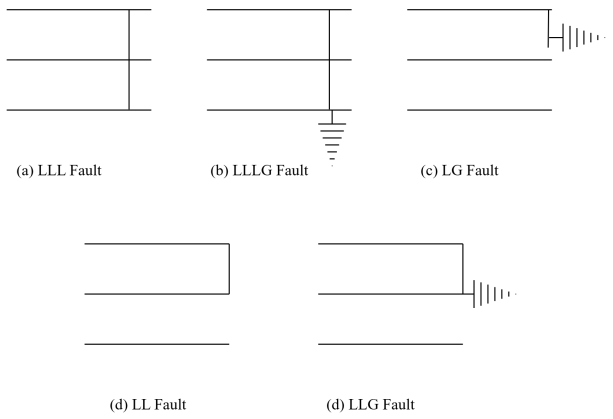

Figure 1: Classification of short circuit fault

A fault in a distribution system refers to abnormal conditions that cause current to flow along unintended

paths, often with a larger magnitude than normal. A Short circuit faults can be classified as [4]:

1.1.1 Symmetrical Short Circuit Fault

A symmetrical short circuit fault occurs when all three phases are involved in a short circuit. In this type of fault, the fault current in each phase is equal, and the phase angles remain the same. It can be further classified into LLL (three-line) and LLLG (three-line-to-ground) faults. Although this type of fault is rare, its impact is severe.

1.1.2 Unsymmetrical Short Circuit Fault

During the short circuit condition either one or two phase involve, this type of fault is termed as unsymmetrical fault. During this type of fault magnitude of fault current through each phase are different as well as change in phase angle. Further, this type of fault can be classified as single phase to ground (LG) fault, double line to ground (LLG) fault, and double line (LL) fault.

- Single Line to Ground (LG) Fault: In case of LG fault, there is involvement of only single line to ground. When bolted LG fault occurs, the healthy phases voltage may vary from phase voltage to line voltage that depends upon the earthing condition.
- Double Line (LL) Fault: In case of LL fault, there is involvement of two line. When bolted LL fault occurs in system, the healthy phase voltage remains as same.
- Double Line to Ground (LLG) Fault: In case of LLG fault, there is involvement of two phase to ground. When bolted LLG fault occurs in system, the healthy phase voltage varies from phase voltage to 1.5 times of phase voltage depending upon condition.

The classification of short circuit faults is illustrated in figure 1.

1.2 Occurrence Probability of Fault

Various of short circuit fault types, the relative frequency of occurrence [5] of fault in distribution system in order to decreasing severity is presented in table 1.

Table 1: Relative frequency of occurrence of fault

Type of faults	Percentage occurrence
Three phase (3L) fault	5%
LLG fault	10%
LL fault	15%
LG fault	70%

1.3 Fault Localization Method

Various methods have been successfully applied to fault location in transmission lines with high accuracy. However, their implementation in distribution systems is challenging due to the presence of multiple laterals, load taps, the heterogeneous nature of the network, and varying load conditions. [6]. The popular method of fault localization is listed below with brief summary about its strengths as well as limitations.

1.3.1 Traveling Wave Based Method

The traveling wave-based method is perfectly localized fault in transmission line, but their application in distribution system becomes very complicated due to presence of multiple laterals, and resulting reflecting wave. Moreover, this method requires expensive equipment with high sampling rate capable of detecting waveform traveling near speed of light [7].

1.3.2 Impedance Based Method

The calculation between substation and fault point is required to calculate for fault localization. These methods are problem providing multiple fault localization point. One of the tested cases in the paper is for single line to ground fault, the impedance-based algorithm gives four possible locations of the fault if only three smart energy meter is deployed in the system [8].

1.3.3 Super Imposed Component Method

It calculates the faulted system's state by superimposing the normal (pre-fault) system state with the deviation caused by the fault, known as the superimposed components. By isolating these deviations, the method simplifies fault location and analysis by focusing only on the incremental changes. This approach is effective for analyzing transient and steady-state fault behavior, especially in radial distribution systems. However, its limitations include sensitivity to measurement inaccuracies, dependency on accurate pre-fault conditions, and reduced

effectiveness in complex, meshed systems where multiple pathways can dilute the superimposed signals. Additionally, integrating it with real-time monitoring systems can be computationally intensive [8].

1.3.4 Intelligent System Based Method

It employs artificial intelligence (AI) techniques, such as neural networks, fuzzy logic, expert systems, and machine learning, to analyze and locate faults in power distribution systems. These methods utilize historical and real-time data to identify patterns and anomalies associated with faults. They can handle the complexities of nonlinear, dynamic systems and adapt to changing system conditions, making them suitable for modern smart grids. However, their limitations include the need for large datasets for training, potential over-fitting, and challenges in interpreting the model's decision-making process. Additionally, their accuracy heavily depends on the quality and quantity of input data and the robustness of the system's design [8].

1.3.5 Voltage Sag Based Method

The voltage sag-based method identifies and locates faults in distribution systems by analyzing the voltage sags caused by faults. When a fault occurs, it creates a characteristic drop in voltage magnitude at different buses, with the severity and pattern of the sag depending on the fault's location, type, and impedance. By comparing the measured voltage sags with a pre-calculated fault signature database or using analytical models, the fault's location can be pinpointed. This method is particularly effective for radial networks. Artificial intelligence-based algorithms, trained using voltage sag data, require multiple fault scenarios to be simulated. However, their accuracy is affected when faults occur under conditions not covered in the training data, such as variations in fault resistance and distributed generation penetration. Similarly, some methods leverage both voltage magnitude and phase angle, with meters strategically placed at the beginning of multiple branch nodes [8].

The major objective of this paper is to develop a robust approach for fault localization in the Nepalese distribution system, along with a novel fault classification method. We propose a mean deviation-based fault classification technique that utilizes the calculated fault current from two synchronized measurement units.

The paper is organized as follow. Section II consists of proposed methodology for fault localization and classification. Section III consists of modeling of system for verification of methodology. Section IV present's fault localization and classification result and discussion. Conclusion and future scope of this research is presented in section V.

2. Proposed Methodology

2.1 Fault Localization

The fault localization method proposed in this paper relies on calculating the voltage sag between the pre-fault and during-fault voltages. Since two nodes are equipped with a synchronized time measurement unit, the subsystem containing this unit is utilized. To determine the fault location, the fault current, voltage, and error calculations are essential, with references drawn from [9, 10].

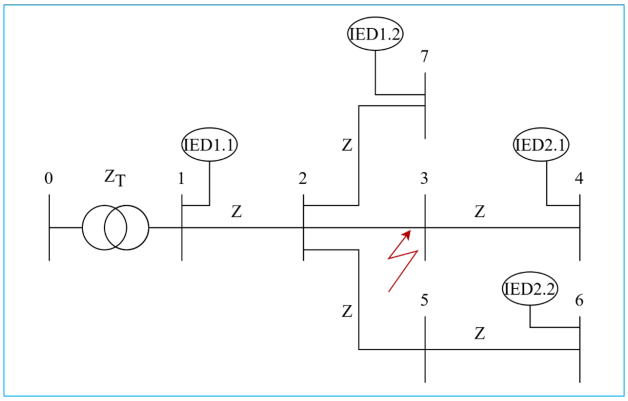

Figure 2: Sample 7 node distribution feeder

Figure 2 illustrates a sample distribution feeder layout with seven nodes. Node 1 represents the substation, while terminal node 7 is also equipped with a synchronized time measurement unit. Additionally, terminal nodes 4 and 6 are equipped with smart meters that transmit the magnitude of voltage both before and during a fault.

The nodes equipped with synchronized time measurement units are responsible for determining two nodal currents. In this calculation, all other branches are neglected, and only the branch between the substation node and the synchronized time measurement unit-equipped terminal node is considered. For this sample system, the two nodal currents at nodes 1 and 7 are determined using

equation (1).

Here, m represents the substation node equipped with the synchronized time measurement unit, while n denotes any lateral node within the subsystem where a synchronized time measurement unit is installed.

The fault current, as expressed in equation (2), is obtained by summing the two nodal currents from equation (1). Since fault resistance and the integration of distributed generation (DG) have already been accounted for through measurements from the synchronized time measurement unit, the calculated fault current inherently depends on both fault resistance and distributed generation.

$$\begin{bmatrix} i_m^{\text{abc}} \\ i_n^{\text{abc}} \end{bmatrix}_{6\times1} = \begin{bmatrix} Z_T & Z_T \\ Z_T & Z_T + 2Z \end{bmatrix}_{6\times6}^{-1} \begin{bmatrix} \Delta \dot{V}_m^{\text{abc}} \\ \Delta \dot{V}_n^{\text{abc}} \end{bmatrix}_{6\times1} \quad (1)$$

$$i_f^{abc} = i_m^{abc} + i_n^{abc} \quad (2)$$

Here i_f^{abc} represents the calculated fault current from voltage sag, and for each phase a,b and c. Similar way, i_m^{abc} and i_n^{abc} represent three phase voltage of substation node and terminal node.

The calculated fault current is then injected at each node in the substation, and the resulting voltage sag at the terminal nodes is measured. For each subsystem, a candidate fault node is identified. Finally, using a weight matrix, the fault location closest to the affected bus is determined.

2.2 Fault Classification

By analyzing various scenarios of the calculated fault current in equation (2), it is observed that in the case of a three-phase fault, the fault currents in all three phases have nearly identical values. However, for a line-to-ground (LG) fault, the faulted phase exhibits a significantly higher current, while the healthy phases show very low values. Similarly, in a double-line fault, two phases experience substantial fault currents, whereas the remaining phase remains relatively unaffected.

Based on these observations, a novel fault classification method is developed. This paper proposes an innovative approach to fault classification using the mean current and the per-unit deviation of the mean phase current. The mean current, given by equation (3), is calculated by summing the absolute values of the phase currents from equation (2). The mean deviation for each phase is then computed using equations (4)–(6).

$$I_m^f = \frac{abs(i_f^a) + abs(i_f^b) + abs(i_f^c)}{3} \quad (3)$$

$$D_{IA} = \frac{abs(i_f^a) - I_m^f}{I_m^f} \quad (4)$$

$$D_{IB} = \frac{abs(i_f^b) - I_m^f}{I_m^f} \quad (5)$$

$$D_{IB} = \frac{abs(i_f^c) - I_m^f}{I_m^f} \quad (6)$$

The proposed fault classification approach is illustrated in the flowchart 3. In the case of a three-phase fault, the mean deviation of each phase is very low, nearly zero. Therefore, a tolerance level of $1e-5$ is defined. If the mean deviation of each phase falls below this threshold, a three-phase fault is identified.

For a single line-to-ground fault, if the mean deviation of one phase exceeds 1.5 while the other two phases approximately sum to that value, the condition for a single line-to-ground fault is met. The phase with a mean deviation greater than 1.5 is identified as the faulted phase.

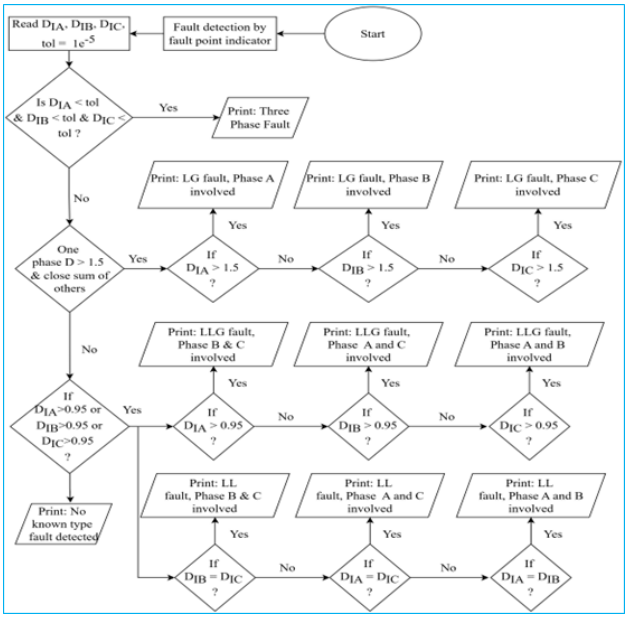

Figure 3: Flowchart showing developed fault classification approach

If the above two conditions—single line-to-ground or three-phase faults—are not met, and the mean

deviation of any phase exceeds 0.95, the fault is classified as a double-line fault. The two phases involved in the fault are those other than the phase with the highest deviation above 0.95.

3. System Modeling

3.1 Implemented Methodology for Fault Localization

The fault localization methodology is developed and implemented using **OpenDSS** and **Python**, following a structured approach to accurately identify fault locations in a power distribution network. The methodology involves multiple sequential steps, as shown in flochart 4.

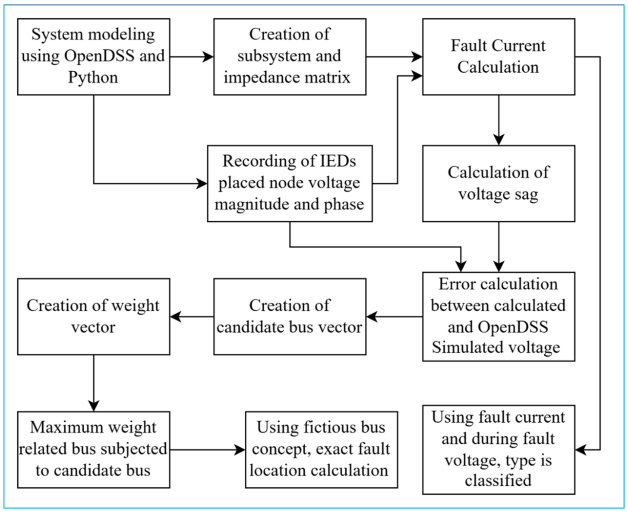

Figure 4: Overall Fault localization and classification methodology

3.1.1 System Modeling Using OpenDSS and Python

The distribution system is modeled using **OpenDSS**, where network parameters such as bus data, line data, and load data are incorporated. Python is used to automate the simulation and extract the necessary system information.

3.1.2 Creation of Subsystem and Impedance Matrix

A subsystem is defined based on the network topology, and the **impedance matrix** is formulated. This helps in determining the voltage response of different nodes in the system during normal and fault conditions.

3.1.3 Fault Current Calculation

A fault is introduced at different locations in the system, and the corresponding fault current is calculated. This current provides critical information regarding the severity and type of fault.

3.1.4 Calculation of Voltage Sag

Voltage sag levels are computed based on the simulated fault conditions. The reduction in voltage at different buses serves as an indicator of fault presence and propagation.

3.1.5 Recording of IEDs Placed Node Voltage Magnitude and Phase

Intelligent Electronic Devices (**IEDs**) placed at specific nodes record voltage magnitudes and phase angles. These measurements are used for comparison against simulated fault scenarios.

3.1.6 Error Calculation Between Calculated and OpenDSS-Simulated Voltage

The voltage sag values obtained from fault simulation in OpenDSS are compared with the measured values from IEDs. The error between these values helps in refining the fault location estimates.

3.1.7 Creation of Candidate Bus Vector

A candidate bus vector is generated, containing the buses that are most likely to have experienced the fault based on error analysis.

3.1.8 Using Fault Current and During-Fault Voltage for Fault Type Classification

The fault type is classified by analyzing the fault current and the voltage profile during the fault event. This aids in further narrowing down the potential faulted location.

3.1.9 Using Fictitious Bus Concept for Exact Fault Location Calculation

A fictitious bus concept is employed to refine the fault location estimation. This concept helps in identifying the **exact** faulted node by analyzing voltage deviations in a theoretical extended network.

3.1.10 Creation of Weight Vector

A weight vector is generated based on the probability of fault occurrence at different candidate buses. The

weights are assigned based on the error values and the voltage sag levels.

3.1.11 Maximum Weight Related Bus Subjected to Candidate Bus

The bus with the highest assigned weight is identified as the most probable fault location. This final step confirms the faulted bus based on systematic ranking and analysis.

3.2 Distribution Feeder Modeling Approach

A Python-based distribution system modeling program has been developed, which imports input data from Excel and conducts the final system modeling in OpenDSS. Serving as a bridge between the input data and the OpenDSS model, the program requires line data, bus data, load data, and bus coordinates to generate a complete system model.

3.3 Creation of Subsystem

The fault localization algorithm requires the creation of subsystems that extend from substation nodes to the end of each branch, while other branches are disregarded. Each subsystem consists of lines connecting the substation node to the terminal point of a branch. The total number of subsystems formed corresponds to the number of branches in the system.

OpenDSS is interfaced with Python using the win32com library, which provides full control and access to OpenDSS elements. In the modeling process, it is assumed that the substation node is connected to bus number 1. After identifying the substation node, the next key task is to determine the nodes at the ends of branches (i.e., the terminal nodes of each branch). The implemented logic for identifying these end nodes is based on connectivity: if a bus is connected to only one line, it is considered a terminal node; otherwise, if it is connected to at least two lines, it is not an end node.

In some cases, the substation node may only be connected to a single line or branch. In such instances, this node could be identified as a terminal node. To prevent this, a discarding function is implemented to exclude the substation node from being classified as a branch terminal node. This ensures that the substation node is not treated as the end of a branch.

Now, it is necessary to determine the shortest distance between the substation node and the branch lateral nodes. Here, the shortest distance is defined not by the physical length of the lines but by the number of connected buses from the substation node to the end of the branches. This is accomplished using the Breadth-First Search (BFS) method.

Breadth first search (BFS) is an algorithm for traversing or searching tree or graph data structures. It starts at the root and explores all the neighbor nodes at the present depth level before moving on to nodes at the next depth level [11]. BFS starts at source node, and uses a queue to keep track of the nodes to visit next, ensuring that nodes are explored level by level. The algorithm adds the starting node to the queue and marks it as visited. Then this algorithm enters a loop where it removes a node from the front of the queue, and visits all unvisited neighboring nodes (or children, in tree terms), marking them visited and adding them to the queue. This process is continuing until the queue is empty or specific condition is met. The specific condition means targeted nodes.

Finally, each line containing the subsystem is saved in the data base for further analysis. The overall process is shown in flowchart 5.

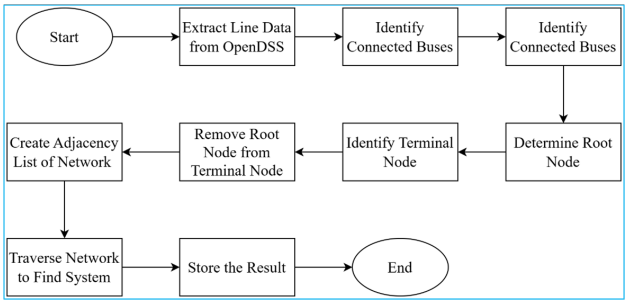

Figure 5: Flowchart showing methodology of subsystem creation using OpenDSS and Python

4. Result and Discussion

In order to validate the proposed method, an 11 kV distribution feeder, namely the Solati distribution feeder, originating from the Barahathawa distribution feeder in Sarlahi district, is simulated. The feeder comprises 22 load centers, supplied by 2 transformers of 25 kVA, 5 transformers of 50 kVA, and 15 transformers of 100 kVA. The total length of the feeder, including all branches, is 25.58 km, with the longest segment extending 17.121 km. The network consists of 36 nodes, where buses serve as junction points for laterals, load centers, or conductor type changes. The distribution line is heterogeneous, consisting of a mix of dog and rabbit conductors. The

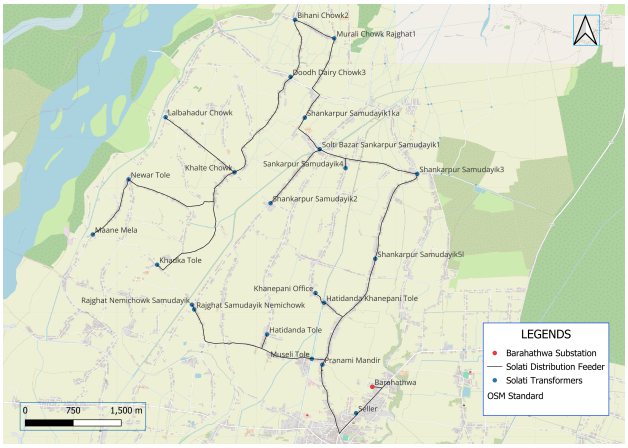

Figure 6: GIS diagram of Solati distribution feeder

GIS diagram of the simulated feeder is shown in Figure 6.

4.1 LLLG Fault Scenario

A three-phase fault is applied at various locations along the distribution feeder. Due to page limitations, results for only selected buses are reported. In OpenDSS, faults are applied at buses, and for fault simulation on line sections, a virtual bus is created. When an LLLG fault is introduced at different locations, the fault detection error remains minimal, with a maximum deviation of 2.01 km in fault distance estimation. In all cases, the fault classification achieves 100% accuracy. The detailed results are presented in Table 2.

Table 2: Bolted LLLG fault at different length of line

S.N.	Simulated Distance (km)	Calculated Distance (km)	Detected Fault Type
1	0.15	0.15	LLLG
2	2.43	2.43	LLLG
3	3.58	3.58	LLLG
4	4.12	3.58	LLLG
5	4.79	5.06	LLLG
6	3.7	3.7	LLLG
7	7.84	7.86	LLLG
8	10.83	10.83	LLLG
9	11.91	11.92	LLLG
10	13.93	11.92	LLLG

4.2 LLG Fault Scenario

When an LLG fault is introduced at different locations, the fault detection error remains minimal, with a maximum deviation of 2.01 km in fault distance estimation. In all cases, the fault classification achieves 100% accuracy. The detailed results are presented in Table 3.

Table 3: Bolted LLG fault at different length of line

S.N.	Simulated Distance (km)	Calculated Distance (km)	Detected Fault Type
1	0.15	0.15	LLG
2	2.43	2.43	LLG
3	3.58	3.58	LLG
4	4.12	3.58	LLG
5	4.79	5.06	LLG
6	3.7	3.7	LLG
7	7.84	7.86	LLG
8	10.83	10.83	LLG
9	11.91	11.92	LLG
10	13.93	11.92	LLG

4.3 LL Fault Scenario

When an LL fault is introduced at different locations, the fault detection error remains minimal, with a maximum deviation of 2.01 km in fault distance estimation. In all cases, the fault classification achieves 100% accuracy. The detailed results are presented in Table 4.

Table 4: Bolted LL fault at different length of line

S.N.	Simulated Distance (km)	Calculated Distance (km)	Detected Fault Type
1	0.15	0.15	LL
2	2.43	2.43	LL
3	3.58	3.58	LL
4	4.12	3.58	LL
5	4.79	5.06	LL
6	3.7	3.7	LL
7	7.84	7.86	LL
8	10.83	10.83	LL
9	11.91	11.92	LL
10	13.93	11.92	LL

4.4 LG Fault Scenario

When an LG fault is introduced at different locations, the fault detection error remains minimal, with a maximum deviation of 2.01 km in fault distance estimation. In all cases, the fault classification achieves 100% accuracy. The detailed results are presented in Table 5.

Table 5: Bolted LG fault at different length of line

S.N.	Simulated Distance (km)	Calculated Distance (km)	Detected Fault Type
1	0.15	0.15	LG
2	2.43	2.43	LG
3	3.58	3.58	LG
4	4.12	3.58	LG
5	4.79	5.06	LG
6	3.7	3.7	LG
7	7.84	7.86	LG
8	10.83	10.83	LG
9	11.91	11.92	LG
10	13.93	11.92	LG

From the results reported in table 2-5, it is observed that fault location accuracy remains consistent across different fault types, demonstrating the effectiveness of the fault classification approach. Sensitivity analysis is conducted by varying the load, incorporating distributed generation, and adjusting fault resistance from 0.1Ω to 250Ω. Due to page limitations, this paper presents sensitivity analysis results only for single-line-to-ground faults.

4.5 Load Variation Scenario

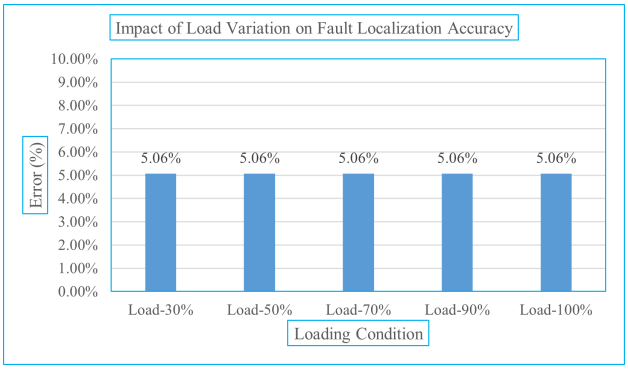

Figure 7: Impact of load variation on fault localization accuracy in LG fault scenario

In the base case, all transformers are assumed to operate at 70% loading, and the results presented in the table are based on this condition. Additionally, four more cases are simulated by varying transformer loading to 30%, 50%,90%, and 100%. For a bolted fault, across all loading conditions, the average error in fault location for an LG fault is found to be 5.06%, as illustrated in figure 7. This indicates that the fault localization method remains unaffected by load variations. As the fault location accuracy is found independent of fault type, the impact of load variation, DG penetration and resistance variation are studied for LG fault type.

4.6 DG Placement Scenario

Currently, the simulated distribution feeder does not include any distributed generation (DG). However, with the power system trend shifting towards locally generated power sources, it is essential to validate the proposed method under the presence of DG. To achieve this, five random locations 5, 13, 20, 33, and 36 are selected for DG placement having capacity of 640 kW, and . The simulation is performed for a bolted LG fault, and across all DG locations, the average fault location error is found to be 5.06%, as illustrated in figure 8. Since the impact and flow of current have already been accounted for in the fault current calculation, the average fault localization error remains constant regardless of the fault location.

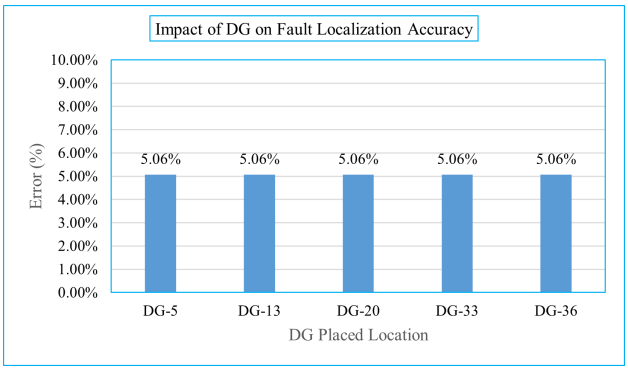

Figure 8: Impact of DG variation on fault localization accuracy in LG fault scenario

4.7 Fault Resistance Variation Scenario

A fault resistance can vary significantly in practical scenarios, influencing the accuracy of the method. To validate the proposed approach under different fault conditions, the fault resistance is varied from 0.1Ω to 250Ω, considering values of 0.1Ω, 10Ω, 50Ω, 100Ω, and 250Ω. The simulation results, illustrated in figure

9, show that as the fault resistance increases, the accuracy of the method improves. Specifically, for fault resistances up to 50Ω, the average fault location error is found to be 5.06%. For fault resistances above 50Ω, the average fault location error decreases to 2.09%, indicating an improvement in the method's performance as the fault resistance increases.

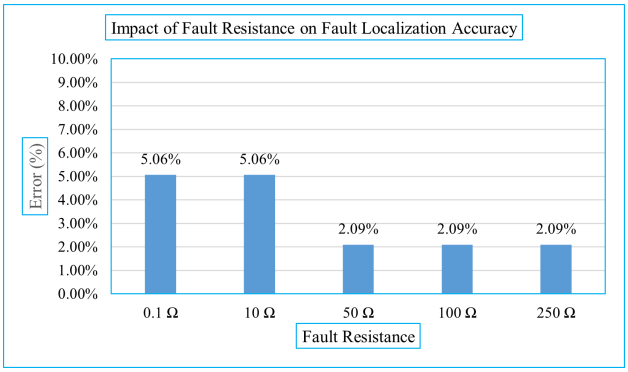

Figure 9: Impact of fault resistance variation on fault localization accuracy in LG fault scenario

5. Conclusion

The developed fault classification approach demonstrates 100% efficacy in accurately classifying faults under various conditions, including varying fault resistance, the presence of Distributed Generations (DGs), fluctuating loading conditions, and the heterogeneous nature of distribution lines. The maximum error in fault localization is observed to be 5.06% under bolted fault conditions, despite the presence of different fault types, DGs, and the varied characteristics of the distribution network. Additionally, as fault resistance increases, the accuracy of fault localization improves.

A key advantage of the proposed methodology is its ability to minimize the number of smart meters required, significantly reducing the cost of practical implementation. By utilizing both synchronized and non-synchronized measurement devices, strategically placed across the network, the approach ensures cost-effectiveness without compromising on performance. Notably, only two synchronized time measurement units are required for fault classification in the distribution network.

These results highlight the methodology's potential for real-world applications, positioning it as a promising solution to enhance the reliability and efficiency of fault management in Nepalese distribution networks. Since this method effectively operates in distribution systems with multiple laterals, heterogeneous line characteristics, varying load conditions, and a high R/X ratio, it is also well-suited for transmission lines.

Future work may explore the integration of additional features, such as real-time data analysis and scalability for larger systems, to further enhance the effectiveness and applicability of the approach.

Acknowledgments

The authors extend their special thanks to Sagar Dharel for his invaluable guidance and insightful feedback throughout this research. They are also deeply grateful to Nikee Thakur and Neema Mishra for their unwavering support and encouragement during the course of this work.

Additionally, the authors express their appreciation to the Department of Electrical Engineering, IoE Pulchowk Campus, TU, for providing excellent infrastructure and resources that facilitated this research.

References

[1] Zbigniew Łukasik and Zbigniew Olczykowski. Quality and reliability of electricity supply. In *2020 ELEKTRO*, pages 1–6. IEEE, 2020.

[2] R Billinton, L Salvaderi, JD McCalley, H Chao, Th Seitz, RN Allan, J Odom, and C Fallon. Reliability issues in today's electric power utility environment. *IEEE Transactions on Power Systems*, 12(4):1708–1714, 1997.

[3] Mehrdad Majidi and Mehdi Etezadi-Amoli. A new fault location technique in smart distribution networks using synchronized/nonsynchronized measurements. *IEEE Transactions on Power Delivery*, 33(3):1358–1368, 2017.

[4] Felix Ghislain Yem Souhe, Alexandre Teplaira Boum, Pierre Ele, Camille Franklin Mbey, Vinny Junior Foba Kakeu, et al. Fault detection, classification and location in power distribution smart grid using smart meters data. *Journal of Applied Science and Engineering*, 26(1):23–34, 2022.

[5] D. P. Kothari and I. J. Nagrath. *Modern Power System Analysis*. McGraw Hill Education (India) Private Limited, Chennai, India, 2016.

[6] Po-Chen Chen, Vuk Malbasa, Yimai Dong, and Mladen Kezunovic. Sensitivity analysis of voltage sag based fault location with distributed generation. *IEEE Transactions on Smart Grid*, 6(4):2098–2106, 2015.

[7] Denis Sodin, Miha Smolnikar, Urban Rudež, and Andrej Čampa. Precise pmu-based localization

and classification of short-circuit faults in power distribution systems. *IEEE Transactions on Power Delivery*, 38(5):3262–3273, 2023.

[8] Saeed Lotfifard, Mladen Kezunovic, and Mirrasoul J Mousavi. Voltage sag data utilization for distribution fault location. *IEEE Transactions on Power Delivery*, 26(2):1239–1246, 2011.

[9] Awnish Kumar Thakur, Sagar Dharel, Nikee Thakur, Raunak Ghimire, Rojina Sharma, and Sher Singh Bhat. Implementation of voltage sag based fault localization algorithm in nepalese distribution system considering the impact of fault resistances. *International Journal of Innovative Science and Research Technology (IJISRT)*, 9(11):2355–2361, November 2024. Accessed: 2025-02-09.

[10] Ricardo Fonseca Buzo, Henrique Molina Barradas, and Fábio Bertequini Leão. A new method for fault location in distribution networks based on voltage sag measurements. *IEEE Transactions on Power Delivery*, 36(2):651–662, 2020.

[11] Ji-Soo Kim, Chul-Hwan Kim, Yun-Sik Oh, Gyu-Jung Cho, and Jin-Sol Song. An islanding detection method for multi-res systems using the graph search method. *IEEE Transactions on Sustainable Energy*, 11(4):2722–2731, 2020.